

**Oxygen isotope microanalysis of silicates
with application to fluid-rock interfaces**

Dissertation

zur Erlangung des Doktorgrades

der Mathematisch-Naturwissenschaftlichen Fakultäten

der Georg-August-Universität zu Göttingen

vorgelegt von

Jens Fiebig

aus Bremen

Göttingen 1999

D 7

Referat: Prof. Dr. J. Hoefs

Correferat: Prof. Dr. G. Wörner

Tag der mündlichen Prüfung: 27.01.2000

Acknowledgements

First of all I like to thank all my co-workers from the Geochemical Institute for their contribution to having a pleasant time throughout the last three years.

I would like to express my sincere thanks to Prof. Dr. J. Hoefs. He has been an excellent mentor and gave me strong support throughout the course of the work. I also like to thank Prof. Dr. G. Wörner for his interest in the present thesis and for taking on the function of co-advisor.

I greatly appreciate the help of R. Przybilla. With his tremendous technical knowledge he was instrumental for the progress of the present work. I also appreciate many fruitful scientific discussions with him.

Special thanks go to Dr. Uwe Wiechert, who set up the former UV-laser microprobe, which has been a prerequisite for starting this study. Especially the first part of the present thesis benefited from his CO₂-laser analyses of various quartz samples at the Geophysical Lab, Washington, and from his critical and detailed reviews.

Dr. K. Simon is thanked for his patience throughout many discussions concerning the alteration history of granites from the Schwarzwald. In this way he kindly taught me the basics for an understanding of the hydrothermal event that occurred within the Schwarzwald.

For many constructive remarks regarding the process of laser ablation and kinetics and thermodynamics of fluid-rock interaction I wish to thank Prof. Dr. K. Luther from the Institute of Physical Chemistry, Göttingen. From the same institute, Prof. Dr. H.-Gg. Wagner is thanked for serving as a member of my candidacy examination committee, though he has already retired.

I further acknowledge Dr. A. Kronz and D. Strohmeyer for giving support during electron microprobe investigations. P. Bogaard is thanked for a final correction of the English.

Finally, greatest thanks go to my parents, who enabled me 10 years of education at the University of Göttingen and to my girl-friend Annett, who encouraged me within the last two years.

Table of contents

D 7	2
Acknowledgements.....	3
Table of contents	4
A. Introduction	7
1. In situ oxygen isotope analysis of quartz.....	10
1.1. Introduction.....	10
1.2. Instrumentation.....	11
1.3. Samples and procedures.....	11
1.4. Basic principles of laser fluorination	15
1.5. Ablation of quartz using ultra-violet laser light pulses	18
1.5.1. ArF-laser ablation.....	18
1.5.2. KrF-laser ablation.....	19
1.6. Oxygen isotope data of different quartz samples.....	21
1.6.1. Comparison of ArF-laser, CO ₂ -laser and conventional data.....	21
a) Dörentrup.....	21
b) Granite quartz.....	24
c) Suprasil	24
1.6.2. Single grain versus thick section analysis.....	26
a) Granite quartzes.....	27
b) Dörentrup.....	27
1.6.3. Data correction	29

1.7. Application: oxygen isotope analysis of a hydrothermal cap quartz.....	30
Appendix I.....	33
Appendix II.....	34
Appendix III.....	36
Appendix IV.....	38
2. Set up of a rapid technique enabling precise determinations of 18/16-ratios within silicate extracted oxygen.....	40
2.1. Introduction.....	40
2.2. Silicate oxygen and irm-GC-MS.....	40
2.3. Equipment.....	41
2.4. Set up of the continuous flow technique.....	42
2.4.1. Characteristics of the DeltaPlus concerning oxygen isotope measurements in a contiuuous flow mode.....	42
2.4.1.1. Peak shape.....	42
2.4.1.2. Optimization of ion source parameters.....	43
2.4.2. Set up of irm-GC-MS.....	44
2.4.2.1. Linearity.....	47
2.4.2.2. Factors influencing linearity.....	47
2.4.3. Calibration to V-SMOW-scale.....	49
2.4.4. Combination of UV-laser oxygen extraction system and irm-GC-MS.....	51
2.4.5. Gaseous interferences during detection of $^{18}\text{O}/^{16}\text{O}$ -ratios.....	53

3. Exchange mechanisms, fluid flow and fluid evolution during hydrothermal alteration of granites from the southeastern Schwarzwald, Germany	55
3.1. Introduction	55
3.2. Geological setting and sample description	56
3.3. Analytical procedure	58
3.4. Principles of fluid-rock interaction	61
3.5. Scale of disequilibrium	62
3.5.1. Km-scale: averaged in situ data.....	63
3.5.2. Cm-sub-mm-scale: implications by in situ analysis.....	67
3.6. Mechanisms and interfaces of hydrothermal interaction.....	77
3.6.1. Biotite	77
3.6.2. Plagioclase.....	78
3.6.3. K-feldspar	78
3.6.4. Quartz.....	79
3.7. Fluid evolution and alteration history.....	80
3.8. Comparison of conventional and in situ data	85
B. Conclusions.....	88
References	91
Curriculum vitae.....	99

A. Introduction

The present dissertation entitled: "Oxygen isotope microanalysis of silicates with application to fluid-rock interfaces" has been submitted to the Natural Science Faculty of the University of Göttingen, December 9th, 1999. It is the result of approximately 3 years work (the project was initiated in February, 1997). The thesis is embedded as "Teilprojekt C2" in the "Sonderforschungsbereich (SFB) 468: Wechselwirkungen an geologischen Grenzflächen" of the "Deutsche Forschungs-Gemeinschaft (DFG)". The SFB 468 has been founded in January 1997 to investigate processes at geological interfaces including organic and inorganic compounds. The supervisor of this work has been Prof. Dr. Jochen Hoefs from the Center of Earth Sciences, University of Göttingen.

Scientific Background

The application of oxygen isotope analysis in order to investigate geochemical and cosmochemical processes is tremendous. An overview has recently been given by Hoefs (1997).

Amongst these, the determination of $^{18}\text{O}/^{16}\text{O}$ -ratios within coexisting minerals to elucidate "temperatures of formation" (e.g. Urey, 1947; Bottinga & Javoy, 1973) and to characterize fluid-rock processes (e.g. Sheppard et al., 1969; Taylor, 1974) is well known. Therefore, oxides and silicates have been analysed for many years using the technique of Clayton & Mayeda (1963): Oxygen is released by thermal fluorination, subsequently converted to CO_2 and finally detected using mass spectrometers with dual inlet. Generally, 5-20 mg of sample material are necessary to obtain reproducible results.

A general prerequisite for doing oxygen isotope thermometry is that the investigated system has fully equilibrated. Using the technique of Clayton & Mayeda (1963) it has long been recognised that oxygen isotope thermometers often record discordant temperatures in slowly cooled metamorphic rocks, that result from diffusional re-equilibration during cooling (Giletti, 1986). Hence, slowly cooled coexisting minerals often exhibit disequilibrium over the range of their size, which is -within single grains- documented by oxygen isotope gradients from cores to rims (e.g. Eiler et al., 1995). Monitoring the isotopic composition of cores of neighbouring minerals would result in more accurate determinations of peak-metamorphic temperatures.

Disequilibrium and isotopic gradients also play a significant role in the identification of mechanisms of fluid-rock interactions. Generally, fluid-rock interaction takes place by dissolution-recrystallisation, chemical reaction and diffusion (e.g. Giletti, 1985), each of which leaves characteristic oxygen isotope gradients within altered mineral grains (e.g. Elsenheimer & Valley, 1993). Additionally, oxygen isotopes can be used to identify interfaces of fluid-rock interaction and, hence, to deduce the style of fluid flow through the rock. An interaction along

grain boundaries reveals an oxygen isotope zonation pattern distinct from an exchange along a multiple set of microcracks (Elsenheimer & Valley, 1993, Valley & Graham, 1996).

It is straightforward that isotopic gradients within single mineral grains can not be monitored using the technique of Clayton & Mayeda (1963). A new door has been opened by the introduction of IR-laser fluorination for oxygen extraction, by which the necessary amount of analyte material has been reduced to 0.1 mg (Sharp, 1990). Nevertheless, due to pit rim fractionations, IR-laser are not suitable for in situ analysis of minerals (Elsenheimer & Valley, 1992). This problem has been overcome by using UV- instead of IR-light to induce fluorination of silicates and oxides. The KrF-laser (248 nm) has been the first UV-laser that has been successfully applied to in situ oxygen isotope extraction from various silicates like feldspar, biotite, olivine, garnet and pyroxene (Wiechert & Hoefs, 1995).

However, because of its high transparency in the UV-range, first efforts to ablate quartz at 248 nm failed (Wiechert & Hoefs, 1995). This is a serious problem since quartz is the second most abundant mineral on earth. Additionally, spatial resolution has been restricted to 500 μm , since μmol -amounts of analyte gas have been necessary for reproducible mass spectrometric analyses and a fractionation-free conversion of oxygen to CO_2 prior analysis. Thus, monitoring of oxygen isotope heterogeneities within single mineral grains and an investigation of fluid-rock interfaces remained difficult.

Object of the Ph.D. thesis

The main aim of the thesis has been to investigate fluid flow and exchange mechanisms between hydrothermal fluids and granites using oxygen isotopes as a tracer of fluid-rock interaction. For this purpose, granites from the southeastern Schwarzwald, Germany, have been available, which partly have intensively interacted with a fluid of meteoric origin (Simon, 1990).

Of course, a detailed investigation of oxygen isotope exchange mechanisms between granite and hydrothermal fluid requires an in-situ analysis of both quartz and its coexisting minerals. Additionally, mineral grains of these granites are often less than 1 mm in size. It is obvious that the technique of Wiechert & Hoefs (1995) does not fulfill these prerequisites.

Hence, the above aim also required the development of a new technique, which enables both in situ oxygen isotope analysis of quartz and a detection of nmol quantities of silicate extracted oxygen. The present thesis is therefore structured into three parts:

In chapter 1 experiments regarding in situ oxygen isotope analysis of quartz are described. For these experiments the instrumentation of Wiechert & Hoefs (1995) has been modified by replacing the KrF-laser by an ArF-laser ($\lambda = 193 \text{ nm}$). Further their optical system has been changed in order to obtain twofold energy densities of the focused beam. Within chapter 1 it is shown that the ArF-laser is suitable to perform in situ oxygen isotope analysis on quartz and

fused silica. For selected samples, a comparison of oxygen isotope data obtained by conventional analysis, CO₂- and ArF-laser fluorination is provided. Extracts of this chapter have recently been published in *Geochimica et Cosmochimica Acta* **63**, 687-702.

The implementation of a new technique enabling reproducible quantifications of 18/16-ratios within nmol quantities of silicate extracted oxygen is described in chapter 2. Therefore a continuous flow mass spectrometer (DeltaPlus, Finnigan Inc.) is used, which allows a detection of oxygen as masses 32, 33 and 34. The characteristics of the DeltaPlus concerning oxygen isotope measurements in a continuous flow mode have been investigated and an isotope ratio monitoring Gas Chromatography Mass Spectrometry (irm-GC-MS) system has been set up, which finally has been combined to an UV-laser based oxygen extraction system. Using this technique, spatial resolution during in situ ablation of silicates is improved to 250 µm, while a single analysis takes less than 15 minutes.

Finally, the newly developed technique, which is described in chapter 2, has been applied to in situ oxygen isotope analysis of five samples from the St. Blasien granite, Schwarzwald, Germany (chapter 3). In situ analysis has been carried out on thick sections (ca. 10 x 10 x 4 mm), which afterwards have been investigated by electron microprobe. In situ oxygen isotope data and electron microprobe data is used to discuss fluid-granite interaction on a scale ranging from 250 µm to a few kilometers. For each thick section averaged in situ data is modelled using the kinetic exchange theory of Criss et al. (1987). A comparison of UV-laser data and data obtained by conventional analysis by Simon (1990) is also included. Extracts of chapter 3 will be submitted for publication to the journal *Geochimica et Cosmochimica Acta* in due course.

1. In situ oxygen isotope analysis of quartz

1.1. Introduction

CO₂- and neodymium:yttrium-aluminium-garnet (Nd:YAG) lasers have increased tremendously the number of geochemical problems that can be investigated using oxygen isotopes. The higher temperatures of these lasers techniques now allow refractory minerals to be studied. One of the most exciting example is zircon, that could not be reacted at all, a few years ago (Valley et al. 1994; Gilliam & Valley, 1997). Reacting samples and standards in the same chamber has improved precision by almost an order of magnitude (e.g. Valley et al. 1995) and permits the investigation of very small isotopic variations in igneous and metamorphic rocks (e.g. Matthey et al. 1994, Yui et al. 1995, Eiler et al. 1996, Eiler et al., 1997). In addition, sample size has been reduced by a factor of ten, and has lead to studies of oxygen isotope variations in single quartz crystals (Conrad & Chamberlain, 1992; Elsenheimer & Valley, 1993, Kirschner et al., 1993, Young & Rumble, 1993, Onasch & Vennemann, 1995). Although CO₂- and Nd:YAG-laser techniques are very successful, in-situ measurements with CO₂- or Nd:YAG-lasers are very difficult (Sharp, 1990, 1992; Elsenheimer & Valley, 1992; Conrad & Chamberlain, 1992; Young & Rumble, 1993; Kirschner et al., 1993). This is because steep thermal gradients in the sample during in-situ analysis induce isotopic fractionation. Such thermal effects have recently been overcome by vaporizing samples with high power ultra-violet (UV) KrF-laser ($\lambda = 248\text{nm}$), thus making possible in-situ oxygen isotope analysis of silicate minerals (Wiechert & Hoefs, 1995; Rumble et al. 1997). In contrast to ablation with CO₂-and Nd:YAG-lasers that radiate in the infrared (IR) region, UV-lasers release oxygen not by heating but by electronic excitation. A long list of minerals have been analyzed with the KrF-laser: olivine, pyroxenes, garnet, spinels, chromites, amphibole, biotites, feldspar and phosphates, but efforts to study highly transparent minerals like quartz failed (Wiechert & Hoefs, 1995). This is a serious problem, because most conventional silicate analyses refer to NBS-28, and quartz is one of the most abundant minerals in the continental crust.

Within this chapter it is demonstrated that high precision in-situ oxygen isotope analysis of silica and quartz can be done using the ArF-laser ($\lambda = 193\text{ nm}$). Photon energy of the ArF-laser is sufficient for exciton creation by a two-photon process, which seems to be the initial step for breaking Si-O bonds. Isotopic ratios are not affected by low oxygen yields, and the ArF-laser can probably be used to study oxygen isotopes of all types of minerals. It is also shown that quartz measurements affected either by neighboring feldspar or other contaminations can be corrected only by using a standard which has $\delta^{18}\text{O}$ close to the sample quartz.

1.2. Instrumentation

The UV-laser microprobe has been described by Wiechert & Hoefs (1995). It consists of an optical bench enabling sample observation and laser focussing (Fig. 1.1), a vacuum extraction line with fluorine generator (Fig. 1.2) and a MAT 251 mass spectrometer. For the analysis of quartz, the KrF-laser ($\lambda = 248$ nm) has been replaced by an ArF-laser (Compex 205, Lambda Physik Inc.), that emits radiation at 193 nm. It is characterized by a maximum pulse energy of 400 mJ and a repetition rate ranging from 1 to 50 Hz. The laser provides a maximum of 15 Watts average power and a pulse duration of 16 ns. In addition to replacing KrF with ArF fillgas, two cylindrical lenses have been added to the laser beam optics (Fig. 1.1). The lenses are placed directly beside the output coupler window, changing the laser beam dimensions from a 28 x 14 mm cross-section to a square of 14 x 14 mm. The laser beam then passes through two apertures, which reduce the amount of divergent light. After passing through these apertures, the beam is reflected into the viewing optic via a dielectric mirror, and is finally focused onto the sample surface. The viewing optic is identical to the configuration described by Wiechert & Hoefs (1995).

The sample chamber of Wiechert & Hoefs (1995) has been replaced by one that is 20 cm³, i.e. 6 times smaller by volume (Fig. 1.1). It is made of stainless steel and has a cylindrical shape. The chamber is open only at the top and sealed by a KalRez O-ring and Suprasil 1 window. The smaller chamber uses less fluorine gas without reducing gas pressure. A Suprasil 1 window is used for two reasons: 1) The strength of Suprasil gives a thinner, less absorbing and more durable window than fragile fluorides such as MgF₂; 2) Fluoride reaction products adhering to the inside of the window and obscuring the operator's view of samples are easily removed by the ArF laser beam from Suprasil but are difficult to remove from MgF₂ windows. The window is undamaged by the laser beam, as long as it is not placed close to the focus (see Fig. 1.1). Another modification of the technique described in Wiechert & Hoefs (1995) for this study is the use of commercially available NaCl, pretreated with BaCl₂ to remove sulfate, as a fluorine getter. The use of chemically cleaned NaCl instead of KCl, in combination with smaller amounts of fluorine, leads to a lower oxygen blank. As a consequence, different $\delta^{18}\text{O}$ values for pure oxygen and oxygen/fluorine mixtures (see Fig. 3 in Wiechert & Hoefs, 1995) are not seen. The previously used KCl contained contaminants, probably SO₄²⁻, which were released during the reaction with surplus fluorine.

1.3. Samples and procedures

A variety of samples were used for the different experiments of this study, both as single grains (< 1 mm size) and thick sections (2 - 5 mm thickness). The ablation behavior of quartz

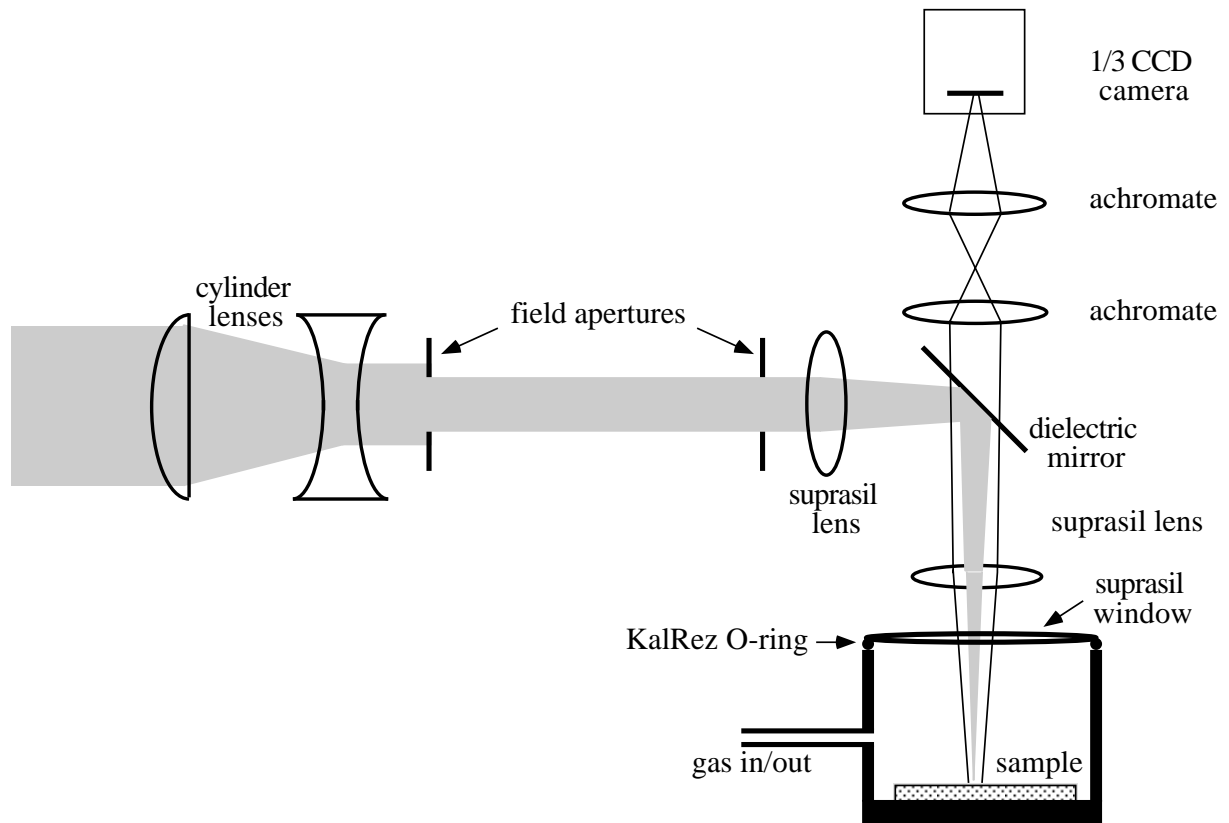


Fig. 1.1. Optical system and sample chamber of the UV-microprobe. After the output coupler the original beam profile of 14 x 28 mm is reduced to a square of 14 x 14 mm using two antireflection-coated cylindrical lenses set up in telescope mode. Energy loss is minimized thereby when passing through the first aperture, which transmits only the flat top of the square beam profile. Before being slightly prefocused by a first Suprasil lens, a second aperture reduces divergent light. A dielectric mirror, that transmits visible light, reflects the prefocused beam towards a second Suprasil lens, by which it is finally focused onto the sample surface. Suprasil 1 is used as window material since it is highly transparent for non-focused UV-light. The window is sealed by a KalRez O-ring to the sample chamber, which is made of stainless steel. Sample observation is performed by a 1/3" CCD camera and two achromats enabling a magnification from 10-100 (see also Wiechert & Hoefs, 1995).

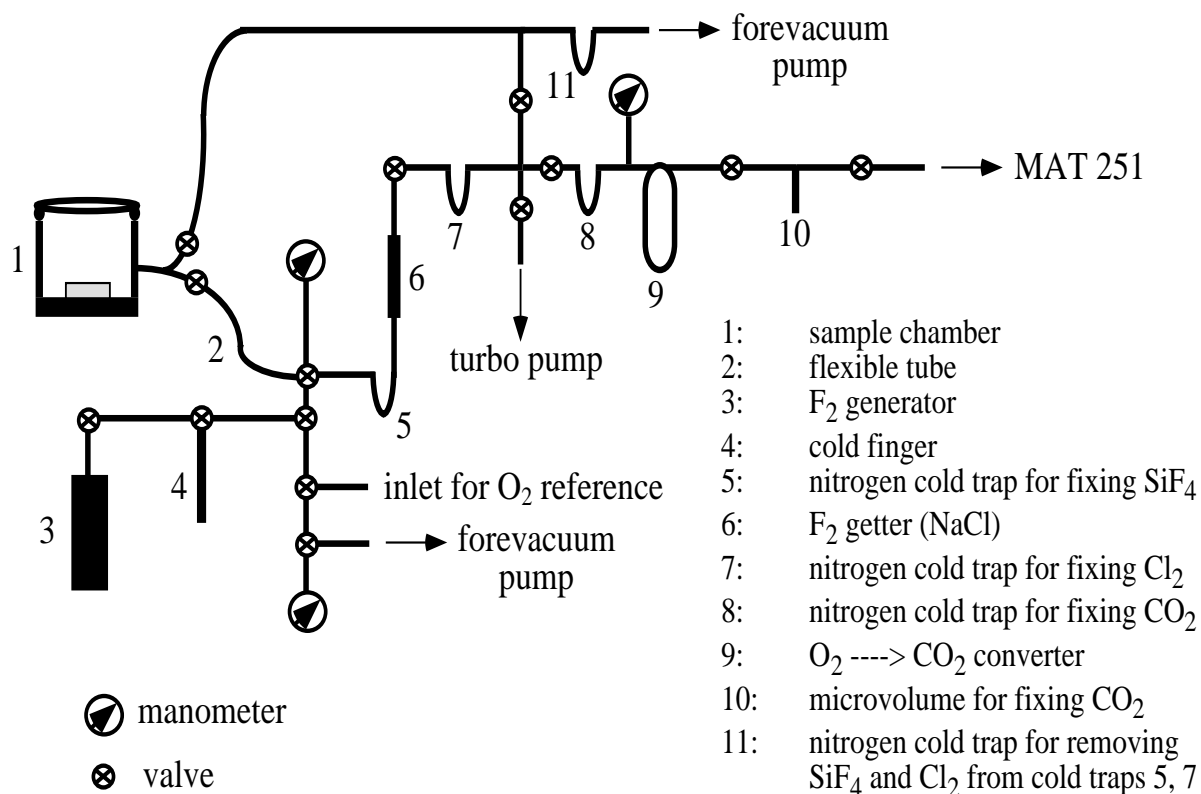


Fig. 1.2. Vacuum extraction line and fluorine generator of the UV-microprobe. Pure F₂ is generated by heating K₃NiF₇ in a nickel vessel (3) (Asprey, 1976). After expanding to 10 bars pressure, amounts of F₂ necessary for daily analyses are condensed in a cold finger (4) at liquid nitrogen temperature. Before laser ablation is started the sample chamber (1) is filled with 50 mbar F₂. Oxygen is released from the sample by laser ablation and plasma fluorination. When enough oxygen is released the valve of the sample chamber is opened and oxygen passes a NaCl-trap (6), where surplus F₂ is reacted at 150 °C to Cl₂ and NaF. Cl₂ is frozen out in nitrogen cold trap (7), while other condensable gases like SiF₄ freeze out in liquid nitrogen cold trap (5). Oxygen streams into a glass vial (9) and is converted to CO₂ on red hot diamonds, which are fixed in a small platinum crucible. Generated CO₂ is frozen out in nitrogen trap (8) and yields can easily be determined using a Pirani gauge. To guarantee a viscous flow into the mass spectrometer generated CO₂ is frozen out a second time in a microvolume (10). The minimum amount of CO₂ for a reliable analysis must be more than 1 μmol. For detailed information see Wiechert & Hoefs (1995).

has been studied by analyzing hydrothermally grown quartz from **Brasil**, because it was found to be free of large inclusions. **Dörentrup** quartz, which is the in-house standard for conventional silicate analysis in Göttingen, has been used to test whether isotope fractionation occurs during the ablation process. For laser analysis the standard was converted to a glassy mass by melting in a vacuum oven. In this way rods of nearly cylindrical shape are produced. Analyses were made on thick sections and on single fragments of these after crushing. Other samples include quartz from the **Schluchsee** granite, Black Forest, Germany and from **Weinsberg**, Bohemian Massif, Austria, which were analyzed both as single grains and in thick section in order to study the effect of feldspar on quartz measurements. Oxygen isotope analysis was also performed on **Suprasil 2**, a commercially available silica glass with less than 1000 ppm OH, highly transparent to ultra-violet light. Glasses of the Suprasil family are commercially generated by hydrolysis of SiCl₄ at high temperatures. Suprasil 1 (used as window material) and Suprasil 2 have identical compositions, but different optical characteristics: Suprasil 1 is optically isotropic, whereas Suprasil 2 is anisotropic. The concentrations of impurities in glasses of the Suprasil family are given in Table 1.1. Finally, the ability of the ArF-laser to study heterogeneity in single quartz crystals is demonstrated by analyzing hydrothermally grown quartz from **Usingen**, Rhenish Massif, Germany.

impurities	concentration (ppm)
Al	0.05
Ca	0.05
Cr	0.005
Cu	0.01
Fe	0.02
K	0.01
Li	0.01
Mg	0.005
Na	0.05
Ti	0.05
OH	<1000

Table 1.1. Concentrations of impurities for glasses of the Suprasil family.

For UV-laser analysis single grains and thick sections were purified ultrasonically in distilled water and dried at 300 °C under vacuum for more than 10 hours. Mineral and rock thick sections were placed on the bottom of the sample chamber, without the use of a sample holder. In contrast, single grains were loaded into 2-mm deep holes that were drilled into a nickel disk. This sample holder is necessary to hold small mineral fragments that might otherwise jump out of the laser focus. After loading the chamber is evacuated and heated over night. Typically the vacuum is better than 10⁻⁵ mbar after six hours. Before lasing, the sample chamber is filled with

50 mbar F₂ in order to remove remnants of adsorbed water. Once the blank is reduced to less than 50 nmol by repeated fluorination, analysis proceeds as described by Wiechert & Hoefs (1995).

The CO₂ laser technique at the Geophysical Laboratory is essentially the same as described by Sharp (1990). A 25-watt, Synrad Series 48 CO₂-laser is used for sample evaporation. In contrast to Sharp (1990), oxygen is not converted to CO₂ after reaction of samples with BrF₅, but frozen on a 5Å mol sieve. Its isotopic composition is determined on masses 32, 33, and 34 using a Finnigan MAT-252 mass spectrometer.

Samples for CO₂ laser analysis were first crushed with a BN pestle and mortar. A typical analysis requires the evaporation of 1 - 3 large quartz fragments (1.5 to 2.2 mg) in order to avoid grain size effects (Fouillac & Girard, 1996). Analysis of NBS-28 was performed by rapid heating with a defocused laser beam (RHD-technique) similar to that described in Spiccuza et al. (1998). The RHD-technique immediately melts small quartz grains together. Only a few grains are lost which are probably not even touched by the laser light, but are pushed away by the shock wave that is initiated by the heating process. After a few seconds the laser power is reduced to avoid expulsion of partly reacted melt droplets. In this study, only NBS-28 analyses, for which more than 95 % oxygen has been recovered, are considered. Ejection of melt droplets was observed to be minor while evaporating larger fragments of Suprasil 2 and Dörentrup, whereas violent reaction and loss of material was observed for Weinsberg quartz. The latter is probably caused by large fluid inclusions. All CO₂-laser data are corrected for daily variations with an olivine standard ($\delta^{18}\text{O} = 5.20 \text{ ‰}$). Corrected analyses of NBS-28 have a value of $9.57 \pm 0.09 \text{ ‰}$ (n = 4), and UWG-2, a garnet standard ($\delta^{18}\text{O}_{\text{corr.}} = 5.8 \text{ ‰}$ by Valley et al., 1995), has a value of $5.85 \pm 0.03 \text{ ‰}$ (n = 2).

Conventional analyses in Göttingen and Tübingen were performed in nickel vessels using ClF₃ (Göttingen) and BrF₅ (Tübingen) as reagents (Borthwick & Harmon, 1982; Clayton & Mayeda (1963).

1.4. Basic principles of laser fluorination

Most laser-based oxygen isotope analyses of quartz have been performed with a CO₂-laser (Sharp, 1990; 1992; Conrad & Chamberlain, 1992; Young & Rumble, 1993; Elsenheimer & Valley, 1993; Kirschner et al., 1993; Onasch & Vennemann, 1995; Fouillac & Girard, 1996; Kirschner & Sharp, 1997; Spiccuza et al., 1998). Infrared radiation from a CO₂-laser ($\lambda = 10600 \text{ nm}$) acts to increase the vibrational energy of quartz - in other words the laser heats the sample. Oxygen is subsequently released by a thermally controlled reaction between vibrationally excited silica and fluorine. Incomplete sample evaporation in combination with a coexisting temperature gradient leads to significantly lowered $\delta^{18}\text{O}$ values (Fouillac & Girard,

1996). Probably this is caused by a preferential release of ^{16}O from cooler sample parts, since ^{16}O is bonded slightly weaker to Si than ^{18}O . As a consequence, accuracy of single quartz grain analysis depends on factors like grain size (Fouillac & Girard, 1996) as well as laser power (Spicuzza et al., 1998). Recent improvements in the accuracy of fine-grained quartz analysis have been made by techniques that increase oxygen yields close to 100 % by reducing the loss of ejecta during laser heating: Kirschner & Sharp (1997) used LiF as a binder, while Spicuzza et al. (1998) operated with a defocused beam (see also chapter 1.3). But, generally, during in-situ analysis only a minor percentage of the sample can be vaporized. This means that high precision in-situ analysis of quartz is very difficult with CO_2 -laser (Sharp, 1990, 1992; Conrad & Chamberlain, 1992; Young & Rumble, 1993; Kirschner et al., 1993). Consequently, some workers prefer to cut thick sections into small chips prior to CO_2 -laser analysis, producing 0.2 - 1.5 mg size samples, which can be vaporized almost completely (Elsenheimer & Valley, 1993; Onasch & Vennemann, 1995).

Nd:YAG-lasers operating at 1064 nm have also been used for oxygen isotope analyses. Due to the high transparency of quartz at this wavelength, however, it is necessary to mix an absorber into the sample. Akagi et al. (1995) used submicron nickel powder as an absorber, whereas Matthey et al. (1994) mixed NBS-28 with olivine of a known oxygen isotope composition. The principle of the absorber is straightforward: laser light is converted into heat by the absorber with the result that neighboring quartz is heated by conduction, and then reacts with ClF_3 . The $\delta^{18}\text{O}$ values reported by Akagi et al. (1995) for NBS-28 are much lower than the reference value, whereas more accurate $\delta^{18}\text{O}$ values are reported by Matthey et al. (1994). The reproducibility of this technique ($\pm 0.2\text{‰}$, 1 S.D.) seems to be only slightly lower than what is achieved by direct heating with a CO_2 -laser ($< 0.1\text{‰}$, Spicuzza et al., 1998). It is clear that the absorber technique is not suitable for in-situ measurements of quartz.

In the ultra-violet range KrF-lasers ($\lambda = 248\text{ nm}$) are used for oxygen isotope analysis (e.g. Wiechert & Hoefs, 1995; Wiechert et al., 1997 a, b; Rumble et al., 1997). KrF-lasers are not used to heat the sample but to break bonds by electronic excitation. Ablation of insulators with nanosecond pulsed ultra-violet lasers is initiated by promoting an electron of the valence band into the conduction band by absorption of one or more photons (Fig. 1.3). In this way not only a free negatively charged electron is formed, but also a positive charge (hole) in the crystal lattice is left behind (Pompe et al., 1992; Haglund & Itoh, 1994). The hole may increase its potential energy by absorption of an additional photon and, accordingly, the free electron may increase its kinetic energy. Within a short period of 10^{-12} seconds electrons and holes reunite and form localized excited states, so-called excitons, which are able to relax to defects. Excitons and defects are both precursors for the absorption of additional photons, by which their potential energy is further increased. Generally, bond breaking and subsequent particle emission can occur in different ways. For example, the potential energy of the hole, exciton or

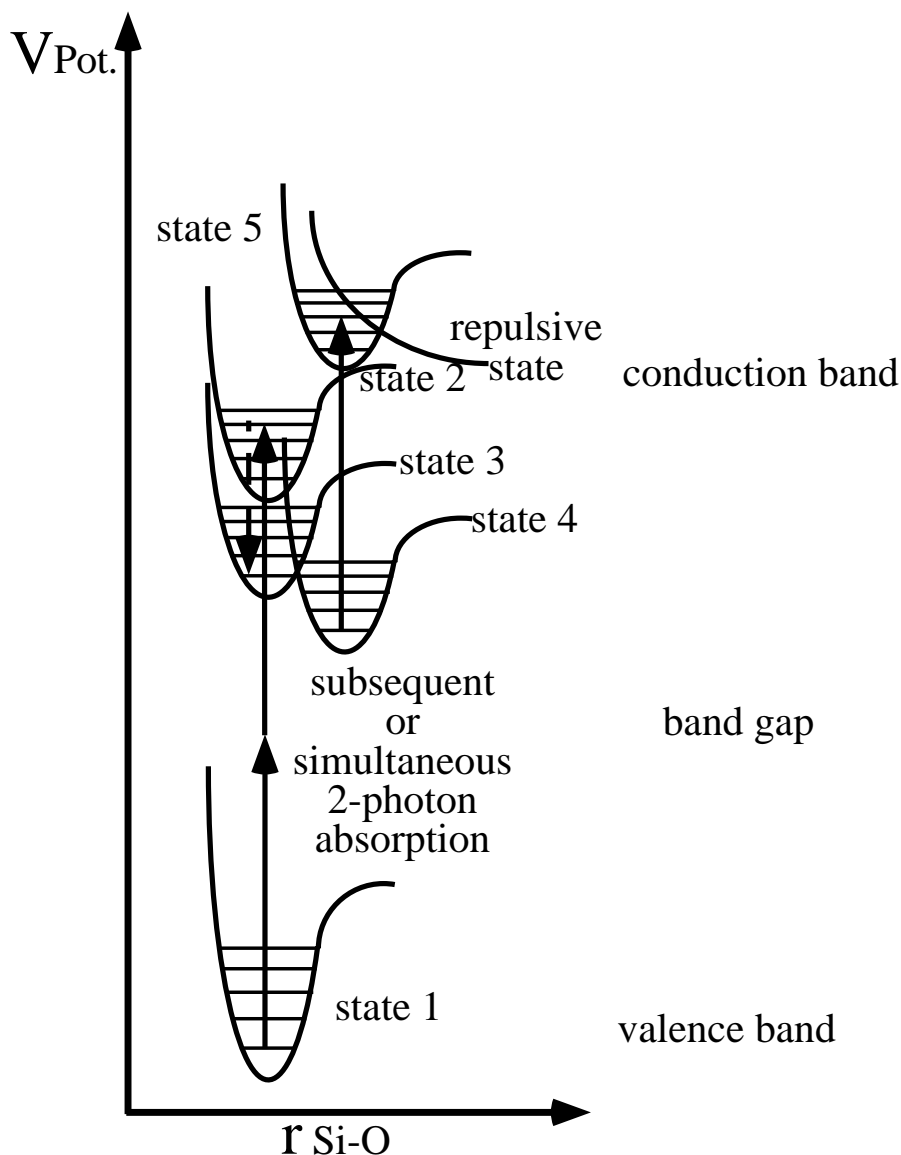


Fig. 1.3. Schematic illustration of one possible Si-O bond-breaking mechanism using ArF-laser light with a single photon energy of 6.4 eV. The potential energy ($V_{Pot.}$) of a SiO-cluster directly depends on the distance r of both atoms from each other (anharmonic oscillator). Anharmonic oscillators and possible vibrational modes are shown for different electronic states. For each state bonding is strongest when $V_{Pot.}$ reaches a minimum. UV-light induces an electronic excitation of the irradiated sample. Insulators are electronically excited by promoting an electron from the valence band into the conduction band. Since the band gap for silica is about 9 eV, a subsequent or simultaneous absorption of two photons is required for band gap crossing. An electron hole pair is created (state 2), which recombines to an exciton (state 3). Excitons relax to defects (state 4) by internal conversion. Excitons and defects might be able to absorb one additional photon by which potential energy is further increased, e.g. to state 5. If any of these states is crossed by a repulsive state, bonding dissociation and oxygen release occurs, as shown for state 5.

defect can be transferred to a repulsive electronic state via internal conversion (Haglund & Itoh, 1994), as it is schematically shown in Fig. 1.3. The flux of particles ablated from the sample is directed away from the irradiated surface. Some of the particles absorb photons from the laser beam, which causes the formation of a plasma plume. Due to the high temperature of the plasma, ablated particles are fluorinated within the plume. Once the light is off and the plasma is cooling, excess fluorine may prevent recombination of oxygen with other atoms.

1.5. Ablation of quartz using ultra-violet laser pulses

1.5.1. ArF-laser ablation

The ablation behavior of quartz in a fluorine atmosphere was studied using a highly pure druse quartz from Brasil in order to limit possible effects of impurities. The relationship between ablation rate, oxygen yield and energy density is shown in Fig. 1.4:

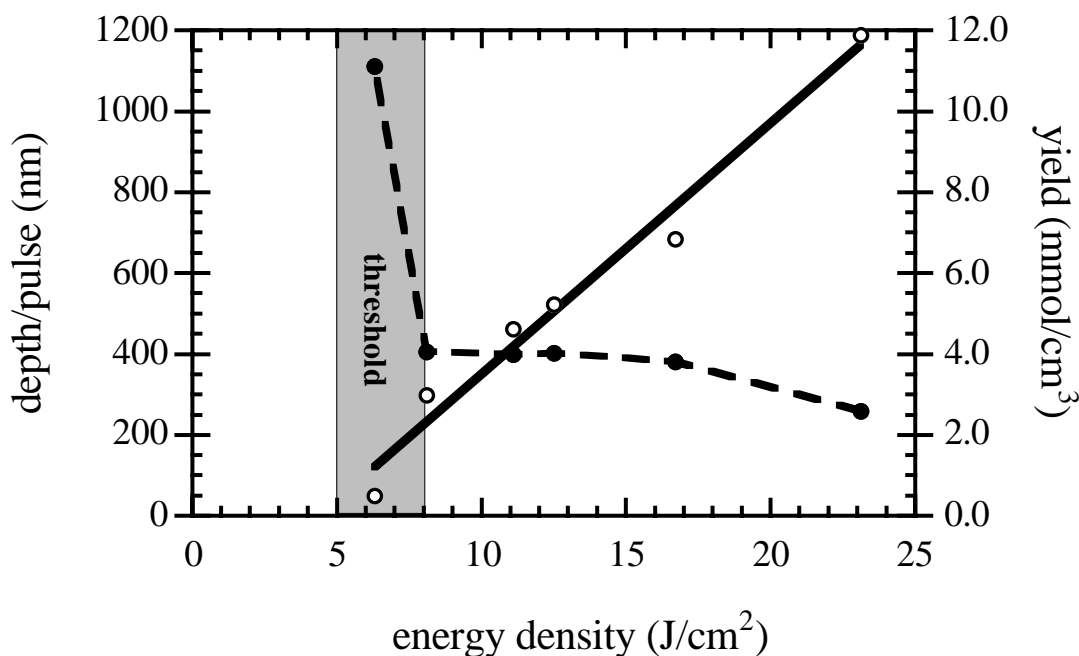


Fig. 1.4. Relationship between ablation depth/pulse, yield and energy density for Brasilia quartz at 193 nm. Ablation depth per pulse (filled circles, dashed line) has been determined by dividing ablation depth of the laser holes by the number of laser pulses. Yield in mmol/cm^3 (open circles, solid line) has been calculated by dividing the total amount of released oxygen by the volume of the holes. In this way the amount of released oxygen depends not on the focus diameter. For discussion see text.

Ablation starts above $5 \text{ J}/\text{cm}^2$ with rates as high as $1.1 \mu\text{m}$ per pulse, but almost no molecular oxygen is observed. The ablation rate drops dramatically between 5 and $8 \text{ J}/\text{cm}^2$, whereas it only

slightly decreases above 8 J/cm^2 . Additionally, a linear correlation between energy density and oxygen yield is observed above 5 J/cm^2 . These observations can be described by two different, competitive ablation mechanisms:

ArF-laser light has a photon energy of 6.4 eV. Since the energy gap between the valence and the conduction band is about 9 eV for silica, an absorption of two photons is required for exciton creation by bandgap crossing. Tsai et al. (1988), Devine (1989) and Rothschild et al. (1989) found strong evidence for a simultaneous two photon absorption for exciton creation in Suprasil using excimer lasers. Single photon transitions can only occur at preexisting defects or inclusion sites, such as the alkalis, which are present in all types of natural quartz. At low energy densities single photon absorptions will dominate over two photon absorptions. Thus, below 8 J/cm^2 , beam energy is exclusively stored at preexisting defects or inclusions, which finally leads to a bursting of the material by bulk evaporation, as described by Pompe et al. (1992) and Ihlemann et al. (1992). As small SiO_2 fragments are ejected and the amount of released oxygen is negligible this process is called explosive ablation. The higher the photon density the higher the probability of a two photon process, which is the precursor step for a break up of Si-O bonds. Above a threshold of 8 J/cm^2 , energy density is sufficient to generate excitons: Now, next to the bulk evaporation a surface evaporation occurs, which is indicated by the steep decrease in ablation depth. Due to surface evaporation much more oxygen is liberated from the sample and a linear correlation between oxygen yield and energy density is observed. The higher the energy density the higher the extent of oxygen release by surface vaporization. Simultaneously, ablation depth decreases slightly implying that explosive ablation is further minimized. Fig. 1.5 shows a SEM picture of an ablation pit in Brasil quartz. The average energy density during this shot was 15 J/cm^2 . Relics of a competitive explosive ablation can be seen from the blocky structure of the crater. It is also obvious that the surroundings of the pit are unaltered. Thus a melting of the surroundings during ablation can be excluded (see also chapter 1.6.1a).

1.5.2. KrF-laser ablation

Experiments on silica using 248 nm light have been carried out by Wiechert & Hoefs (1995) using a LEXTRA 200 excimer laser (Lambda Physik Inc.). Despite the fact that pulse power of this laser ($1.1 \times 10^7 \text{ W/cm}^2$) is significantly higher than that of the ArF-laser ($6.4 \times 10^6 \text{ W/cm}^2$), the KrF-laser with a single photon energy of 5.0 eV liberates only sub μmol amounts of oxygen, even at fluences as high as 20 J/cm^2 (Wiechert & Hoefs, 1995). Using the new optical system described in Fig. 1.1 energy densities of about 40 J/cm^2 can be obtained with the KrF-laser. At such high energy densities, oxygen yields are sufficient to enable a mass spectrometric analysis (see chapter 3). However, explosive ablation remains dominant and spatial resolution is still not as good as when using the ArF-laser and energy densities of 20 J/cm^2 .

There are several reasons that could account for low oxygen yields at 248 nm: E.g. excitons and/or defects created by 248 nm radiation might relax faster than those generated by 193 nm light, so that in the case of 248 nm excitation fewer excitons and/or defects are able to absorb an additional photon during their lifetimes.

To sum up, μmol amounts of oxygen can be released from quartz by ArF-laser induced fluorination. Oxygen yields increase with increasing energy density of the focused beam. At high energy densities oxygen can also be extracted from silicates using a KrF-laser. It is expected that explosive ablation at 193 nm and 248 nm can be further minimised if a beam homogenizer is placed between output coupler window and focussing lens. It has often been observed that explosive ablation starts at the rim of the ablating beam. Here, energy density is lower than in the centre. A beam homogenizer would provide a homogeneous energy distribution over the irradiated area.

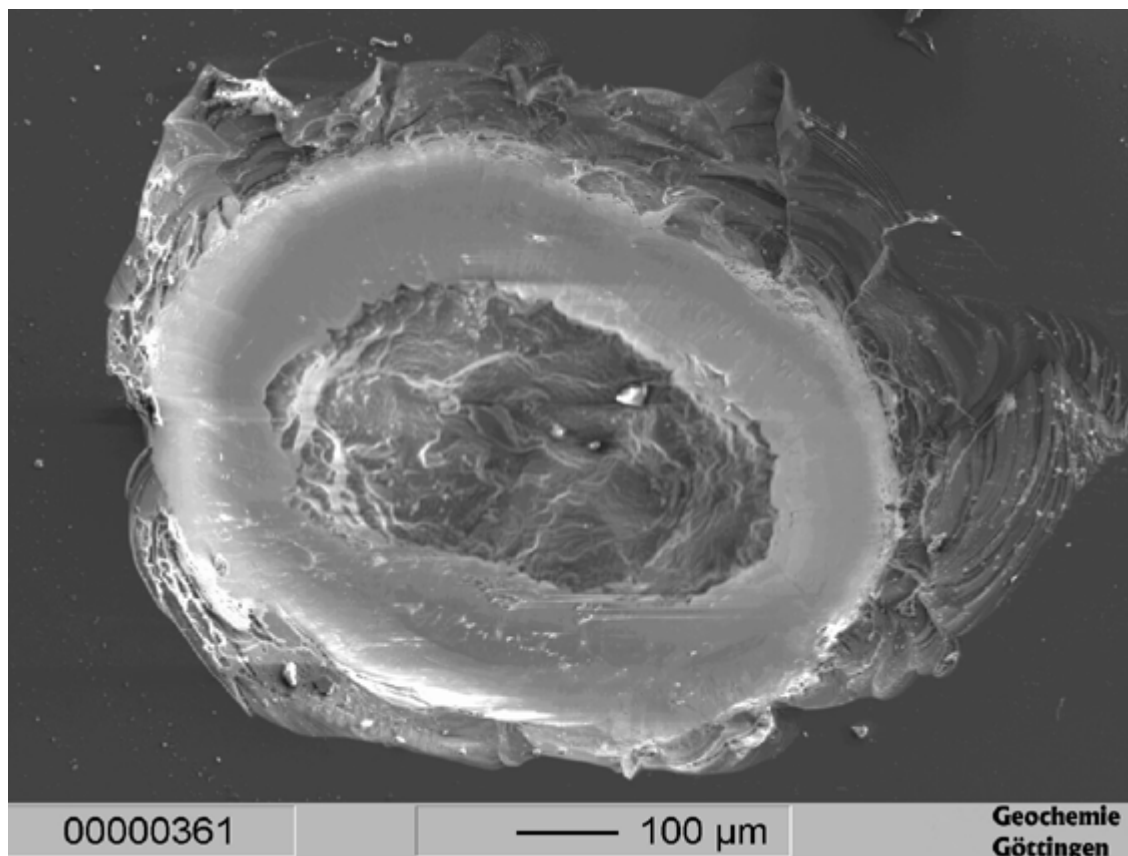


Fig. 1.5. SEM picture of an ablation pit in Brasilia quartz. Surrounding pit areas are unaltered, which excludes a melting process and indicates a release of oxygen by pure electronic excitation of the irradiated sample. Relics of an expulsion of SiO_2 fragments due to an explosive ablation can be seen by the blocky structure of pit margins. The pit is of conical shape as the beam focus had been fixed and ablation only takes place at points of highest energy density. The center of the crater is blocky since energy density decreases with increasing depth (increasing

defocusing of the laser beam with increasing depth). Averaged focus beam energy density has been 15 J/cm^2 .

1.6. Oxygen isotope data of different quartz samples

A multi-step technique for oxygen isotope analysis only results in accurate and precise measurements if no oxygen isotope fractionation occurs during the whole procedure. Our fluorination line consists of a reaction chamber in which ablation occurs, a gas extraction line, an O_2 to CO_2 converter, and a gas source mass spectrometer (see also Fig. 1.2). Given that the mass spectrometer operates without fractionation, the easiest way to avoid any fractionation is trying to keep oxygen yields as high as 100 % for each step. For the fluorination line in Göttingen, the extraction of oxygen from the sample gas and the conversion to CO_2 is quantitative, when analyzing μmol amounts of oxygen (Wiechert & Hoefs, 1995). But during the ablation of quartz at 193 nm, only a small proportion of oxygen is released from the ablated volume. For Brasil quartz, oxygen yields of only 30 % have been calculated, even at fluences as high as 23 J/cm^2 . Thus it is necessary to prove whether isotopic fractionation occurs during the ablation step.

1.6.1. Comparison of ArF-laser, CO_2 -laser and conventional data

Dörentrup quartz, a granite quartz from the Bohemian Massif (Weinsberg, Austria) and Suprasil have been analysed by ArF-laser fluorination, CO_2 -laser fluorination and conventional 'thermal' fluorination to test the reliability of ArF-in-situ measurements. CO_2 -laser analysis was carried out at the Geophysical Laboratory in Washington, while conventional analysis was performed in Tübingen and Göttingen.

a) Dörentrup

Dörentrup quartz powder is the working standard for conventional analysis in Göttingen. For ArF- and CO_2 -laser analysis it was melted at $1700 \text{ }^\circ\text{C}$ to form glassy rods, as well as for conventional analysis in Tübingen. These rods were cut to form thick sections, which were analyzed by ArF-laser fluorination in Göttingen. For CO_2 -laser analysis in Washington and conventional analysis in Tübingen, Dörentrup rods were crushed. Conventional analysis in Göttingen was performed on the original quartz powder.

Fig. 1.6 shows the average and 1 standard deviation for the ArF-long term run of Dörentrup from June 1997 to January 1998. Daily analyses are also listed in Appendix I. No corrections have been made to these data. The average value of 33 analyses is 11.99 ‰ with a single

standard deviation of 0.20 ‰. A change of markers indicates a new loading of the sample chamber. The first standard analysis of a day sometimes deviates from the daily mean by more than three standard deviations and have been discarded. The trend in $\delta^{18}\text{O}$ does not seem to be systematic within each loading of the sample chamber, but over all fillings, and might reflect a variety of factors including e.g. buildup of contaminants in the sample chamber, or outgassing of the diamonds and of the fluorine getter.

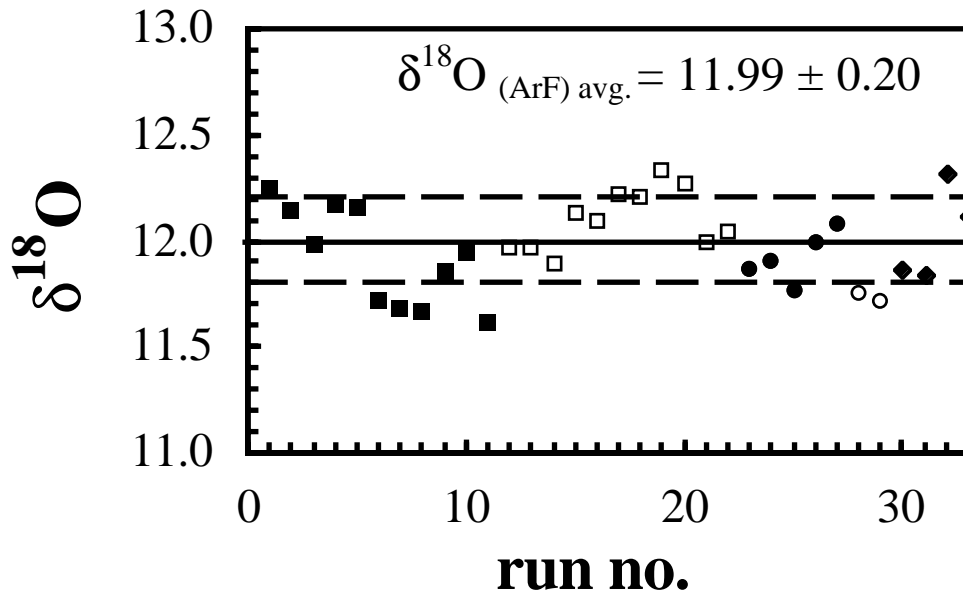


Fig. 1.6. Thick section ArF-laser data for Dörentrup-quartz from June 1997 to January 1998. The long term average (11.99 ‰) is in excellent agreement with the mean of six conventional analyses (12.1 ‰) accomplished in triplicate in Göttingen and Tübingen. The first two analyses after loading a fresh sample chamber are not included due to possible contamination by adsorbed water or atmospheric oxygen. Oxygen yields varied between 2 and 5 μmol , and energy densities between 8 and 25 J/cm^2 . Changes in signature indicate new loading of the sample chamber.

Averaged Dörentrup data obtained by each technique are listed in Table 1.2: the ArF-mean value (11.99 ± 0.20 ‰) is within simple standard deviation of conventional (12.1 ± 0.1 ‰) and CO_2 -laser analysis (12.10 ± 0.14 ‰). Slightly lower ArF-laser averages are probably not random but due to small (≤ 0.2 ‰) fractionation of oxygen in the extraction line (Wiechert & Hoefs, 1995). The very good agreement between ArF-laser, CO_2 -laser and conventional data for Dörentrup is clear evidence that there is no significant fractionation during ArF-laser ablation. Heating of the rim zone of ablation pits therefore is inferred to be negligible. As a consequence, raw data need not be corrected, if contamination can be excluded (see also chapters 1.6.3 and 1.7). In contrast to IR-laser-based techniques high yields are not required

Sample	ArF - laser (thick section)		CO₂ - laser		external heated Ni-vessels	
	n	$\delta^{18}\text{O}_{\text{raw}}$ (‰)	n	$\delta^{18}\text{O}_{\text{corr.}}$ (‰)	n	$\delta^{18}\text{O}_{\text{corr.}}$ (‰)
Dörentrup	33	11.99 ± 0.20	6	12.10 ± 0.14	3	12.1 ± 0.1
					3*	12.1 ± 0.1
Suprasil	10	23.50 ± 0.25	3	24.21 ± 0.15	-	—
Weinsberg	3	11.09 ± 0.18	4	10.79 ± 0.13	7	11.3 ± 0.3
NBS-28	-	—	5	9.57 ± 0.09	3	9.72 ± 0.09

* conventional analyses as quartz powder in Göttingen

Table 1.2. Comparison of ArF-laser data with CO₂-laser and conventional analyses. CO₂-laser fluorination was carried out at the Geophysical Laboratory, Washington DC, conventional analyses of Dörentrup quartz in Göttingen and Tübingen and conventional analyses of granite quartz from the Weinsberg in Göttingen, only. Analyses of NBS-28 in Washington show that calibration of both techniques is accurate assuming that the $\delta^{18}\text{O}$ -value of NBS-28 is +9.6 ‰ relative to V-SMOW.

with the UV-laser. Even if oxygen yields are low, the method results in accurate and reproducible $\delta^{18}\text{O}$ values. Oxygen yields do not measure the quality of UV-laser analyses. This is a great advantage of using UV-lasers since it permits real in-situ analyses. Thick sections analyzed for oxygen isotopes with an UV laser are still available for an investigation by additional techniques, like e.g. LA-ICP-MS.

b) Granite quartz

Averaged thick section raw data of Weinsberg quartz is listed in Table 1.2, while single analyses are listed in Appendix II. The mean value ($11.09 \pm 0.18 \text{ ‰}$) is within the range of suspected heterogeneity given by seven conventional analyses ($11.3 \pm 0.3 \text{ ‰}$). In contrast, the mean $\delta^{18}\text{O}$ for Weinsberg quartz obtained by CO_2 -laser analysis ($10.79 \pm 0.13 \text{ ‰}$) is significantly lower than the conventional and ArF-laser mean values. This lowering may be explained by an ejection of melt droplets, which has been observed during CO_2 -laser heating of Weinsberg quartz. Once ejected, melt droplets are no longer heated by the laser beam and thus, during cooling, ^{16}O enriched oxygen may be preferentially released (see also chapter 1.4). The violent sputtering of Weinsberg quartz under the CO_2 -laser beam is probably caused by decrepitation of large fluid inclusions which are abundant in the sample.

c) Suprasil

Suprasil glass is free of large inclusions and can be vaporized completely using CO_2 -laser fluorination. For this reason the CO_2 -laser average ($24.21 \pm 0.15 \text{ ‰}$, Table 1.2) is believed to be accurate. Analysis of Suprasil with an ArF laser, however, reveals analytical problems caused by its transparency to 193 nm light. The raw average of 10 ArF-laser analyses ($23.50 \pm 0.25 \text{ ‰}$, for single data see Appendix II) is 0.7 ‰ below the mean value of CO_2 -laser analysis and $\delta^{18}\text{O}$ decreases with decreasing oxygen yields (Fig. 1.7e). Suprasil is characterized by absence of impurities, lack of defects and inclusions and thus by lack of sites for photon absorption. In fact it is observed that many photons go through the thick section of Suprasil and hit the bottom of the ablation chamber. When the Suprasil section is removed, ablation textures of the transmitted laser beam are visible on the metal floor of the sample chamber beneath where the section lay during laser fluorination. Secondary holes are found on the bottom of Suprasil thick sections directly beneath primary ablation craters on top of the sections. The secondary holes have a 1 mm wide rim of altered material, the inner part of which is colored brown. It is proposed that the holes with brown alteration rims result from a second plasma plume caused by ablation of the stainless steel reaction chamber by laser light transmitted through the thick section of Suprasil. The second plasma plume is located between the inside surface of the

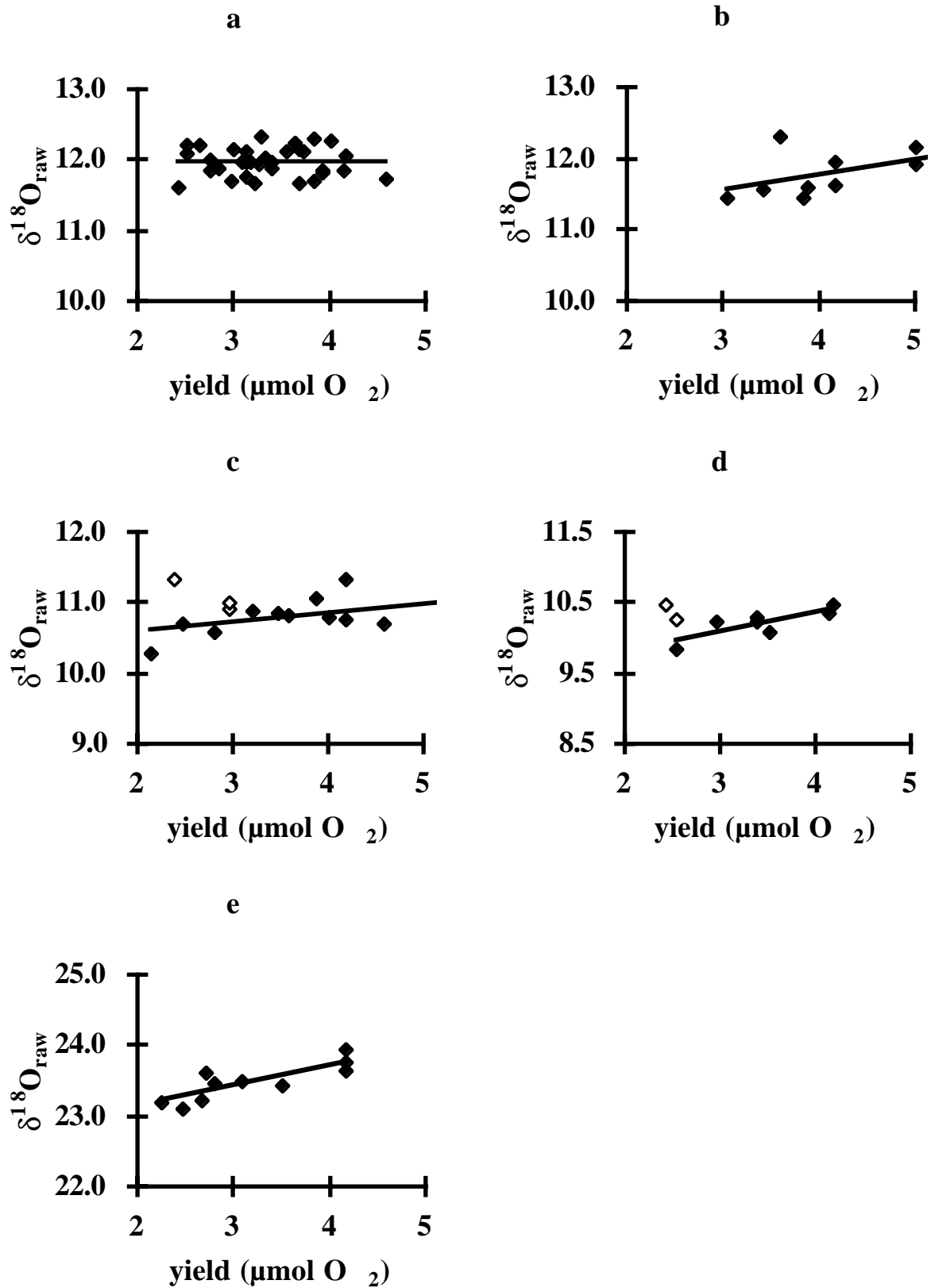


Fig. 1.7. Dependence of $\delta^{18}\text{O}$ on the total amount of released oxygen, both for single grain and thick section measurements:

(a) and (b): thick section (a) and single grain measurement (b) of Dörentrup-quartz;

(c) and (d): single grain (filled diamonds) and thick section (open diamonds) measurement of granite quartzes from the Weinsberg (c), Bohemian Massif, Austria, and Schluchsee (d), Black Forest, Germany;

(e) in-situ measurement of Suprasil 2. For discussion see text.

reaction chamber and the lower side of the Suprasil thick section inducing a thermal reaction between stainless steel, silica and fluorine. Such a process may become proportionately more pronounced if less oxygen due to electronic excitation is released and may explain the yield dependent fractionations shown in Fig. 1.7e. As known from CO₂-laser fluorination, lowered $\delta^{18}\text{O}$ -values are characteristic of a thermally induced release of oxygen.

In contrast, yield dependent fractionations are not observed for thick section analysis of Dörentrup quartz glass (Fig. 1.7a): This is because the transparency of glassy Dörentrup is not as high as for Suprasil glass. In addition, the rods obtained from melted Dörentrup quartz powder are generally 4 mm thick and thus of double thickness compared to the analyzed Suprasil sections. Moreover, thick section analysis of Dörentrup glass and granite quartz from the Weinsberg indicate that no significant oxygen isotope fractionation occurs during ArF-laser ablation of less transparent silica. The generally lower transparency of most natural quartzes should be sufficient for accurate and reproducible thick section analysis (see also chapter 1.7). For in-situ analysis of highly transparent silica an improvement in accuracy should be expected by analyzing thicker sections.

1.6.2. Single grain versus thick section analysis

Laser-based in-situ oxygen isotope analysis can be performed on thick sections as well as on single grains or crystal fragments. For single grain analysis, fragments need to be fixed in a sample holder, otherwise the repulsion of the laser plasma hurls even large fragments out of the focus (Wiechert & Hoefs, 1995). This technique is favored above thick section analysis if a large number of samples have to be analyzed. Additionally it is preferred if there is any material within the thick section that reacts with fluorine at room temperature contributing oxygen to that derived from the ablated sample. Such a fluorine reactive mineral is feldspar which has been found to affect oxygen isotope measurements of neighboring quartz during IR-laser fluorination (Elsenheimer & Valley, 1993). In this case much better accuracy should be obtained by analyzing single quartz grains instead.

Two granite quartzes (Weinsberg, Bohemian Massif, Germany, and Schluchsee, Black Forest, Germany) have been measured both as single grains (see Appendix III) and as thick sections (see Appendix II) to investigate the effect of feldspar on accuracy of quartz measurements during UV-laser fluorination. Additionally, for a general comparison of both

techniques, Dörentrup glass has been analyzed the same way. Averaged raw data are also listed in Table 1.3.

a) Granite quartzes

Thick section raw averages of Weinsberg ($11.09 \pm 0.18 \text{ ‰}$) and Schluchsee quartz ($10.39 \pm 0.11 \text{ ‰}$) are within one standard deviation of single grain raw averages ($10.83 \pm 0.26 \text{ ‰}$ and $10.26 \pm 0.20 \text{ ‰}$, respectively). In addition, as mentioned earlier, the raw mean value ($11.09 \pm 0.18 \text{ ‰}$) for Weinsberg quartz is in good agreement with conventional data ($11.3 \pm 0.3 \text{ ‰}$; Table 1.2). Thus it appears that feldspar does not have any effect on oxygen isotope measurements of quartz (see also discussion in chapter 1.6.3).

Instead, the slight lowering of single grain data is once again most likely caused by a yield dependent fractionation, as indicated in Fig. 1.7c for Weinsberg quartz and in Fig. 1.7d for Schluchsee quartz. For single grain analysis, quartz crystals of about 1 mm size have been put into drilled holes of a nickel holder. Crystal size and hole diameter generally differ in size, so that many grains are not fixed in the hole and rotate during ablation due to plasma repulsion. Explosive ablation rapidly minimizes crystal size. In addition, a significant proportion of the laser light goes through the quartz fragments. Thus it cannot be avoided that the laser beam hits the bottom of the nickel holder inducing a slight reaction between metal, quartz and fluorine, as described before. As expected, yield dependent fractionations do not occur for thick section analyses of Weinsberg and Schluchsee quartz (open symbols in Fig. 1.7c and Fig. 1.7d).

b) Dörentrup

An increase in $\delta^{18}\text{O}$ with increasing oxygen yield (Fig. 1.7b) indicates a yield dependent fractionation for single grain measurements of Dörentrup. The mean raw value of ArF-laser single grain analyses ($11.81 \pm 0.29 \text{ ‰}$) is slightly below thick section raw average ($11.99 \pm 0.20 \text{ ‰}$) and this shift becomes more pronounced when only those single grain analyses with amounts of 2-4 $\mu\text{mol O}_2$ are considered ($11.68 \pm 0.32 \text{ ‰}$ and $11.99 \pm 0.20 \text{ ‰}$, respectively). In contrast, thick section analyses of Dörentrup are not susceptible to yield dependent fractionations (Fig. 1.7a): Dörentrup rods are generally 4 mm thick, whereas single grains are only of 1 mm size. Considering the decrease in sample size during UV-ablation due to explosive ablation, many more photons may hit the metal surface during single grain analysis than during thick section analysis.

From these results it is concluded that thick section analysis should be preferred over single grain analysis. However, the effect of plasma heating on $\delta^{18}\text{O}$ is very small ($\leq 0.2 \text{ ‰}$) and single grain analysis might be considered if a large number of samples have to be analyzed or

Sample	thick section			single grain		
	n	$\delta^{18}\text{O}_{\text{raw}}$ (‰)	$\delta^{18}\text{O}_{\text{corr.}}$ (‰)	n	$\delta^{18}\text{O}_{\text{raw}}$ (‰)	$\delta^{18}\text{O}_{\text{corr.}}$ (‰)
Dörentrup (2-5 $\mu\text{mol O}_2$)*	33	11.99 \pm 0.20	—	10	11.81 \pm 0.29	11.80 \pm 0.18
Dörentrup (2-4 $\mu\text{mol O}_2$)*	29	11.99 \pm 0.20	—	5	11.68 \pm 0.32	11.69 \pm 0.11
Weinsberg*	3	11.09 \pm 0.18	10.44 \pm 0.18	12	10.83 \pm 0.26	10.50 \pm 0.22
Weinsberg#	3	11.09 \pm 0.18	11.03 \pm 0.17	6	10.99 \pm 0.21	10.93 \pm 0.21
Schluchsee 5#	2	10.39 \pm 0.11	10.61 \pm 0.11	8	10.26 \pm 0.20	10.47 \pm 0.19

Table 1.3. Comparison of single grain and thick section analyses using ArF-laser. All analyses are also listed in Appendix II and III

* corrected by an intralaboratory olivine standard (UGO-1: $\delta^{18}\text{O} = 5.20$ ‰)

corrected by homogeneous Dörentrup quartz ($\delta^{18}\text{O} = 12.10$)

standard deviation refers to 1 σ

rock sections are highly reactive to fluorine. For thick section analysis yield dependent fractionations occur for highly transparent quartz samples, but this problem may be overcome by analyzing thicker sections.

1.6.3. Data correction

Laser fluorination techniques can be subject to two groups of analytical problems: The first group includes contaminants like oxygen blanks which derive from leaks, samples, fluorine and fluorine getter (Valley et al., 1995). The second group comprises oxygen isotope fractionations occurring during the analytical procedure, such as edge effects, which have been observed by many authors during in-situ IR-laser fluorination (Elsenheimer & Valley, 1992; Sharp, 1992; Chamberlain & Conrad, 1991, 1993; Conrad & Chamberlain, 1992; Young & Rumble, 1993) as well as fractionations due to the conversion of O₂ to CO₂ (Mattey & Macpherson, 1993; Wiechert & Hoefs, 1995). Generally, a standard is run along with the sample in order to detect and subsequently correct for these effects. Valley et al. (1995) reported an improvement in accuracy and precision using a garnet standard for sample correction.

In Göttingen, for UV-laser analysis of quartz, the second group of interferences is of only minor importance: Sample ablation has been shown to be (nearly) free from fractionation (see chapter 1.6.1), while fractionations during the conversion of O₂ to CO₂ are not significant when analyzing μmol amounts of oxygen (Wiechert & Hoefs, 1995). Nevertheless, for monitoring and correction of contaminants, two standards have been used:

Raw values have either been corrected for an olivine standard (UGO-1: $\delta^{18}\text{O} = 5.20 \text{ ‰}$) or for Dörentrup glass ($\delta^{18}\text{O} = 12.10 \text{ ‰}$). The latter has been found to be very homogeneous in its isotopic composition (see chapter 1.6.1). In Table 1.3 averaged raw data are listed next to averaged corrected data.

In the case of thick section analysis of Weinsberg quartz all three analyses have been corrected both for the olivine and quartz standard (see also Appendix II for daily analyses). Olivine corrected data gave an average of $10.44 \pm 0.18 \text{ ‰}$, which is significantly lower than the raw mean value ($11.09 \pm 0.18 \text{ ‰}$) and the average obtained from Dörentrup correction ($11.03 \pm 0.17 \text{ ‰}$). This must be caused by contamination, most likely by a reaction of feldspar with fluorine at room temperature releasing small amounts of oxygen blanks (Elsenheimer & Valley, 1993). If such an oxygen blank has a $\delta^{18}\text{O}$ which is only slightly higher than the Dörentrup correction value (12.10 ‰) it would show a larger influence on standard olivine measurements than on Dörentrup quartz analysis. The $\delta^{18}\text{O}$ of Dörentrup glass (12.28 ‰ and 12.10 ‰ , Appendix II) would stay very close to its 'real' value (12.10 ‰), whereas $\delta^{18}\text{O}$ of the olivine standard (5.85 ‰ , Appendix II) is significantly shifted towards the isotopic composition of the blank oxygen. As a result, the average of raw values of Weinsberg quartz ($11.09 \pm 0.18 \text{ ‰}$)

would only be slightly higher than the Dörentrup corrected mean value (11.03 ± 0.17 ‰), but significantly higher than the olivine corrected average of 10.44 ± 0.18 ‰.

Although a reaction of feldspar with fluorine seems to be the likely mechanism for the production of blank oxygen in this study, a completely different contamination process such as degassing of the diamonds or remnants of adsorbed water in the extraction line can not be excluded. However, this example clearly demonstrates that raw data can only be corrected accurately by choosing a standard which has nearly the same isotopic composition as the mineral of interest. The accuracy of such a correction is demonstrated by the coincidence of Dörentrup corrected thick section- (11.03 ± 0.17 ‰) and single grain averages (10.93 ± 0.21 ‰) for Weinsberg quartz and Schluchsee quartz (10.61 ± 0.11 ‰ and 10.47 ± 0.19 ‰, respectively, Table 1.3).

Hence, it is demonstrated that standards which significantly differ from the isotopic composition of the sample, should be used only to guard against unsuspected errors such as leaks, outgassing, contamination, etc. rather than for data correction. The accuracy of in situ ArF-laser data of unknown samples can be improved by choosing a standard with similar isotopic composition. However, in-situ raw data for pure quartz are within 0.2 ‰ of corrected reference values. Data correction for quartz is only necessary if there is any contamination in the oxygen extraction line.

1.7. Application: oxygen isotope analysis of a hydrothermal cap quartz

Cap quartz formation of the quartz vein in Usingen, Rhenish Massif, is assumed to be caused by a mixing of surface waters with basinal brines (Behr & Gerler, 1987). Thus, oxygen isotope variations in single cap quartz sections should result from (1) variations of the amounts of fluids that have been mixed, (2) original variations in $\delta^{18}\text{O}$ of each fluid, (3) variations in temperature during quartz precipitation, (4) fractionations of oxygen isotopes during crystal growth and (5) a combination of those four (Onasch & Vennemann, 1995). Data from Horita & Wesolowski (1994) suggest that beside temperature or compositional parameters also pressure induced fluid boiling might lead to variations in $\delta^{18}\text{O}$ of the precipitating quartz. Therefore several hydrothermal quartz samples from Usingen, Rhenish Massif, Germany, have been screened to find indications for such a process. The purpose of this section is only to demonstrate the high spatial resolution and in-situ capabilities of the ArF-laser technique. One analyzed thick section and $\delta^{18}\text{O}$ -data of a hydrothermal quartz from Usingen is shown in Fig. 1.8.

Three laser runs have been carried out on this sample during a period of two weeks: Run 1 in the upper, run 2 in the middle and run 3 in the lower region of the thick section. To guard against contamination effects, Dörentrup quartz has been used as a standard. All data are listed in Appendix IV. During all thick section analyses, $\delta^{18}\text{O}$ variation of Dörentrup was within the

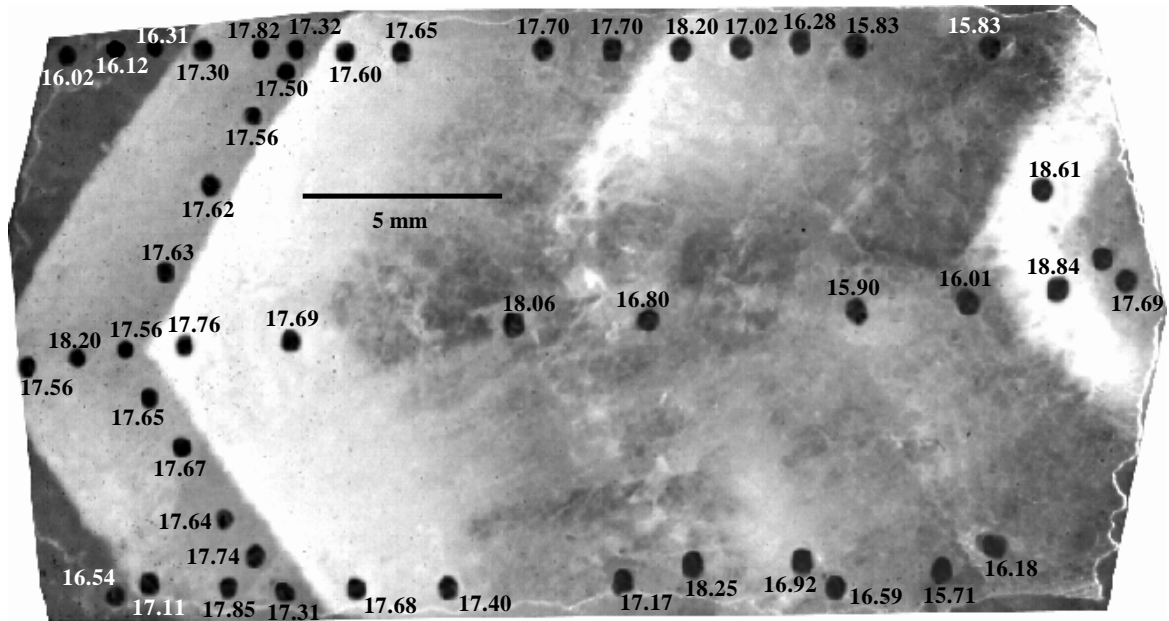


Fig. 1.8. Thick section (25 x 15 x 4 mm) of a hydrothermally precipitated quartz from Usingen, Rhenish Massif, Germany, and its variation in $\delta^{18}\text{O}$. Lateral resolution varied between 500 - 600 μm , vertical resolution between 1 - 2 mm (see text). In some cases mixed analyses of two different growth zones have been obtained, since each growth zone is not perpendicular to the surface. Nevertheless, points of the same growth level show nearly identical isotopic composition. Analyses have been carried out during two weeks and are also listed in Appendix IV. For further discussion see text.

same range shown in Fig. 1.6, suggesting that raw data need not be corrected, as discussed in chapter 1.6. Lateral resolution varied between 500 - 600 μm . Measurements of Usingen hydrothermal quartz were carried out at an early stage of the investigation, before the installation of cylindrical lenses to achieve higher fluence (see chapter 1.2). Thus only a maximum energy density of 15 J/cm^2 and a vertical resolution of 1 - 2 mm was obtained. With beam intensifier optics in place, however, a nearly twofold increase in fluence is realized. Since the yield increases two- to threefold when doubling the energy density (Fig. 1.4), pit depth decreases by the same factor. Thus, a much better vertical resolution would now be obtained with the rebuilt beam delivery system. However, even without beam intensification high precision data have been produced. Absolute values vary between 15.7 ‰ and 18.8 ‰. It is apparent that cloudy zones of quartz are systematically higher in $\delta^{18}\text{O}$ than clear ones. Additionally, laser pits in the same growth level have nearly identical isotopic composition. Especially when considering that these analyses have been performed during two weeks, the constancy of $\delta^{18}\text{O}$ -values demonstrates again the great precision of in-situ analyses using the ArF-laser.

Additional experiments must be carried out to investigate whether pressure induced fluid boiling caused the observed variation in $\delta^{18}\text{O}$ of 3.1 ‰. This can be easily done: In contrast to in-situ studies of single crystals with CO_2 -laser the sample is not lost after oxygen isotope analysis and additional investigations can be performed on the same section. Detailed microthermometric measurements of fluid inclusions would identify temperature changes, whereas trace element profiles using the laser ICP-MS technique and hydrogen isotope analyses would give clues as to the extent of mixing surface sulfate-bicarbonate waters with basinal brines as proposed by Behr & Gerler (1987). The Usingen quartz clearly shows that use of an ArF-laser extends the possibilities of existing laser techniques and increases the number of geochemical problems which can be investigated by oxygen isotope analysis, especially when a combination of oxygen isotopes with other data is needed.

Appendix I

ArF-laser fluorination: long term run for Dörentrup thick sections

date	run no.	yield (μmolO_2)	$\delta^{18}\text{O}_{\text{raw}}$ (‰)
09.06.1997	1	3.63	12.25
09.06.1997	2	3.13	12.14
11.06.1997	3	3.38	11.98
12.06.1997	4	3.67	12.17
12.06.1997	5	3.00	12.16
16.06.1997	6	2.96	11.72
16.06.1997	7	3.67	11.68
16.06.1997	8	3.21	11.67
23.06.1997	9	2.75	11.86
23.06.1997	10	3.25	11.94
23.06.1997	11	2.42	11.62
26.06.1997	12	3.13	11.97
26.06.1997	13	3.17	11.97
26.06.1997	14	2.83	11.89
28.06.1997	15	3.71	12.13
28.06.1997	16	2.50	12.09
28.06.1997	17	2.63	12.22
28.06.1997	18	2.50	12.21
02.07.1997	19	3.29	12.33
02.07.1997	20	4.00	12.27
03.07.1997	21	3.08	11.99
03.07.1997	22	3.33	12.04
08.09.1997	23	3.92	11.87
09.09.1997	24	3.38	11.90
09.09.1997	25	3.13	11.77
09.09.1997	26	2.75	12.00
09.09.1997	27	4.17	12.08
15.09.1997	28	4.58	11.75
15.09.1997	29	3.83	11.72
15.11.1997	30	4.13	11.87
17.11.1997	31	3.92	11.84
17.11.1997	32	3.83	12.32
15.01.1998	33	3.54	12.12
			<hr/> 11.99±0.20

Appendix II

ArF-laser fluorination: thick section analyses

date	sample	daily analysis no.	yield (μmolO_2)	$\delta^{18}\text{O}_{\text{raw}}$ (‰)	$\delta^{18}\text{O}_{\text{corr.}}$ (‰)	
21.04.1997	UGO-1	1	4.17	5.44		
	Suprasil	4	2.25	23.21	22.99	
	Suprasil	5	2.67	23.24	23.02	
	Suprasil	6	2.46	23.12	22.91	
	Suprasil	7	4.17	23.77	23.56	
	Suprasil	8	3.50	23.43	23.23	
	Suprasil	9	3.08	23.51	23.32	
	Suprasil	10	2.71	23.61	23.42	
	Suprasil	11	4.17	23.96	23.78	
	Suprasil	12	4.17	23.66	23.48	
	Suprasil	13	2.79	23.46	23.29	
	UGO-1	15	3.08	5.36		
	Suprasil*				23.50±0.25	23.30±0.26
	28.04.1997	UGO-1	2	2.96	5.85	
		Weinsberg	6	2.38	11.34	10.69
Weinsberg		7	2.96	10.93	10.28	
Weinsberg		8	2.96	11.01	10.36	
UGO-1		9	4.17	5.85		
Weinsberg*				11.09±0.18	10.44±0.18	
28.04.1997	Dörentrup	1	4.17	12.28		
	Weinsberg	6	2.38	11.34	11.26	
	Weinsberg	7	2.96	10.93	10.87	
	Weinsberg	8	2.96	11.01	10.97	
	Dörentrup	10	3.88	12.10		
Weinsberg#				11.09±0.18	11.03±0.17	
11.09.1997	Dörentrup	1	3.38	11.88		
	Schluchsee	2	2.54	10.28	10.50	
	Dörentrup	10	3.21	12.00		

	Dörentrup	1	4.17	11.87	
12.09.1997	Schluchsee	3	2.42	10.49	10.71
	Dörentrup	9	4.17	11.90	

Schluchsee#

10.39±0.11

10.61±0.11

* corrected for ol-Std. ($\delta^{18}\text{O} = 5.20$)

corrected for qz-Std. ($\delta^{18}\text{O} = 12.10$)

Appendix III

ArF-laser fluorination: single grain analyses

date	sample	daily analysis no.	yield (μmolO_2)	$\delta^{18}\text{O}_{\text{raw}}$ (‰)	$\delta^{18}\text{O}_{\text{corr.}}$ (‰)
17.03.1997	UGO-1	1	3.71	5.59	
	Weinsberg	4	2.13	10.28	10.02
	Weinsberg	5	4.17	10.76	10.53
	Weinsberg	6	2.79	10.58	10.38
	Weinsberg	7	3.46	10.87	10.71
	UGO-1	9	3.13	5.30	
21.04.1997	UGO-1	1	4.17	5.44	
	Weinsberg	2	2.46	10.72	10.46
	Weinsberg	3	4.00	10.80	10.51
	UGO-1	15	3.08	5.36	
25.04.1997	UGO-1	2	4.17	5.64	
	Weinsberg	3	7.08	11.13	10.69
	Weinsberg	4	3.88	11.06	10.63
	Weinsberg	5	4.58	10.71	10.28
	Weinsberg	6	3.21	10.89	10.46
	Weinsberg	7	3.58	10.83	10.40
	Weinsberg	8	4.17	11.33	10.91
	UGO-1	9	5.00	5.62	
	Weinsberg*				10.83±0.26
25.04.1997	Weinsberg	3	7.08	11.13	11.07
	Weinsberg	4	3.88	11.06	11.00
	Weinsberg	5	4.58	10.71	10.65
	Weinsberg	6	3.21	10.89	10.83
	Weinsberg	7	3.58	10.83	10.77
	Weinsberg	8	4.17	11.33	11.27
	Dörentrup	10	5.00	12.16	
Weinsberg#				10.99±0.21	10.93±0.21

	Dörentrup	1	3.92	11.87	
	Schluchsee	3	4.17	10.47	10.70
	Schluchsee	4	4.13	10.37	10.59
	Schluchsee	5	3.50	10.08	10.30
08.09.1997	Schluchsee	6	2.54	9.86	10.08
	Schluchsee	7	2.96	10.23	10.45
	Schluchsee	8	3.38	10.30	10.51
	Schluchsee	9	3.38	10.25	10.46
	Schluchsee	10	6.25	10.50	10.64
	Dörentrup	12	3.38	11.90	

Schluchsee#

10.26±0.20

10.47±0.19

	UGO-1	9	5.00	5.62	
25.04.1997	Dörentrup	10	5.00	12.16	11.74
	Dörentrup	11	3.04	12.31	11.89
					11.74
	UGO-1	2	4.17	5.05	11.89
	Dörentrup	3	3.04	11.47	11.61
	Dörentrup	4	3.88	11.59	11.72
	Dörentrup	5	4.17	11.62	11.74
04.06.1997	Dörentrup	6	3.83	11.46	11.57
	Dörentrup	7	5.00	11.92	12.01
	Dörentrup	8	3.42	11.58	11.66
	Dörentrup	9	4.17	11.95	12.02
	Dörentrup	10	5.42	12.02	12.08
	UGO-1	11	4.17	5.15	

Dörentrup*

11.81±0.29

11.80 ± 0.18

* corrected for ol-Std. ($\delta^{18}\text{O} = 5.20$)

corrected for qz-Std. ($\delta^{18}\text{O} = 12.10$)

Appendix IV

ArF-laser fluorination: thick section analyses of hydrothermally precipitated quartz from Usingen, Rhenish Massif, Germany

date	sample / pit no.	daily analysis no.	yield (μmolO_2)	$\delta^{18}\text{O}_{\text{raw}}$ (‰)
23.06.1997	Dörentrup	2	2.75	11.86
	1	3	2.71	16.02
	2	4	2.71	16.12
	3	5	2.71	16.31
	4	6	2.83	17.30
	5	7	2.71	17.82
	6	8	2.67	17.32
	7	9	2.58	17.60
	8	10	2.29	17.65
	Dörentrup	11	3.25	11.94
	24.06.1997	Dörentrup	1	2.71
9		2	2.08	17.70
10		3	2.08	17.70
Dörentrup		4	2.46	12.02
26.06.1997	Dörentrup	3	3.13	11.97
	11	4	3.00	18.20
	12	5	3.29	16.28
	13	6	3.21	15.83
	14	7	3.21	17.02
	15	8	3.58	15.83
	16	9	3.29	17.56
	17	10	3.00	17.56
	18	11	2.79	17.76
	19	12	2.79	17.69
	20	13	2.63	18.06
	21	14	2.79	16.80
	22	15	2.33	15.90
	23	16	2.79	16.01
	24	17	3.42	18.84
	25	18	2.08	17.69
	Dörentrup	19	3.17	11.97

	Dörentrup	3	2.50	12.09
	26	4	2.50	17.31
28.06.1997	27	5	2.50	17.68
	28	6	2.96	16.54
	29	7	2.92	17.11
	30	8	2.75	17.85
	Dörentrup	9	2.63	12.22
	31	10	1.92	17.40
28.06.1997	32	11	2.38	17.17
	33	13	2.21	17.50
	Dörentrup	14	2.50	12.21
	Dörentrup	2	3.29	12.33
	34	3	3.04	18.25
	35	4	3.33	16.92
02.07.1997	36	5	2.83	16.59
	37	6	2.79	15.71
	38	7	2.96	16.18
	Dörentrup	11	4.00	12.27
	Dörentrup	2	3.08	11.99
	39	3	2.63	17.56
	40	4	2.92	17.62
	41	5	3.08	17.63
03.07.1997	42	6	3.21	18.20
	43	7	3.33	17.65
	44	8	3.33	17.67
	45	9	3.42	17.64
	46	10	3.25	17.74
	Dörentrup	11	3.33	12.04

2. Set up of a rapid technique enabling precise determinations of $^{18}\text{O}/^{16}\text{O}$ -ratios within silicate extracted oxygen

2.1. Introduction

The spatial resolution of the UV-laser based oxygen isotope microprobes described in chapter 1.2 is restricted to 500 μm . This is not caused by focal properties of UV-light. Generally, UV-light can be focused down to spot sizes of less than 1 μm . Instead, it is limited by the amount of oxygen necessary for the maintenance of a viscous flow of analyte gas into the ion source: For conventional mass spectrometers with dual inlet a change towards a fractionating molecular flow occurs when sub- μmol amounts of analyte gas are introduced (Bridger et al., 1974). Additionally, these mass spectrometers are not suitable to measure oxygen directly, so that oxygen must be first converted to CO_2 before entering the ion source. The conversion is tied to fractionations if less than μmol amounts of oxygen are reacted to CO_2 (Mattey & MacPherson, 1993).

A new generation of continuous flow mass spectrometers uses He as a carrier gas for the transportation of analyte gas into the ion source. By adding He the mean free path of analyte molecules decreases such that nmol quantities can be introduced without any fractionation. Widely varying ion currents are accepted, which allows a continuous observation of gas chromatographic effluents. This set up is known as irm-GC-MS (isotope ratio monitoring gas chromatography mass spectrometry; e.g. Matthews & Hayes, 1978; Hayes et al., 1990). Additionally, these newly developed mass spectrometers are equipped with a cup configuration for a detection of masses 32, 33 and 34, so that oxygen can be measured directly as O_2 and conversion to CO_2 is not necessary anymore (Newman, 1996).

In the following a UV-laser based microprobe for monitoring $^{18}\text{O}/^{16}\text{O}$ -ratios within silicates is described. For oxygen isotope detection a DeltaPlus mass spectrometer (Finnigan, Inc.) with continuous flow inlet is used. Spatial resolution is about 250 μm , but can easily be improved to smaller spot sizes. Due to the fact that only an aliquot of released oxygen is finally analysed, the duration of a single analysis is reduced to less than 15 minutes.

2.2. Silicate oxygen and irm-GC-MS

Prior to irm-GC-MS, analyte oxygen is liberated from silicates by UV-laser fluorination. Principles of this method have been already described by several authors (e.g. Wiechert & Hoefs, 1995; Farquhar & Rumble, 1998; Young et al., 1998b; Fiebig et al., 1999) as well as in chapter 1.4.

Using continuous flow mass spectrometers, analyte and standard oxygen are only once introduced into the ion source. This is in contrast to conventional mass spectrometers, where it is continuously switched between analyte and standard gas. In order to obtain reproducible and accurate signals, the oxygen signal must be distinguishable from the background signal. Hence, nmol quantities of analyte oxygen are packaged prior to introduction into the ion source. Generally, this is done by cryofocusing it over molsieve 5A at $-196\text{ }^{\circ}\text{C}$. When cryofocusing is quantitative, the molsieve is heated up to $100\text{ }^{\circ}\text{C}$ and analyte oxygen, immediately desorbing, is purged with He towards the mass spectrometer.

Before mass spectrometric analysis takes place, analyte oxygen is usually set apart from interferences (e.g. NF_3 , Rumble et al., 1997; N_2 , Young et al., 1998a). After cryofocussing oxygen therefore passes a GC equipped with a molsieve 5A column. Finally, analyte oxygen enters the ion source via an open split, the function of which is described by Merrit & Hayes (1994). The open split additionally allows an introduction of standard oxygen.

2.3. Equipment

For oxygen isotope detection a DeltaPlus mass spectrometer (Finnigan, Inc.) equipped with continuous flow- and dual inlet system is used. It is characterised by an accelerating voltage of 3 kV and a Faraday cup collector system for masses 32 ($R = 3 \cdot 10^8\ \Omega$), 33 ($R = 3 \cdot 10^{11}\ \Omega$) and 34 ($R = 1 \cdot 10^{11}\ \Omega$). The DeltaPlus mass spectrometer has so far been applied to quantify isotope ratios of $^{18}\text{O}/^{16}\text{O}$, $^{15}\text{N}/^{14}\text{N}$, $^{13}\text{C}/^{12}\text{C}$ and $^{34}\text{S}/^{32}\text{S}$ measured as CO_2 , CO, N_2 and SO_2 . For a detection of N_2 , CO_2 and CO, the resistor of cup 33 ($R = 3 \cdot 10^{11}\ \Omega$) must be replaced by one with $R = 3 \cdot 10^{10}\ \Omega$.

The detector system accepts varying ion currents, such that chromatographic signals can be integrated. Peak detection parameters have been set to 0.1 mV/s both for the starting and ending slope of each signal and to a minimum amplitude of 50 mV. Integration time has been fixed to 0.125 seconds. Background correction is done individually for each peak. Therefore, the intensity of the background signal five integration units prior to peak detection is taken.

All parameters of oxygen isotope detection can be easily controlled using the computer programm ISODAT (Finnigan, Inc.). This program also guarantees a conversion of measured signal areas into corresponding $\delta^{18}\text{O}$ -data.

The continuous flow inlet of the ion source can either be connected to a Conflo II- or to a GP-Interface (Finnigan, Inc.). The Conflo II-interface consists of a single open split, by which both sample and standard oxygen are introduced into the mass spectrometer. It is suitable to reduce from μmol to nmol amounts of oxygen. In contrast, the GP-interface has two open splits, one for the standard and the other for the analyte gas. Compared to the Conflo II-interface, the

"loss" of analyte gas at the open split is much smaller. Hence, the GP-interface is usually taken, when only nmol amounts of analyte gas reach the open split.

In contrast to the Conflo II-interface double amount of He enters the ion source when the GP-interface is used. This leads to a working pressure of $3.6 \cdot 10^{-6}$ mbar within the ion source ($1.8 \cdot 10^{-6}$ mbar in the case of using the Conflo-interface). Both interfaces can also be controlled by the software programm ISODAT (Finnigan, Inc.).

The GC used is a Hewlett Packard 5890 Series II equipped with a PoraPLOT Q column (25m length, 0.53 mm inner diameter). This column is suitable for separating hydrocarbons and fluorocarbons, but not oxygen from nitrogen.

The characteristics of the used ArF-laser and the oxygen extraction system are described in chapter 1.2.

2.4. Set up of the continuous flow technique

The putting into operation occurred in three steps:

- (1) The DeltaPlus mass spectrometer is used for the first time worldwide to determine oxygen as O_2 . Therefore an optimal adjustment of the mass spectrometer concerning oxygen isotope measurements in a continuous flow mode was necessary.
- (2) Cryofocus and GC have been connected to the DeltaPlus including its GP-interface to set up an irm-GC-MS-system. This was done separately from (1) to recognize possible fractionations due to cryofocussing.
- (3) UV-fluorination and oxygen extraction system were coupled to the system given by (2).

2.4.1. Characteristics of the DeltaPlus concerning oxygen isotope measurements in a continuous flow mode

2.4.1.1. Peak shape

First runs regarding oxygen isotope detection as O_2 in a continuous flow mode demonstrated that a differential pumping system is necessary in order to avoid tailing effects. In the absence of a differential pump mass 32 is partly scattered on higher mass cups 33 and 34. Impacts between He and O_2 within the ion source can not account for this feature, as these would lead to lower kinetic energies of O_2 prior to acceleration and thus to a tailing of high masses on lower mass cups. Moreover, O_2 must interact with He within the fly tube, such that the impact-induced loss in kinetic energy is overcompensated by a directional effect.

However, using a differential pump the vacuum within the fly tube is improved. Tailing nearly vanishes and reproducible $\delta^{18}\text{O}$ -analyses can be carried out.

2.4.1.2. Optimization of ion source parameters

Optimal ion source parameters were adjusted by looking for best linearity. The software programm ISODAT allows linearity to be automatically checked. Throughout this check one bellow of the dual inlet system is used for the introduction of oxygen into the ion source. As a reference, the oxygen 32 signal was set to 2 V and was afterwards increased in 1 V steps up to 8V. In order to simulate continuous flow conditions He was additionally added via the continuous flow inlet.

Non-linearity was observed, the extent of which could be decreased by optimising the extraction voltage of the first aperture behind the slit of the ion source. Fig. 2.1 shows non-linearities obtained for an optimised extraction voltage of 40 %. It is evident that the extent of non-linearity is a function of He-pressure within the ion source. Obviously, non-linearity arises from a reaction of molecular and/or ionised oxygen within the ion source (e.g. with the W-filament) and can be buffered by the amount of He (dilution effect). The more He is within the ion source, the smaller the non-linearity turns out to be.

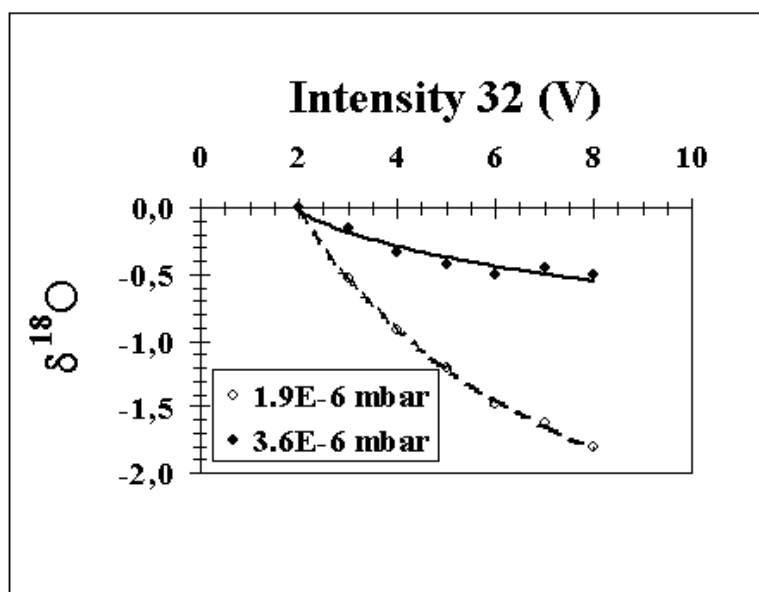


Fig. 2.1. Linearity check using the dual inlet. Optimal ion source parameters was given by an extraction voltage of 40 %. The first signal of 2V was taken as reference. By further compression of the bellow oxygen signals were increased in 1V steps. Parameters were chosen as follows: IDLE-time: 30 s, Integration time: 8 s, Delay time: 2 s. He was continuously added via Conflo (1.9E-6 mbar) or GP-interface (3.6E-6 mbar). For further discussion see text.

A reaction of oxygen within the ion source is supported by the observation that the extraction voltage had to be optimised daily to achieve smallest non-linearities. Within one month it increased from 40 % to 70 %, and from that time on it was observed that a variation in extraction voltage only led to an increase in the extent of non-linearity. Hence, in spite of a non-linearity of about 0.15 %/V, the optimal adjustment of ion source conditions for oxygen isotope measurements with the DeltaPlus has been found.

The linearity check described above does not really represent irm-GC-MS-conditions: Oxygen was continuously entering the ion source from the bellow and He and O₂ described different flow paths. In contrast, under irm-GC-MS conditions, oxygen is introduced into the ion source in intervals and the flow path of He equals that of O₂. Therefore it has to be verified if an extraction voltage of 70% represents optimum source conditions for irm-GC-MS, too (see chapter 2.4.2.1).

2.4.2. Set up of irm-GC-MS

Fig. 2.2 shows the instrumentation which was set up to simulate irm-GC-MS conditions: In position I of Valko 1 oxygen (purity 4.5) and He (purity 4.6) are mixed in a sample loop, which is afterwards purged with He (purity 6.0) switching Valko 1 to position II. While Valko 2 is in position II oxygen is cryofocused over molsieve 5A at -193 °C. When cryofocussing is quantitative, valko 2 is switched to position I and the molsieve is now purged with He 5.6. Due to heating with boiling water oxygen desorbs and is carried by He via GC (which is at room temperature) and sample open split into the ion source. Fig. 2.3 exhibits a typical modus of measurement: First, oxygen (which is the same oxygen taken for the sample loop) is introduced for 20 s via the standard open split into the ion source. This is to precondition the ion source for oxygen measurements. A second introduction of oxygen for 20 s then serves as a reference. Afterwards oxygen from the sample loop enters the ion source via the sample open split. Finally, oxygen is once again introduced via the standard open split in order to be able to quantify probable drifts during a single analysis.

In contrast to "flat top" peaks obtained by an inlet of oxygen via the standard open split, the signal shape of analyte oxygen resembles a "Gaussean" peak. This shape reflects variations of oxygen partial pressure within the ion source and is mainly caused by the process of oxygen desorption during heating of the cryofocus. Additionally, the molsieve cryofocus retards ³⁴O₂ relative to ³²O₂. Hence, the latter enters the ion source slightly before the heavier isotopomer. This is different from "flat top" signals, which arise from a simultaneous introduction of both isotopomers into the ion source. Therefore, the 34/32-ratio of the introduced analyte oxygen varies by time, while it is constant during the detection of standard oxygen (see Fig. 2.3). δ¹⁸O-values are not influenced that way since only integrated peak areas are considered for their calculation.

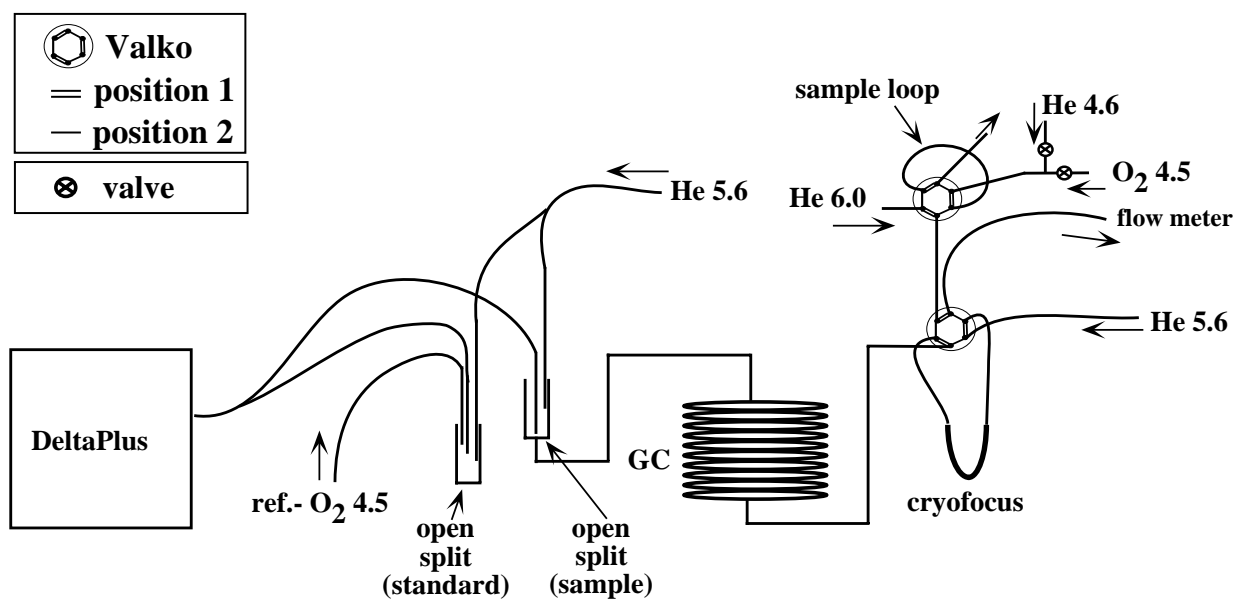


Fig. 2.2. Configuration to simulate irm-GC-MS-conditions. For explanation see text in chapter 2.4.2.

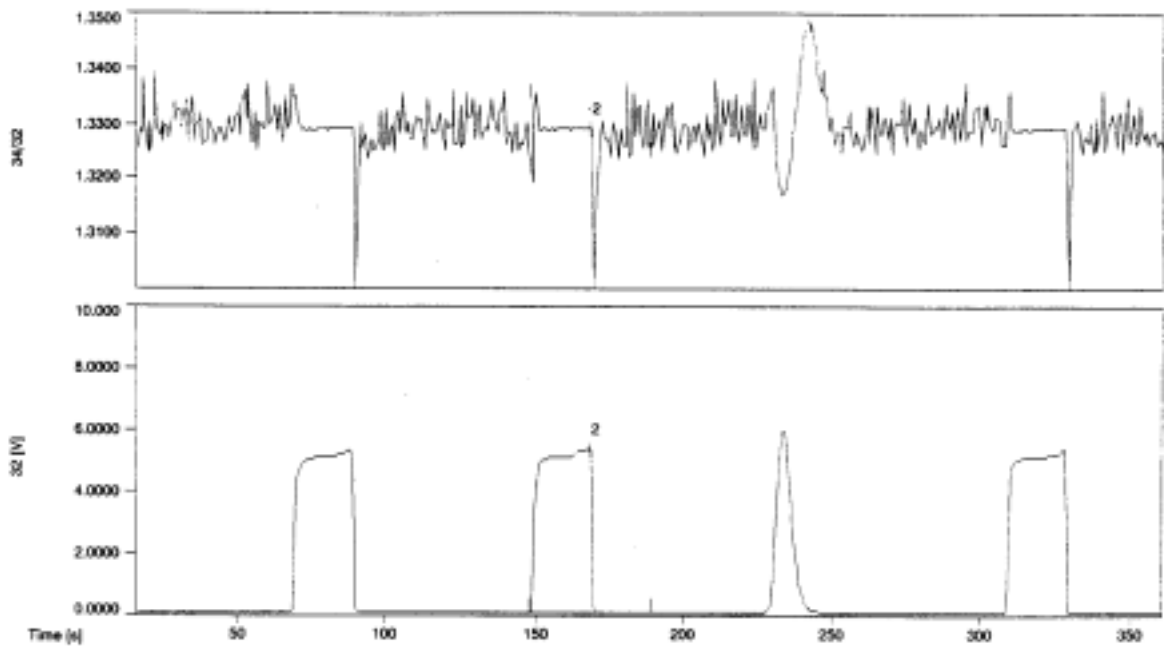


Fig. 2.3. Typical measuring modus using irm-GC-MS. Standard oxygen occurs as "flat top" signal and enters the ion source via the standard open split, such that mass 32 and 34 are not separated prior to their introduction. The first standard signal derives from a preconditioning of the ion source with oxygen. The second signal was taken as reference. In contrast, analyte oxygen ("Gaussean" signal) passes a cryofocus and a PoraPLOT Q column. Due to oxygen desorption from the cryofocus, mass 32 is slightly separated from mass 34 before entering the ion source. The extent of separation is about 40 %. The last standard introduction is done to be able to quantify possible drifts occurring within a single measuring cycle. For further explanation see chapter 2.4.2.

2.4.2.1. Linearity

To check linearity under irm-GC-MS conditions, the reference signal was set to an intensity of 5 V for mass 32. The intensity of the sample peak was varied between 0.1 and 10 V by mixing He and oxygen to different amounts within the sample loop (see Fig. 2.2). Fig. 2.4 shows the results of the linearity test:

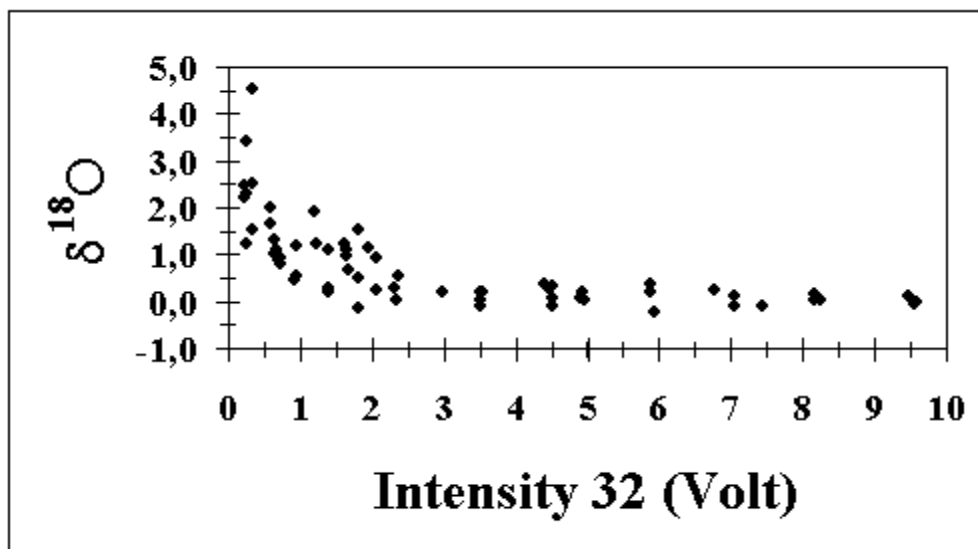


Fig. 2.4. Linearity check carried out in an irm-GC-MS mode (see Fig. 2.3 and chapter 2.4.2). Reference and analyte oxygen derive from the same flask. Linearity occurs between 3.0 and 9.5 V. For further discussion see text.

In contrast to non-linearity obtained for an inlet of oxygen via bellow, now, linearity within a range of 3.0 and 9.5 V occurs. Oxygen isotope fractionation due to cryofocussing was not observed. Non-linearity below 3.0 V is presumably due to an increasing contribution of blank oxygen, non-separated interferences (e.g. N₂; Young et al., 1998a) and shot noise with decreasing amounts of sample oxygen (Young et al., 1998a). At least 30 nmol of oxygen must be cryofocused to obtain an intensity of 3 V for mass 32. Assuming an open split ratio of 1/3, the minimum amount of O₂ necessary for a reproducible analysis is thus about 10 nmol.

2.4.2.2. Factors influencing linearity

Non-linearity is observed when oxygen enters the ion source via the bellows, whereas linearity occurs for irm-GC-MS conditions. To explain this feature two tests were performed:

i) Oxygen was exclusively introduced into the ion source by the standard open split, such that only "flat top" signals were obtained. As for the experiment before, the third peak was taken as analyte signal, while the second one served as reference. Intervals of oxygen injection (80 s) remained the same as for the previous experiment. The reference signal was fixed to 5 V and the analyte signal, now also occurring as "flat top" peak, was varied inbetween 2 and 10 V by changing the flow rate of oxygen into the standard open split: While an extraction voltage of 70 % still represents best source conditions, again, a non-linearity of ca. 0.1 %/V is observed within a range of 3 and 9 V (Fig. 2.5). Obviously, the filament preferentially reacts with $^{34}\text{O}_2$ when partial pressure of oxygen within the ion source decreases.

ii) To investigate the effect of variations of oxygen partial pressure during analyte inlet on the extent of non-linearity, a "Gaussean" profile for the sample peak was simulated by reducing the duration of oxygen inlet from 20 to 6 s during the third introduction. This signal was referenced towards a "flat top" signal, which had been obtained by an injection of oxygen for 20 s. Fig. 2.6 gives evidence that the shape of the signal does not have any significant influence on the extent of non-linearity. The latter rather seems to be a function of relative differences of maximum peak intensities between standard and sample oxygen. Thus, the extent of non-linearity mostly depends on the difference of maximum oxygen partial pressure between analyte and reference oxygen.

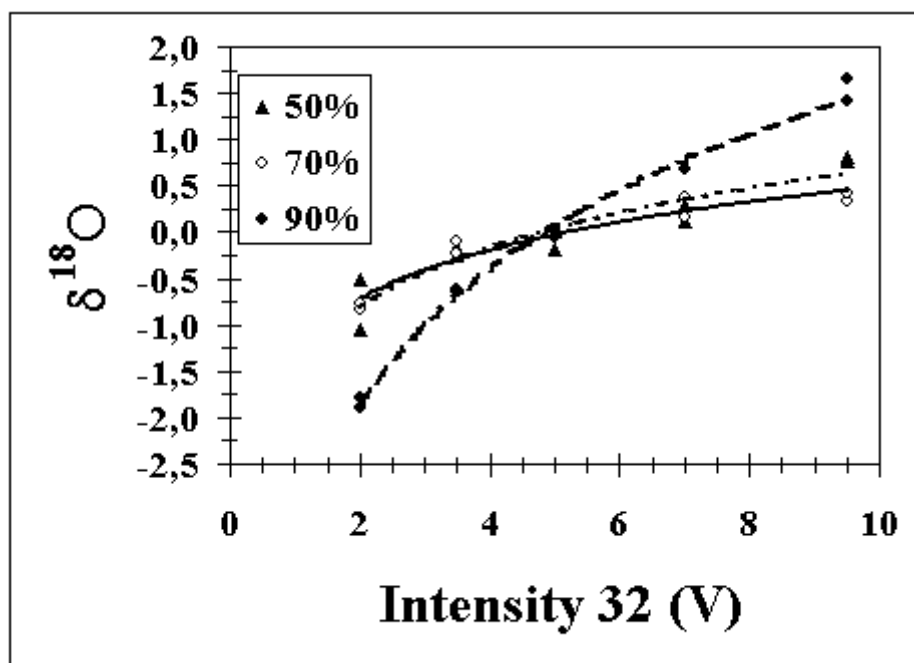


Fig. 2.5. Linearity check carried out by introducing both standard and analyte oxygen via the standard open split. This way, standard and analyte oxygen describe equal flowpaths and mass 32 and 34 of the analyte oxygen are not separated prior to introduction. As for the reference oxygen, corresponding mass signal of analyte oxygen now occurs as "flat top" peak. The reference signal was fixed to 5 V. Reference and analyte oxygen derive from the same flask.

The extent of non-linearity is smallest when using an extraction voltage of 70 % (see also chapter 2.4.2.2).

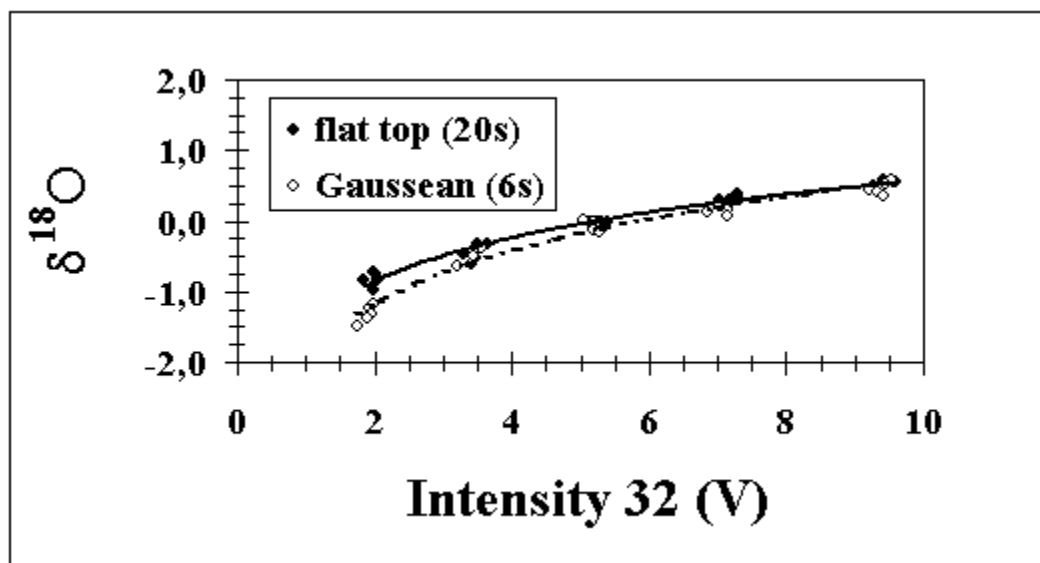


Fig. 2.6. Dependence of the extent of non-linearity on signal shape. "Gaussean" shape of analyte peak was obtained by introducing oxygen via the standard open split for only 6s. This was referenced against a "flat top" signal obtained by an inlet of the same oxygen for 20 s. For discussion see text.

Using irm-GC-MS conditions the maximum intensity of the sample peak coincides with a minimum in the corresponding $^{34}\text{O}_2/^{32}\text{O}_2$ -ratio (Fig. 2.3). The extent of separation between $^{32}\text{O}_2$ and $^{34}\text{O}_2$ is about 40 %. This slight separation seems to be sufficient to make non-linearities of about 0.1 ‰/V disappear, such that linearity between 3.0 and 9.5 V is obtained (Fig. 2.4). Before the ion source can significantly react with $^{34}\text{O}_2$, it is probably already preconditioned by 500-fold more abundant $^{32}\text{O}_2$. In contrast, non-linearity was always obtained within experiments where $^{34}\text{O}_2$ and $^{32}\text{O}_2$ had been introduced simultaneously into the ion source.

2.4.3. Calibration to V-SMOW-scale

For the above experiments sample and reference oxygen derived from the same flask. The $\delta^{18}\text{O}$ -value relative to V-SMOW was unknown, such that it was arbitrarily fixed to 0.0 ‰ and relative deviations from this value were measured.

In order to be able to measure $\delta^{18}\text{O}$ -values relative to SMOW the system was calibrated against oxygen, which had been conventionally determined to a $\delta^{18}\text{O}$ -value of 15.2 ± 0.2 ‰ V-SMOW. Against this, oxygen, which had been taken for linearity checks and which is used as a reference for the following silicate measurements, was determined to a $\delta^{18}\text{O}$ of 8.5 ± 0.2 ‰.

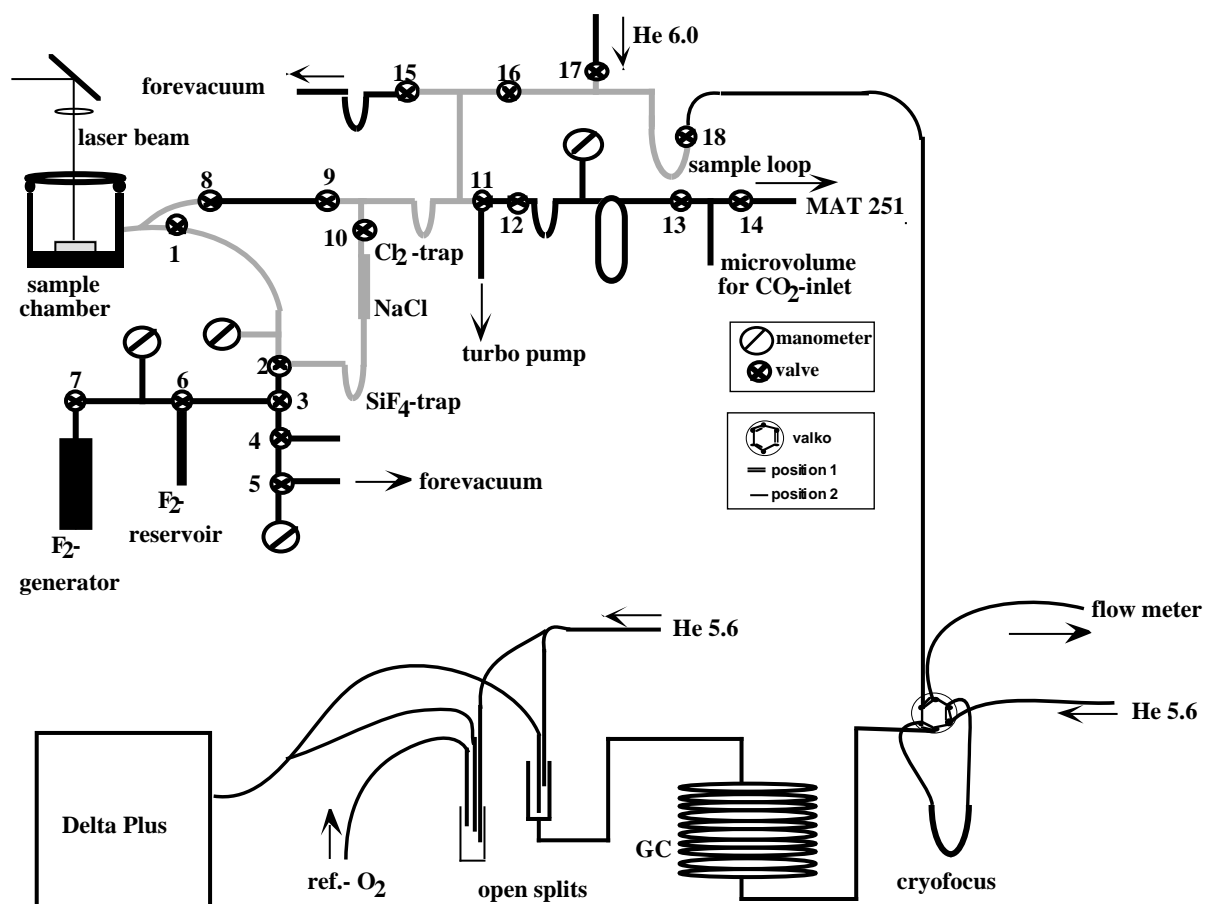


Fig. 2.7. Schematic drawing of the whole preparation line. Oxygen is liberated from silicates by ArF-laser ablation within a sample chamber filled with 10 mbar of fluorine. After the release of 300 nmol of oxygen, the oxygen/fluorine/SiF₄-mixture is expanded into a volume indicated by the grey colour. Fluorine is converted to chlorine on hot NaCl and chlorine and SiF₄ are frozen out in corresponding liquid nitrogen cold traps. After 3 minutes, valve 16 is closed and valves 17 and 18 are opened, such that an aliquot of oxygen is purged with 20 ml/min He towards the cryofocus where it is packaged. For the introduction of cryofocused analyte oxygen and reference into the mass spectrometer see chapter 2.4.2. The oxygen extraction part is still connected to an O₂-CO₂ converter and MAT 251, such that silicate released oxygen can be detected as CO₂ alternatively (see Wiechert & Hoefs, 1995).

2.4.4. Combination of UV-laser oxygen extraction system and irm-GC-MS

The irm-GC-MS part shown in Fig. 2.2 was coupled to a UV-laser oxygen extraction system, which has already been described in chapter 1.2. Fig. 2.7 gives an overview of the instrumentation.

Oxygen from silicates is released by UV-laser fluorination and is subsequently expanded into an evacuated volume defined by closed valves 8, 3, 9, 11, 15, 16, 17 and 18. Surplus fluorine is thereby converted on hot NaCl (150 °C) to chlorine, which is frozen out by liquid nitrogen in the Cl₂-trap. After 3 minutes ³⁴O₂ and ³²O₂ have homogeneously distributed within the defined volume and valve 16 is closed. The volume between valves 16, 17 and 18 serves as a sample loop and oxygen within that volume is purged by He towards the cryofocus by opening valves 17 and 18. Flow rates are about 20 ml/min and cryofocussing is quantitative after additional 3 minutes. Sample and reference oxygen are finally introduced into the ion source as described in chapter 2.4.2.

Two silicate standards of known isotopic composition were analysed repeatedly to look for accuracy and precision of this instrumentation (Fig. 2.8). Within errors the averages agree with recommended values: Finero 9506-1 olivine and Dörentrup quartz were determined to 5.08 ± 0.14 ‰ (n = 10) and 11.99 ± 0.20 ‰ (n = 33), respectively, using the technique of Wiechert & Hoefs (1995) modified after Fiebig et al. (1999). Using the newly developed continuous flow technique, means of 5.04 ± 0.14 ‰ (n = 19) and 11.87 ± 0.17 ‰ (n = 7), respectively, were obtained. The intensity of standard oxygen was set to 5V during all measurements. Fig. 2.8 also shows the obtained δ¹⁸O-values as a function of signal intensity of mass 32. Thereby it is once again demonstrated that linearity occurs for oxygen isotope quantifications carried out under irm-GC-MS conditions.

It is straightforward that the spatial resolution depends on the ratio of sample loop volume and expansion volume. During laser fluorination of the silicate standards this ratio was 1/10. In order to get a sample signal of 3 V, 300 nmol of oxygen had to be extracted totally, which corresponds to a spatial resolution of 250 μm.

Due to a volume ratio of 1/10, 90 % of the total amount of oxygen, that is released by laser fluorination, is discarded. Thus further improvements of the spatial resolution by optimising the volume ratio of sample loop and expansion volume should be possible.

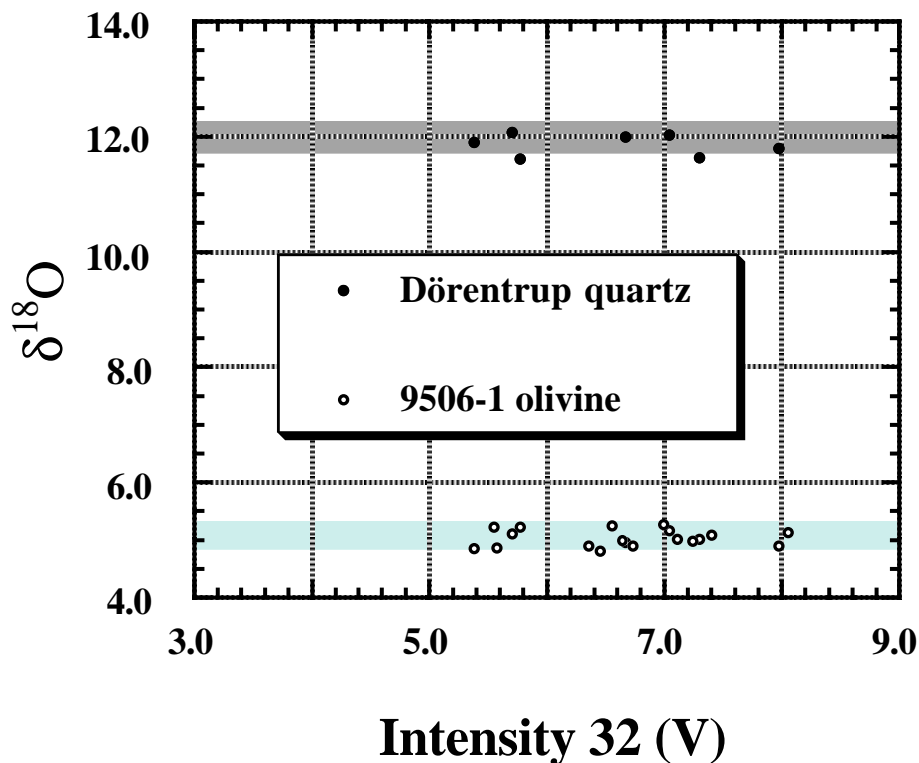


Fig. 2.8. Accuracy and precision of the new technique by running two standards from January to February, 1999. All Dörentrup-quartz- and 9506-1-olivine- $\delta^{18}\text{O}$ -data plot very well within recommended ranges (dark grey: recommended Dörentrup- $\delta^{18}\text{O}$ range; light-grey: recommended olivine $\delta^{18}\text{O}$ -range) previously obtained by oxygen isotope analysis using the technique of Wiechert & Hoefs (1995) modified after Fiebig et al. (1999). For means and standard deviations (1σ) see text.

The great advantage of discarding an aliquot of the released oxygen is the short duration for a single analysis, which is less than 15 minutes. Usually, much more time is needed when liberated oxygen is quantitatively cryofocused in the vacuum (Young et al., 1998a,b). Additionally, it would take much more time if the released oxygen is purged quantitatively all the way from the sample chamber to the molsieve, since the volume which has to be purged increases that way.

2.4.5. Gaseous interferences during detection of $^{18}\text{O}/^{16}\text{O}$ -ratios

Clayton & Mayeda (1983) and Rumble et al. (1997) suggested NF_3 to be an interferent component for mass 33, which, amongst others, decomposes by electron bombardement within the ion source to NF^+ . Rumble et al. (1997) obtained a signal for mass 52 and ascribed it to NF_2^+ . However, the contribution of mass 33 to the $\delta^{18}\text{O}$ -calculation (Santrock et al, 1985) is negligible and due to the low abundance of ^{15}N a significant interference of $^{15}\text{NF}^+$ with mass 34 can be ruled out.

Young et al. (1998a) reported significant errors in oxygen isotope measurements if oxygen is co-eluted simultaneously with small amounts of nitrogen. Nitrogen entering the ion source most likely causes drifts in the background signal inducing a significant signal in the 34/32-ratio and corresponding $\delta^{18}\text{O}$ -values as high as 72‰. Usually, a separation between oxygen and nitrogen is achieved if the analyte oxygen passes a molsieve 5A column prior to an introduction into the ion source.

$\delta^{18}\text{O}$ -determinations on Dörentrup and 9506-1 olivine using a PoraPLOT Q column demonstrate that analyte oxygen need not pass a molsieve 5A column. Precision is better than 0.2 ‰ even if nitrogen is not separated from oxygen prior analysis. However, one has to keep in mind that Young et al. (1998a,b) liberate amounts as small as 12 nmol oxygen, which are cryofocused quantitatively. Throughout this study, 300 nmol of oxygen are released, from which only 1/10 is cryofocused. Hence, nitrogen interferences due to small leakages within the oxygen extraction system should more affect $\delta^{18}\text{O}$ -measurements in their case.

In order to exclude any possible interference, the PoraPLOT Q column was finally exchanged against a molsieve 5A PLOT column (15m length and 0.53mm inner diameter). As expected, precision was not improved. Fig. 2.9 shows the signals of a measuring cycle obtained by using the molsieve 5A column. A significant nitrogen signal after elution of oxygen was not obtained (compare with Fig. 4 of Young et al. (1998a)). It is further obvious that the extent of separation of $^{34}\text{O}_2$ and $^{32}\text{O}_2$ is still about 40 ‰ indicating that $^{34}\text{O}_2$ and $^{32}\text{O}_2$ are primarily separated due to cryofocusing over molsieve 5A.

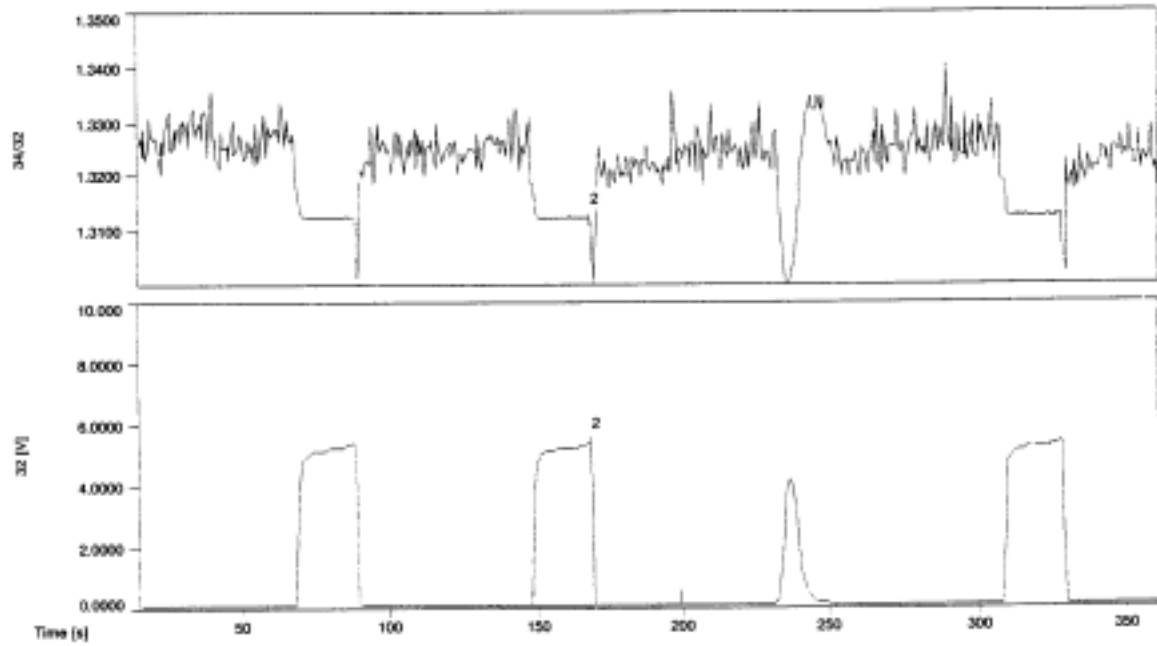


Fig. 2.9. Measuring modus obtained for oxygen isotope analysis of an olivine standard using a molsieve 5A PLOT column. The second signal was taken as reference ($\delta^{18}\text{O} = 8.5 \text{ ‰}$). A significant nitrogen signal after the elution of analyte oxygen -as observed by Young et al. (1998)- was not detected, implying that nitrogen interferences are negligible if more than 300 nmol of oxygen are extracted from the silicate. The extent of separation between masses 32 and 34 is still about 40 ‰ (compare with Fig. 2.3) suggesting that separation between isotopomers of oxygen is mainly caused by the process of oxygen desorption from the heated cryofocus. For the analysed olivine standard (Finero 9506-1) a $\delta^{18}\text{O}$ of 5.2 ‰ was obtained.

3. Exchange mechanisms, fluid flow and fluid evolution during hydrothermal alteration of granites from the southeastern Schwarzwald, Germany

3.1. Introduction

Oxygen isotope data of igneous and metamorphic rocks can provide important information on their origin and alteration history. In numerous studies, Hercynian granites and Pre-Hercynian gneisses from the entire Schwarzwald (Black Forest, Germany) were analysed for their oxygen isotope compositions (Magaritz & Taylor, 1981; Hoefs & Emmermann, 1983; Simon and Hoefs, 1987; Simon, 1988; Simon, 1990; Taylor et al., 1991; Techmer, 1992; Simon & Hoefs, 1998). These studies demonstrate that a complex fossil hydrothermal system was active in the Schwarzwald. While granites from the N-Schwarzwald nearly remained unaffected (Hoefs & Emmermann, 1983; Techmer, 1992), many granites and gneisses from the S-Schwarzwald have been intensively modified at high temperatures by a meteoric fluid (Magaritz & Taylor, 1981; Hoefs & Emmermann, 1983; Simon & Hoefs, 1987; Simon, 1988; Simon, 1990; Taylor et al., 1991, Simon & Hoefs, 1998). Variable degrees of oxygen fractionation between mineral pairs within single granite intrusions were observed implying that hydrothermal interaction took place after the emplacement and solidification of the granites under open system conditions. Equilibrium has not been attained throughout the hydrothermal event (Simon, 1988; Simon, 1990).

All these studies on Schwarzwald granites have in common that oxygen was liberated either from whole rocks or from mineral separates using the conventional fluorination technique of Clayton & Mayeda (1963). This technique is suitable for oxygen isotope analysis of 5-20 mg of crushed material, but not for in situ analysis on a sub-mm scale. Thus, interfaces of fluid-rock interaction can not be investigated using the conventional technique. However, in chapter 2 it is described that a UV-laser system for oxygen isotope extraction has been combined with a continuous flow mass spectrometer. This technique permits in situ analysis of nmol quantities of oxygen and oxygen isotope analysis to be applied to fluid-rock interfaces.

Amongst all southeastern Schwarzwald plutons, meteoric water interactions are especially pronounced in the St. Blasien pluton, as has been shown by Simon (1988; 1990). In situ oxygen isotope analysis with a spatial resolution of 250 μm and electron microprobe analysis is applied on thick sections of four different locations of the St. Blasien pluton. All thick sections were prepared from hand samples that have already been conventionally analysed for oxygen isotopes by Simon (1990). A combination of in situ- and electron microprobe data is used to discuss fluid-rock interaction on a scale ranging from kilometers to sub-millimeters. Among the questions addressed are:

- (1) On which scale does oxygen isotope disequilibrium for the system mineral-fluid in a single intrusion occur?
- (2) At which structural interface did a fluid-rock interaction take place and what have been the main mechanisms of oxygen isotope exchange?
- (3) What new constraints can be drawn by in situ- and electron microprobe data on fluid evolution and alteration history of granites of the southeastern Schwarzwald?
- (4) Does in situ data coincide with conventional data?

3.2. Geological setting and sample description

The Schwarzwald is part of the Moldanubian core zone of the Variscan Fold Belt which extends from the Bohemian Massif (CSFR) to the Massif Central (France), the Pyrenees (Spain) and also to parts of the Appalachian (USA). Fig. 3.1 gives an overview on the southern Schwarzwald and its granitic intrusions. Not all of these granites have been dated, but for the undated granites an appropriate age of emplacement can be made on the basis of the geological map of Metz & Rein (1958) in combination with existing Rb/Sr data by Leutwein & Sonet (1974). A detailed review is given by Taylor et al. (1991).

From structural coherence, the St. Blasien pluton belongs to a group of less-deformed, late-tectonic granites, which further includes the Albtal, Malsburg and Münsterhalden granites. For the latter granite, Leutwein & Sonet (1974) reported Rb/Sr-ages of 314 ± 15 Ma and 322 ± 15 Ma, respectively. According to the petrogenetic model of Emmermann (1977) they represent melts from plagioclase- and biotite-rich paragneisses, producing large volumes of biotite granite. Metz (1964) specified the average modal proportions of minerals for the St. Blasien granite to be 26.8% quartz, 35.7% plagioclase (an_{10-40}), 29.1% alkali feldspar, 8.2% biotite (partly chloritised) and 0.2% accessory minerals (e.g. apatite, zircon).

For oxygen isotope analysis, four samples of the St. Blasien pluton were taken within 10 kilometers distance (Fig. 3.1): GSB 10 derives close to the Badenweiler-Lenzkirch tectonic line, while GSB 7 derives close to the triple junction of Schluchsee-, Bärhalde- and St. Blasien granites. GSB 6 and GSB 14 were taken in one km distance of each other, located inbetween GSB 10 and GSB 7. From averaged in situ oxygen isotope data it appears that GSB 6 interacted to the smallest and GSB 10 to the strongest degree with a fluid low in $\delta^{18}O$ (Tab. 3.2). Therefore, these two samples are petrographically described in detail:

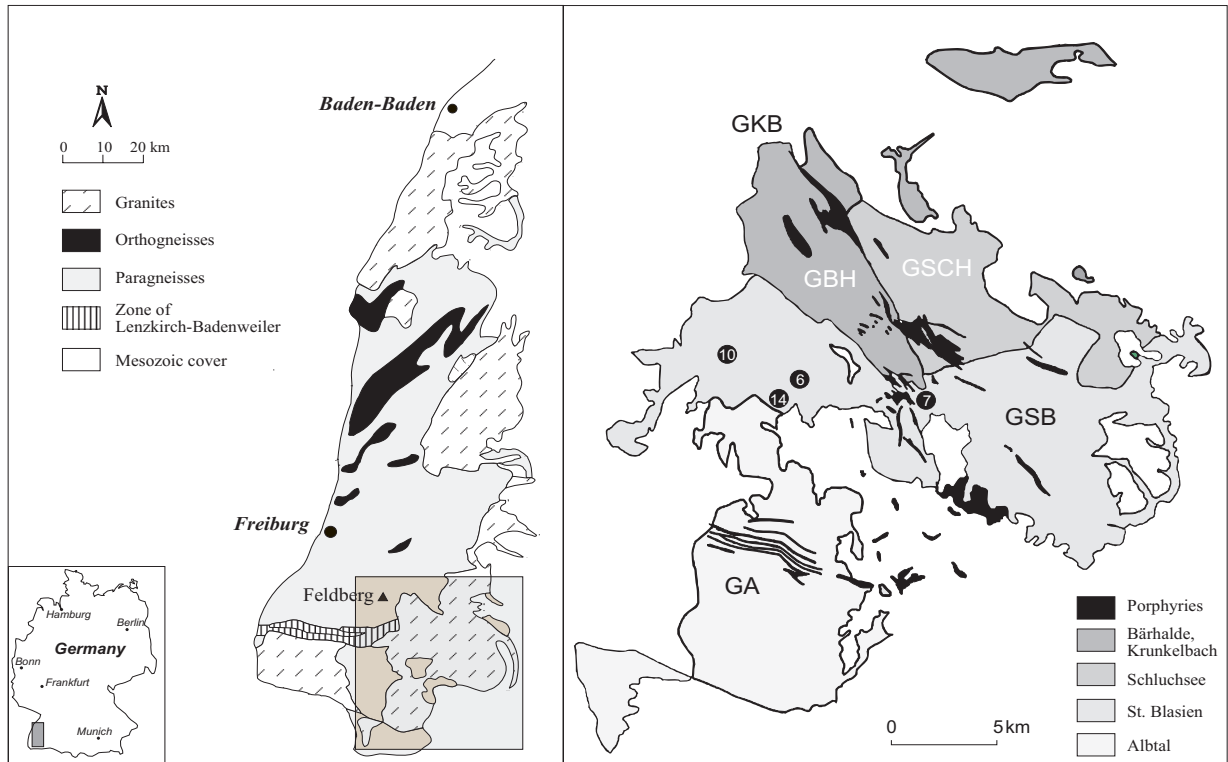


Fig. 1. Geological setting of the southern Schwarzwald and its granite occurrences. Emplacement of syn-tectonic granites (e.g. Rand-Granite; not shown) within the Badenweiler-Lenzkirch tectonic line marked a change in the tectonic regime from collisional shortening to crustal extension at about 340 Ma ago (Taylor et al., 1991; Echtler & Chauvet, 1991-1992). Biotite-rich St. Blasien- and Albtal-Granite probably intruded next (Metz & Rein, 1958; Echtler & Chauvet, 1991-1992), while two-mica granites Schluchsee and Bärhalde are about 300 Ma old and thus of post-tectonic origin (e.g. Müller-Sohnius et al., 1976; Wendt et al., 1974). Samples were exclusively taken from late-tectonic St. Blasien-Granite.

GSB 10:

GSB 10 shows a very intense alteration: Primary magmatic minerals are almost totally replaced by secondary minerals. Multiple sets of microcracks pass through all minerals. Biotite has been completely altered to chlorite, while plagioclase has been converted to albite and calcite. K-feldspar is partly replaced by albite.

GSB 6:

GSB 6 exhibits graphic intergrowth of quartz and K-feldspar. Alteration of biotite to chlorite occurred to a much lesser extent than in GSB 10 and is preferentially observed along microcracks. Plagioclase is often albitised towards the rim, but still shows primary magmatic zonation within the core. In contrast to GSB 10, no calcite has been found and K-feldspar does not include any secondary minerals. Additionally, GSB 6 exhibits much less microcracks than GSB 10.

3.3. Analytical procedure

All granite samples have been analysed as thick sections (ca. 10 x 10 x 4 mm). Prior to analysis, thick sections have been ultrasonically cleaned with distilled water and vacuum dried over night at 300 °C.

In situ oxygen isotope analysis has been carried out using the instrumentation described in chapter 2. For oxygen isotope extraction from GSB 6, 7 and 14 a Lextra 200 excimer laser (Lambda Physik Inc.) has been used ($\lambda = 248$ nm), while GSB 10 has been analysed with a Compex 205 (Lambda Physik Inc.) radiating at 193 nm. At high energy densities (≈ 40 J/cm²), even quartz can be analysed at 248 nm, although oxygen yields are still not as good as when operating with an ArF-laser at 193 nm (see chapter 1.5).

During analyses of GSB 6, 7 and 14, two standards (San Carlos olivine, $\delta^{18}\text{O} = 5.2$ ‰; Dörentrup quartz: $\delta^{18}\text{O} = 12.1$ ‰) have been run along with the samples. For all runs, the standard varied between 5.0 ‰ and 6.2 ‰ for the olivine, and between 10.5 and 11.1 ‰ for Dörentrup quartz, respectively. The observed contaminations are most likely attributable to a reaction of sample feldspar and fluorine, as proposed by Elsenheimer & Valley (1993). Within each run, this contamination seemed to be constant suggesting that both the amount and the $\delta^{18}\text{O}$ -value of blank oxygen stayed constant throughout a daily analysis (Tab. 3.1).

For raw data correction, both the amount and the $\delta^{18}\text{O}$ -value of the blank have been calculated using equation (1):

$$(1) \ x \cdot \delta^{18}\text{O}_{\text{std (corr.)}} + (1-x) \cdot \delta^{18}\text{O}_{\text{blank}} = \delta^{18}\text{O}_{\text{std (raw)}} \text{ with } x = n_{\text{std}} / (n_{\text{std}} + n_{\text{blank}})$$

Standard analyses were performed at the beginning and at the end of each daily run. The amount of released oxygen (n_{std}) has been held constant during all analyses, whereas the amount of blank oxygen (n_{blank}) is assumed to be constant (see observation above). x and $\delta^{18}\text{O}_{\text{blank}}$ can then be calculated by solving equation (1) for each standard. For this calculation only averaged standard raw values have been considered. Each sample raw value has then been corrected for the calculated blank oxygen contribution.

Table 3.1 lists the daily calculated blanks together with the $\delta^{18}\text{O}$ -values of corresponding feldspars. It is obvious that blank $\delta^{18}\text{O}$ -value is always within 2 ‰ of the mean $\delta^{18}\text{O}$ -value of sample feldspar suggesting that the reaction between fluorine and non-irradiated feldspar occurs without much fractionation. Nevertheless, the variation of ± 2 ‰ demonstrates the problems of blank correction by running standards along with the sample. It can not be excluded that both the amount and the $\delta^{18}\text{O}$ -value of blank oxygen is slightly varying from analysis to analysis. For an estimate of the effect of blank variation on data correction two thick sections of one hand sample (GSB 6) have been analysed. However, averaged corrected data of each mineral fraction overlaps within analytical errors for both sections (Tab. 3.2) and demonstrates the accuracy of the above correction.

During in situ analysis of GSB 10 only Dörentrup quartz has been measured along with the sample. In order to calculate the amount of blank oxygen it has therefore been assumed that blank $\delta^{18}\text{O}$ is equal to the average of in situ feldspar analyses.

Electron microprobe investigations have been performed on the same thick sections analysed for oxygen isotopes, using a JEOL JXA 8900 RL, which is equipped with CL- and BSE-detection system.

Date	Sample	$\delta^{18}\text{O}_{\text{Dör.(s)}}$	$\delta^{18}\text{O}_{\text{Dör.(f)}}$	$\delta^{18}\text{O}_{\text{Dör.(avg.)}}$	$\delta^{18}\text{O}_{\text{ol.(s)}}$	$\delta^{18}\text{O}_{\text{ol.(f)}}$	$\delta^{18}\text{O}_{\text{ol.(avg.)}}$	$\delta^{18}\text{O}_{\text{blank}}$	$\delta^{18}\text{O}_{\text{fsp (raw, avg.)}}$
13.07.1999	GSB 6a	10,5	10,9	10,7	5,7	5,0	5,4	6,1	$7.7 \pm 0.3; n = 14$
14.07.1999	GSB 6b	10,6	10,9	10,8	5,6	5,3	5,5	6,5	$7.9 \pm 0.4; n = 4$
16.07.1999	GSB 7	11,0	11,1	11,1	5,8	6,2	6,0	8,3	$6.8 \pm 0.2; n = 6$
12.07.1999	GSB 14	10,6	10,7	10,7	5,3	5,1	5,2	5,2	$5.7 \pm 0.6; n = 7$

Tab. 3.1. Oxygen isotope composition of daily blank oxygen calculated by using equation (1). For each daily load of the sample chamber, two standards have been measured along with the samples (Dörentrup-qtz: 12.1 ‰ and San Carlos olivine: 5.2 ‰). For a calculation of blank oxygen, initial (s) and final (f) standard $\delta^{18}\text{O}$ -raw-values have been averaged for each standard. Raw $\delta^{18}\text{O}$ -values of daily loaded feldspar is listed for a comparison. All $\delta^{18}\text{O}$ -values are given in ‰-deviation relative to V-SMOW.

3.4. Principles of fluid-rock interaction

A knowledge of the mechanisms of oxygen isotope exchange between fluid and rock is a prerequisite to understand disequilibrium and equilibrium systems in nature. Generally, oxygen isotope exchange between fluid and mineral can occur by (Lasaga, 1981a,b; Giletti, 1985):

- (1) diffusion
- (2) dissolution-recrystallisation
- (3) chemical reaction.

Given that meteoric fluid-rock systems are initially far away from chemical equilibrium, processes (2) and (3) should be thermodynamically favored over process (1): The driving force for each type of exchange mechanism is the attempt of the Gibbs free enthalpy (G) to attain a minimum. For a given temperature, the change in Gibbs free enthalpy during one of the above mechanisms is: $\Delta G = \Delta G^{\circ} + RT \ln K$;

ΔG° : standard free molar reaction enthalpy at temperature T ($\Delta G^{\circ} = (\sum_i \nu_i \mu_i^{\circ})_{\text{products}} - (\sum_i \nu_i \mu_i^{\circ})_{\text{educts}}$; where ν is the stoichiometric coefficient and μ the Gibbs free molar enthalpy of any involved species i)

K : equilibrium constant at temperature T

An exchange between fluid and mineral occurs, if the standard Gibbs free reaction enthalpy ΔG° is negative. The exchange proceeds until for each species equilibrium concentrations are attained and ΔG thereby approaches zero. Process (1) occurs under preservation of pre-existing minerals and, thus, ΔG° is already close to zero. For processes (2) and (3) ΔG° is expected to be fairly negative, since either new minerals are formed (process 3) or parts of minerals are dissolved (process 2). Thus, diffusion can be the primary mechanism when equilibrium is nearly attained and processes (2) and (3) are ceasing (Cole et al., 1983; Matthews et al., 1983).

An exchange by dissolution-recrystallisation and chemical reaction is also kinetically favored over diffusional exchange: Activation energies for oxygen isotope exchange by chemical reaction and dissolution processes are usually lower than those for diffusional exchange (Cole & Ohmoto, 1986). Criss et al. (1987) pointed out that no large differences in relative rate constants are required to model fluid-rock exchange trajectories for mineral pairs in δ - δ -space. At a given temperature, diffusion coefficients of natural materials vary by several orders of magnitude, whereas rather similar rates of oxygen isotope exchange are observed in hydrothermal experiments involving dissolution (Wood & Walther, 1983).

These theoretical assumptions are confirmed by both experimental and field studies: Cole et al. (1992) demonstrated by hydrothermal experiments on granites between 170 and 300 °C

that an initial exchange of oxygen isotopes between granite and fluid occurs exclusively by chemical reaction and dissolution-recrystallisation. Rumble et al. (1986) observed that the degree of alteration of quartz and feldspar of granites from South-Central Maine, USA, corresponds with the amounts of secondary minerals. Valley & Graham (1996) determined by a combination of SIMS for oxygen isotope analysis and CL dissolution-recrystallisation to be the exclusive exchange mechanism between hydrothermal fluids and quartz from Skye granites. Their observations are confirmed by King et al. (1997), who analysed hydrothermally altered quartz phenocrysts from the Kidd Creek mine, Ontario, by CL and CO₂-laser fluorination.

For a better understanding of the kinetics of isotopic exchange not only the mechanisms, but also the interfaces of fluid-rock interaction have to be investigated. Generally, subsolidus isotope exchange between fluid and rock is assumed to occur along microcracks, micropores and grain boundaries (e.g. Krantz, 1983; Worden et al., 1990; Arita & Wada, 1990; Fein et al., 1994; Holness & Graham, 1995). In order to deduce the style of fluid flow during hydrothermal alteration, Elsenheimer & Valley (1993) investigated small wafers of quartz and feldspar grains from a Granite, Isle of Skye, Scotland, by IR-laser fluorination. They obtained intragranular oxygen isotope zonation pattern which are best explained by a fluid-rock interaction along a multiple set of microcracks. Within single quartz grains, secondary quartz of low $\delta^{18}\text{O}$ has crystallised along these microcracks (Valley & Graham, 1996). A crack controlled fluid flow also occurred during hydrothermal alteration of quartz from Kidd Creek rhyolites, Ontario (King et al., 1997).

3.5. Scale of disequilibrium

In order to estimate whether equilibrium has been attained throughout a fluid-rock interaction one first has to define the system which is investigated:

First, exchange rates differ from mineral to mineral, such that some minerals of a rock may equilibrate with the fluid during a hydrothermal event, whereas others do not. For granites worldwide it has been observed that quartz is isotopically far more resistant to hydrothermal alteration than is feldspar or biotite in the same rock (e.g. Taylor, 1977; Taylor, 1978; Ferry, 1985; Magaritz & Taylor, 1986; Gregory et al., 1989, Simon, 1990; Elsenheimer & Valley, 1993). Thus, throughout the extent of a hydrothermal event, granitic subsystems excluding quartz are more likely to equilibrate with a fluid than the superior, entire granitic system including quartz.

Secondly, since diffusion is likely to be too slow to show any contribution to hydrothermal granitic alteration (Cole et al., 1992), all minerals that have interacted with a fluid are assumed to be of secondary nature. For an evaluation whether equilibrium between secondary minerals has been attained it is therefore necessary to analyse primary and secondary minerals separately

from each other. This is a serious problem, because it is often difficult and much effort to discriminate between primary and secondary minerals, especially when, such as in the case of conventional analysis, large amounts of sample material are needed. As a consequence, disequilibrium may be the result of mixed analysis of primary and secondary minerals, although both primary and secondary mineral pairs between themselves may exhibit equilibrium fractionations.

Throughout this study, oxygen isotope data will be discussed on a scale ranging from kilometers to the minimum resolution of the applied technique, 250 μm . First, averaged in situ data will be used to describe km processes. Therefore it has not been differentiated between primary and secondary minerals, as it is done for conventional analysis (e.g. Simon, 1990, Taylor et al., 1991). Secondly, single in situ data of coexisting minerals is used to investigate the cm to sub-mm scale. Here, BSE- and CL-visualisations by electron microprobe have been used to differentiate between primary and secondary minerals.

3.5.1. Km-scale: averaged in situ data

All samples were taken within a distance of 10 kilometers. Hence, averaged in situ oxygen isotope data plotted in δ - δ -diagrams exhibit information about the extent of granite alteration, that occurred on a km-scale. For a calculation of averages only those analyses have been considered for which mixed analyses of primary minerals could have been excluded by electron microprobe analysis. An exception has been made for feldspar, which has not been differentiated between its single subphases plagioclase and K-feldspar. Corresponding δ - δ -plots are shown in Figs. 3.2a,b,c. All data is additionally listed in Table 3.2.

All analysed samples have lost their primary magmatic character which is indicated by a shift of oxygen isotope composition of either (both) feldspar (Figs. 3.2a) or (and) biotite/chlorite (Fig. 3.2b) below the primary magmatic fractionation line. Positive slopes of quartz-feldspar and quartz-biotite/chlorite exchange trajectories indicate that the granite interacted with an externally derived fluid enriched in ^{16}O . Additionally, these slopes are different from unity. Thus -on a km scale- equilibrium within the system quartz/feldspar/biotite(chlorite)/fluid has not been attained. GSB 10 has interacted to the greatest extent with the fluid, so that even quartz is slightly depleted in ^{18}O , whereas GSB 6 shows the least extent of fluid-rock interaction.

$\delta^{18}\text{O}_{\text{qtz}}$	$\delta^{18}\text{O}_{\text{fsp}}$	$\delta^{18}\text{O}_{\text{bio}}$	$\delta^{18}\text{O}_{\text{whole rock (calc.)}}$	$\delta^{18}\text{O}_{\text{whole rock}}$
9.3 ± 0.1 (n = 2)	7.7 ± 0.3 (n = 14)	3.9 ± 0.6 (n = 9)		
9.0 ± 0.2 (n = 5)	7.9 ± 0.4 (n = 4)	4.5 ± 1.2 (n = 12)		
9.3 (n = 1)	6.8 ± 0.2 (n = 6)	4.5 ± 0.5 (n = 7)		
6.1 ± 0.5 (n = 4)	0.1 ± 0.6 (n = 14)	-4.0 ± 0.5 (n = 4)		
8.0 (n = 1)	5.7 ± 0.6 (n = 7)	1.5 ± 0.8 (n = 8)		
10.3 ± 0.3	8.3 ± 0.4	3.3 ± 0.8	7.9	
9.7 ± 0.3	8.3 ± 0.5	3.9 ± 1.6	7.9	
9.7	6.3 ± 0.3	3.2 ± 0.7	6.7	
7.1 ± 1.0	0.1 ± 0.7	-4.5 ± 0.5	2.0	
8.8	5.9 ± 0.8	0.5 ± 1.0	6.2	
12.5	10.8	1.9	9.7	8.3
11.6	8.6	4.5	8.8	8.6
9.7	3.4	1.9	5.3	3.7
12.4	5.9	2.1	7.4	7.1

Tab. 3.2. Averaged $\delta^{18}\text{O}$ -values as derived from in situ- and conventional analysis for granites from the St. Blasien pluton (n: number of analysis). Modal compositions for each location, which have been used to calculate whole rock $\delta^{18}\text{O}$ -values, are given by Simon (1990). All $\delta^{18}\text{O}$ -values are given in ‰-deviation relative to V-SMOW.

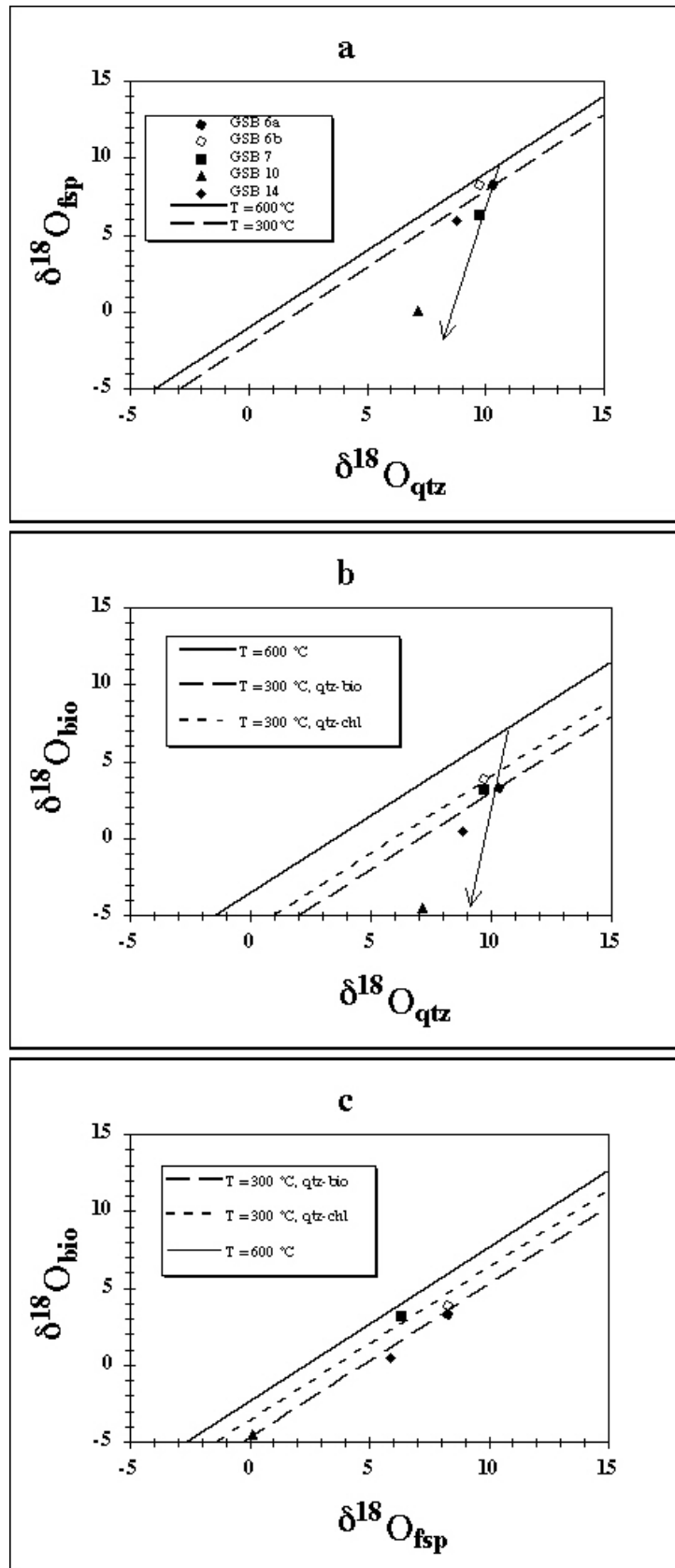


Fig. 3.2. δ - δ -diagrams of coexisting minerals derived from averaged in-situ data. Isothermic equilibrium fractionations have been adopted by Zheng (1993a,b). Diagram sequence: (a) qtz-fsp, (b) qtz-bio, (c) fsp-bio. For further discussion see chapter 3.5.1.

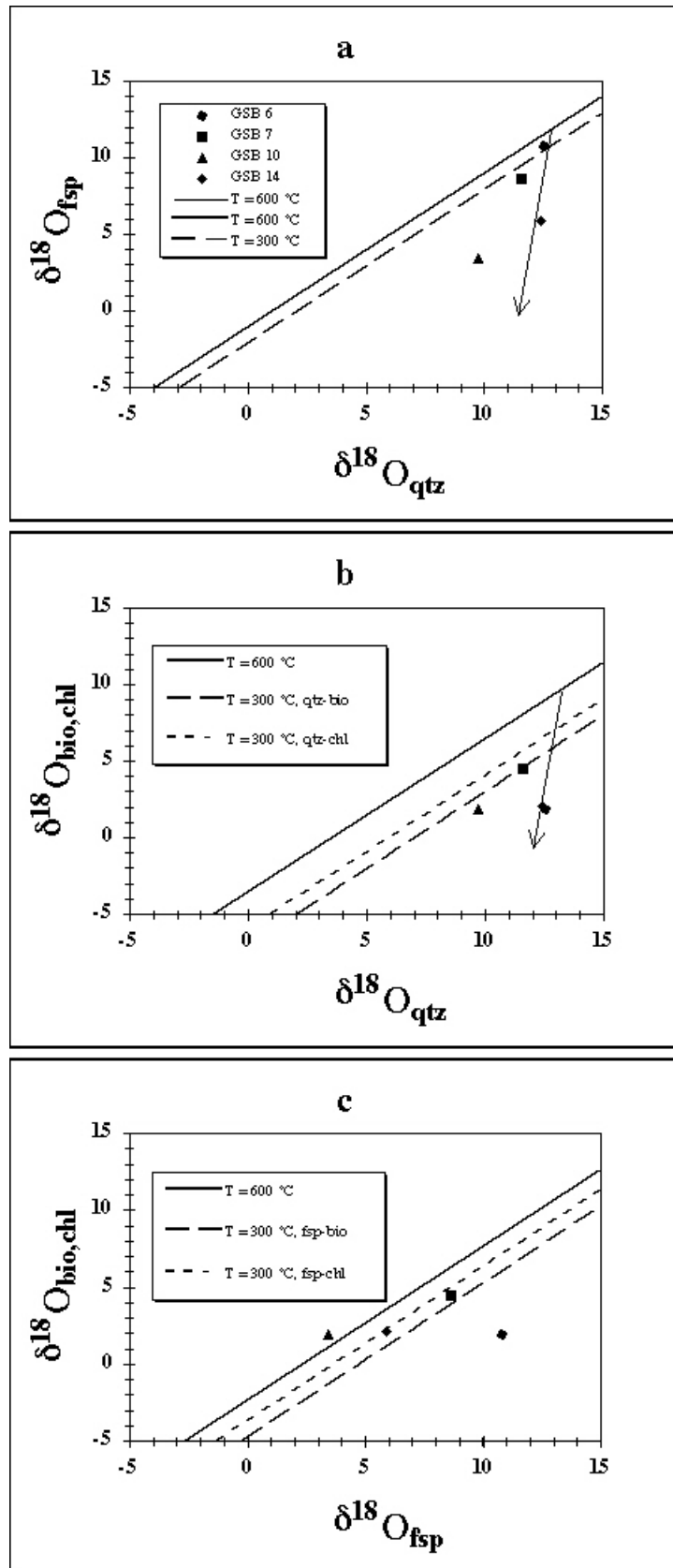


Fig. 3.3. δ - δ -diagrams of coexisting minerals derived from conventional analysis. Sequence chosen as in Fig. 3.2. For further discussion see chapter 3.8.

However, the subsystem feldspar/biotite(chlorite)/fluid seems to have behaved differently from its superior system (Fig. 3.2c): Four of five analysed samples plot very well on a fractionation line for $T = 300\text{ }^{\circ}\text{C}$. Provided that the initial isotopic composition of the fluid has been rather homogeneous (see chapters 3.5.2 and 3.7), the heterogeneity in isotopic composition of different locations that is reflected by the spread along the $T = 300\text{ }^{\circ}\text{C}$ isotherm can be explained in two ways:

(1) Fluid-rock exchange occurred under "closed" system conditions (Gregory & Criss, 1986; Criss et al., 1987), where relative proportions between each mineral and fluid have been constant. Equilibrium has been attained on a km-scale within the subsystem feldspar/biotite(chlorite)/fluid. Heterogeneity results from varying water/rock-ratios.

(2) Fluid-rock interaction took place under open system conditions (Gregory & Criss, 1986; Criss et al., 1987), where an externally derived fluid has been progressively infiltrated. Disequilibrium occurs on a km-scale. The spread along the $300\text{ }^{\circ}\text{C}$ isotherm is caused by varying water-rock ratios, fluid fluxes and time-spans of interaction.

Clearance should be given by in situ data of coexisting, neighbouring minerals. If diffusion can be ruled out (Cole et al., 1992), in the case of (1) all coexisting minerals except quartz should be in equilibrium, whereas in the case of (2) coexisting minerals exhibit disequilibrium fractionations.

Surprisingly, GSB 7 reveals an oxygen isotope composition, that cannot be explained by processes (1) or (2): Its $\delta^{18}\text{O}_{\text{fsp, bio}}$ lies very close to the isotherm of $600\text{ }^{\circ}\text{C}$. Such high temperatures are rather unusual for hydrothermal alterations of granites. It is therefore more likely, that GSB 7 exhibits a complex alteration history due to its nearby location to the Bärhalde- and Schluchsee pluton (see chapter 3.7).

To sum up, quartz/feldspar and quartz/biotite/chlorite exchange trajectories derived from averaged in situ data give evidence that -on a scale of a few kilometers- equilibrium between granite and fluid has not been reached. However, feldspar/biotite/chlorite data fits well to a $300\text{ }^{\circ}\text{C}$ isotherm suggesting that the subsystem feldspar/biotite(chlorite)/fluid might have been able to attain equilibrium.

3.5.2. Cm-sub-mm-scale: implications by in situ analysis

From all samples analysed, GSB 6 shows the least extent of fluid-rock interaction. A BSE-picture and corresponding $\delta^{18}\text{O}$ -values of in situ analysis from a large biotite grain within GSB 6b are shown in Figs. 3.4a,b. The biotite grain is partly chloritised (grey parts). It is obvious that chloritisation occurred preferentially along cleavages and microcracks. Spatial resolution of 250

μm has not been sufficient to analyse biotite and chlorite separated from each other. $\delta^{18}\text{O}$ -values of mixed mineral pairs vary by 4.1 ‰ depending on the degree of chloritisation: Less altered biotite zones exhibit nearly primary magmatic oxygen isotope composition (e.g. 6.3 ‰), whereas strongly chloritised parts are as low as 1.2 ‰. Since only chlorite/biotite mixtures could have been measured, pure chlorite is expected to have a negative $\delta^{18}\text{O}$ -value (see below). However, if equilibrium between biotite and chlorite at $T = 300\text{ }^{\circ}\text{C}$ would have been attained, chlorite should be characterised by a $\delta^{18}\text{O}$ -value which is about 1 ‰ higher than the biotite $\delta^{18}\text{O}$ -value (Zheng, 1993a). Thus, secondary chlorite is in strong disequilibrium with coexisting, primary biotite. Chlorite, that was formed by a reaction of biotite and fluid, must inherit its oxygen mainly from the fluid, as it has been observed by Cole & Ripley (1999).

GSB 10 shows the strongest interactions with a meteoric fluid. Electron microprobe data give evidence that biotite is completely converted to chlorite. Coexisting plagioclase exclusively occurs as low-albite (an_{0-10}) with calcite replacements along microcracks (for detailed discussion see chapter 3.6.2). From in situ oxygen isotope analysis it seems that secondarily formed chlorite and albite have been in equilibrium with the interacting fluid: Chlorite- $\delta^{18}\text{O}$ -values are as low as -4.9 ‰ (Fig. 3.5). A single secondary albite grain within GSB 10 varies between -0.3 ‰ and -0.9‰ (Fig. 3.6). The observed fractionation between chlorite and albite is very close to an equilibrium fractionation of 3.8 ‰ at $T = 300\text{ }^{\circ}\text{C}$ (Zheng, 1993a,b). Slightly higher fractionations obtained by in situ analysis might be due to the simultaneous evaporation of small amounts of fluid equilibrated calcite, which would be about 2 ‰ enriched in $\delta^{18}\text{O}$ compared to secondarily formed albite (Clayton & Kieffer, 1991).

The measured $\delta^{18}\text{O}$ -values for chlorite within GSB 10 are in agreement with $\delta^{18}\text{O}$ -values expected for pure chlorite from mixed biotite/chlorite analysis within GSB 6b. It is therefore suggested that GSB 10 and GSB 6b interacted with a fluid of very similar isotopic composition and that chlorite which had been formed within GSB 6b, has also been in local equilibrium with the fluid.

In contrast, K-feldspar has not equilibrated with the fluid on a scale of a few hundred microns: K-feldspar next to chlorite within GSB 10 exhibits $\delta^{18}\text{O}$ -values around 1 ‰ (Fig. 3.5). At $300\text{ }^{\circ}\text{C}$, equilibrium fractionation between chlorite and K-feldspar is 3.6 ‰ (Zheng, 1993a,b), much less than observed. In chapter 3.6.3 it is shown that alteration of K-feldspar occurred both along grain boundaries and microcracks, but that formation of secondary phases is not complete as in the case of plagioclase. Obviously, K-feldspar interacted at a slower rate with the fluid than plagioclase and smaller amounts of fluid-equilibrated secondary phases have been formed. A resolution of $250\text{ }\mu\text{m}$ is not sufficient to separate between primary and secondary phases (see Fig. 9a,b,c) and disequilibrium for the system K-feldspar/chlorite/fluid is obtained.

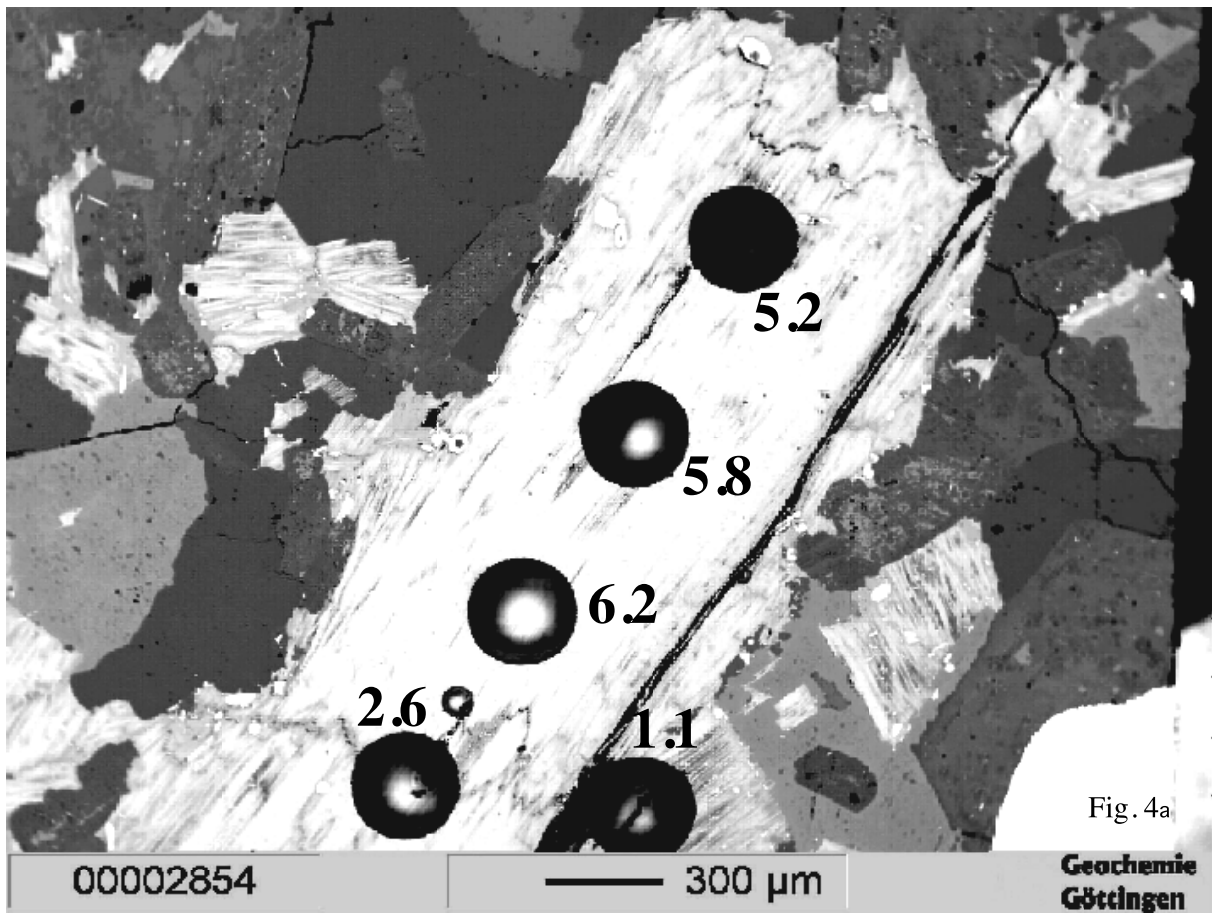


Fig. 4a

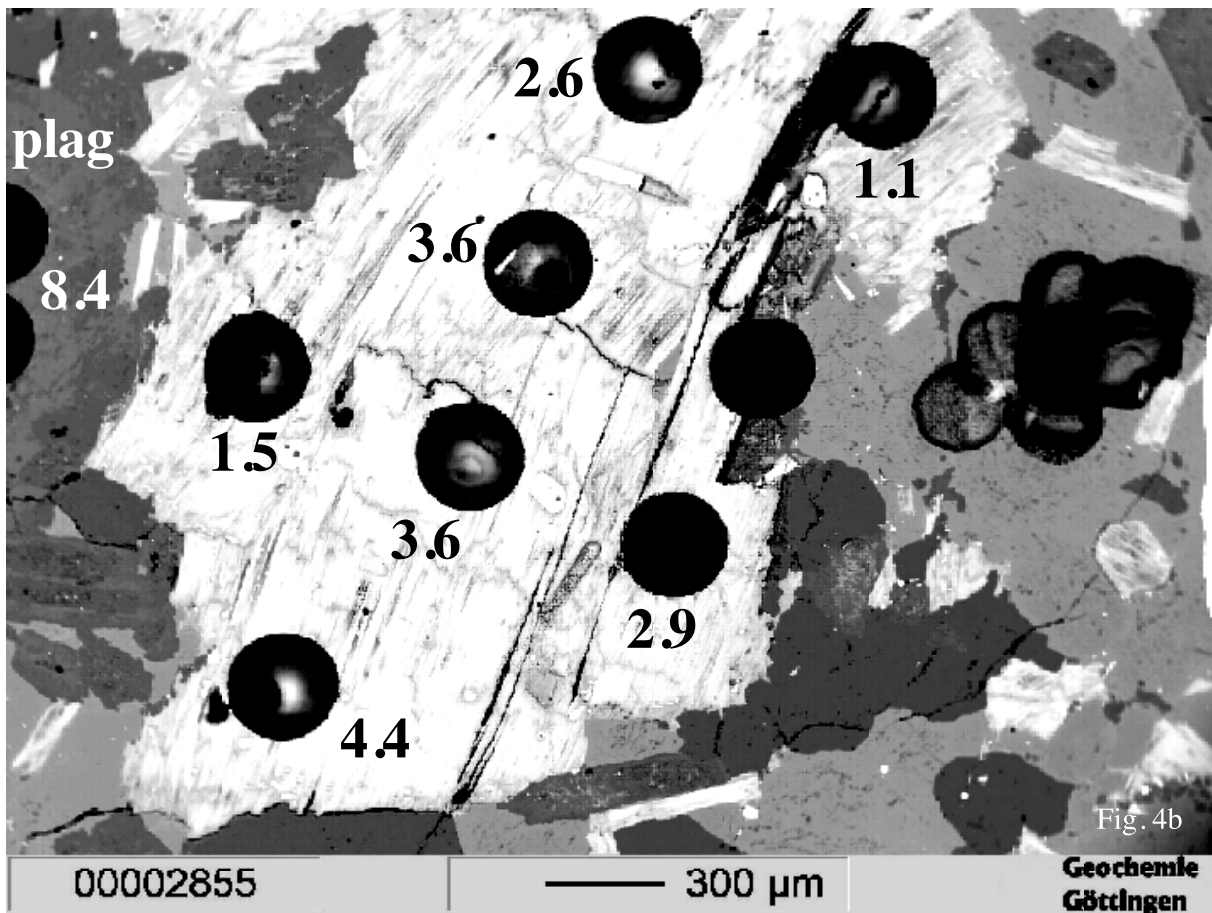


Fig. 4b

Fig. 3.4. BSE-picture of an in situ analysed biotite grain from GSB 6b. Dark grey colour is indicative for chlorite, which has been secondarily formed along microcracks and cleavages.

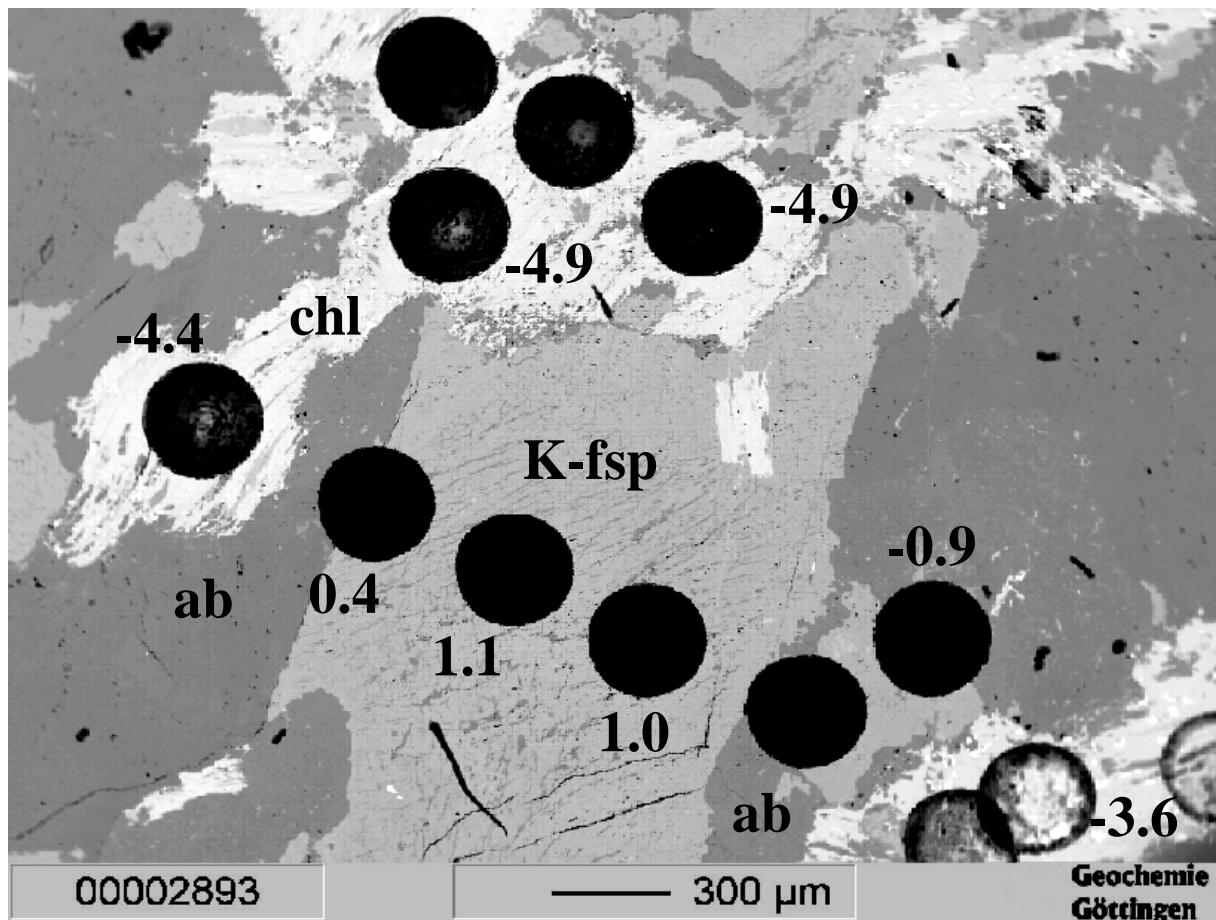
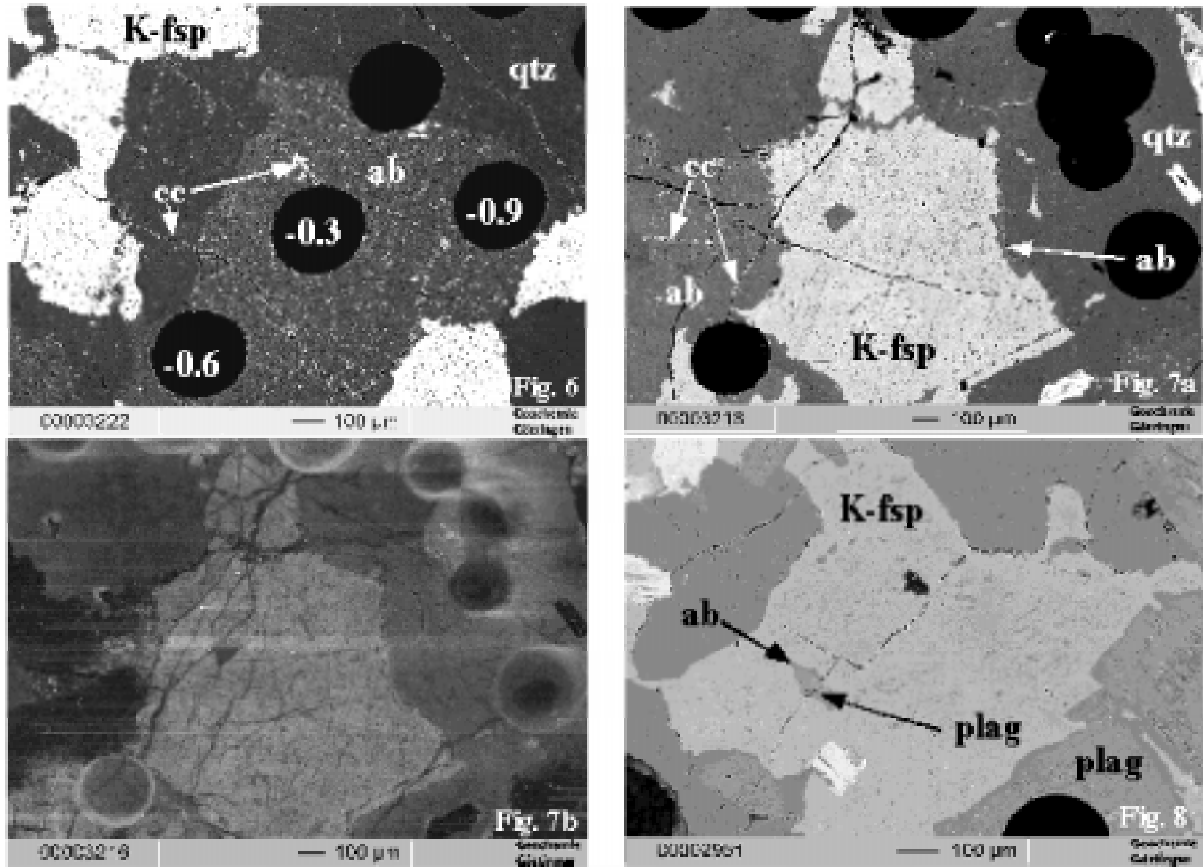
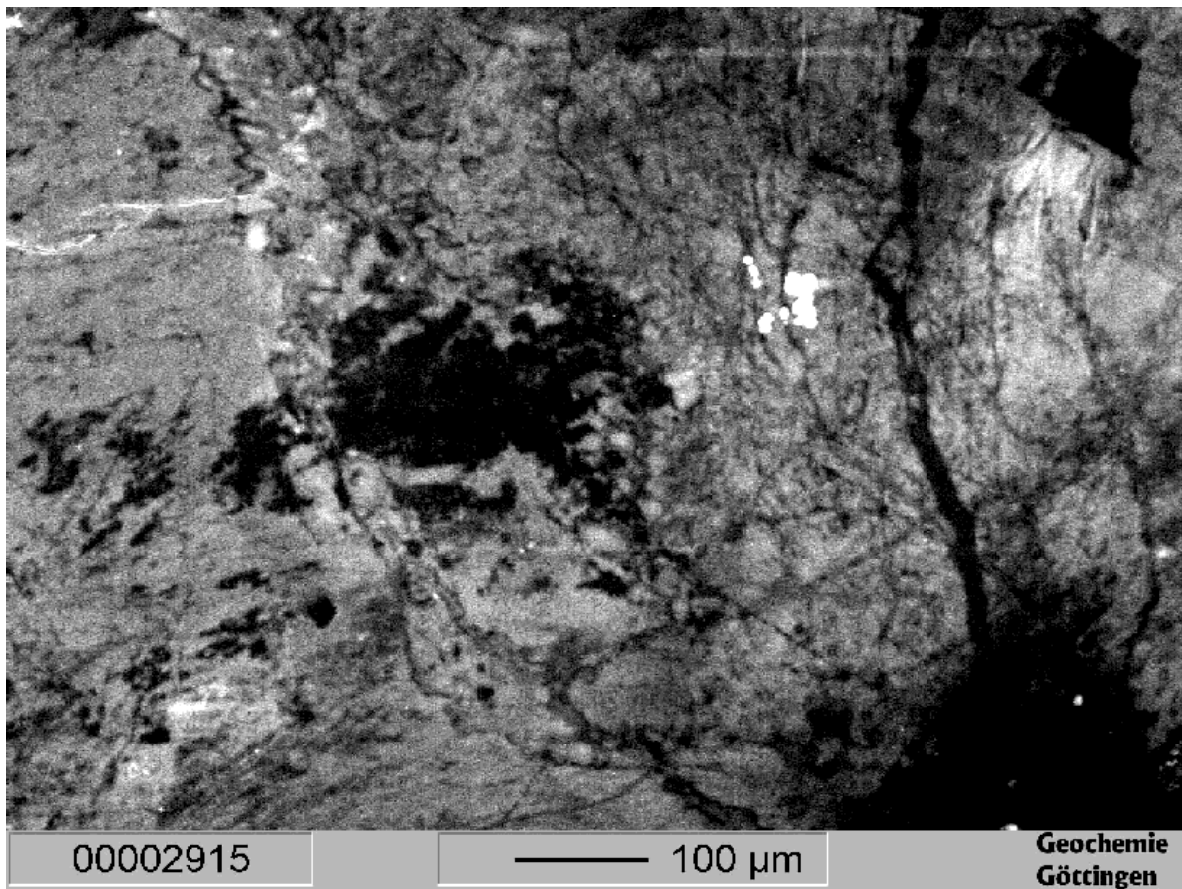
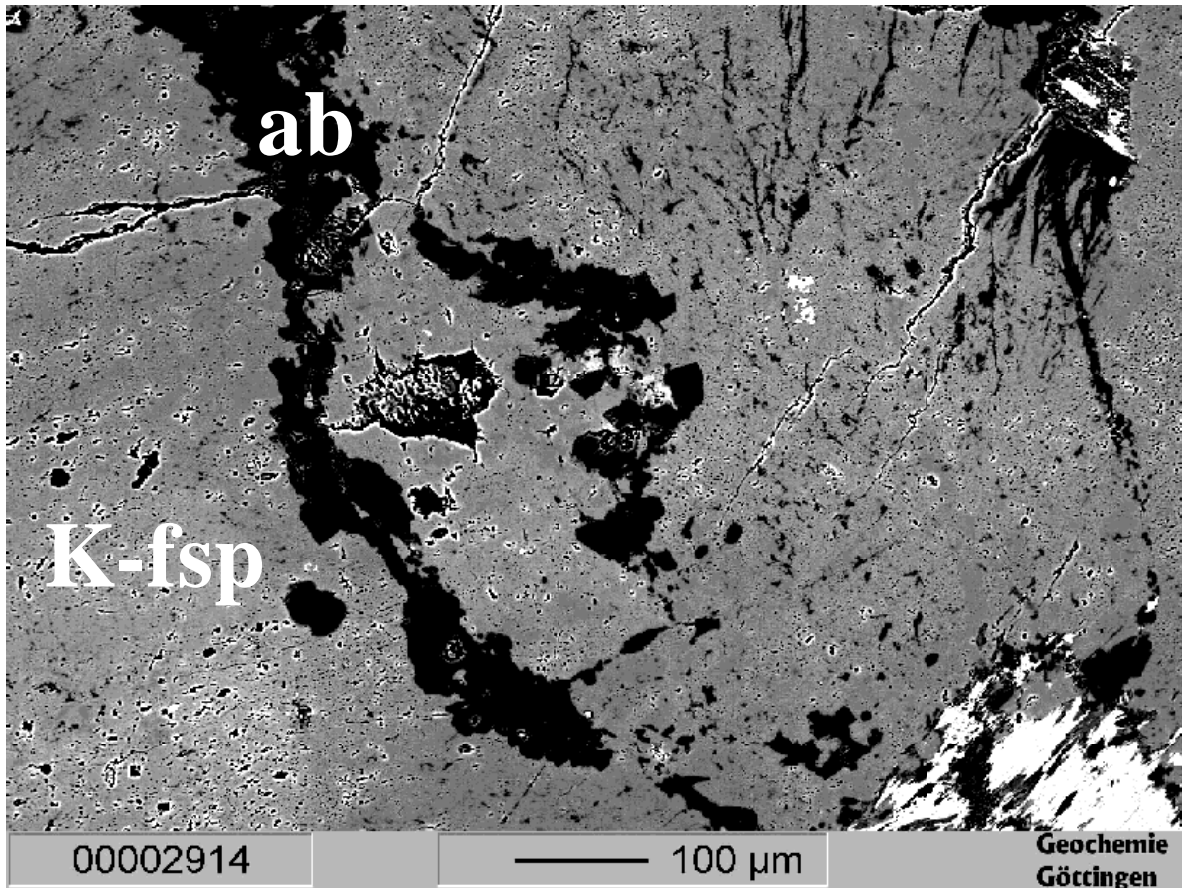


Fig. 3.5. BSE-imaging of chlorite neighbouring K-feldspar within GSB 10.



Figs. 3.6 – 3.8. BSE- and CL- visualisations of granite samples investigated for oxygen isotopes. (6): BSE-imaging of albite with calcite replacements along microcracks within GSB 10; (7a): BSE-imaging of partly albitised K-feldspar and neighbouring quartz within GSB 10; (7b): corresponding CL-imaging of K-feldspar and quartz shown in a BSE-mode in (7a); (8): BSE-imaging of K-feldspar from GSB 6b exhibiting a slightly albitised plagioclase inclusion within K-feldspar. For detailed discussion see chapters 3.5.2 and 3.6.



Figs. 3.9a,b. BSE (9a)- and corresponding CL (9b)-imaging of two neighbouring, albitised K-feldspar grains within GSB 10. Albitisation occurred along the grain boundary between both grains. Lots of microcracks run through both grains.

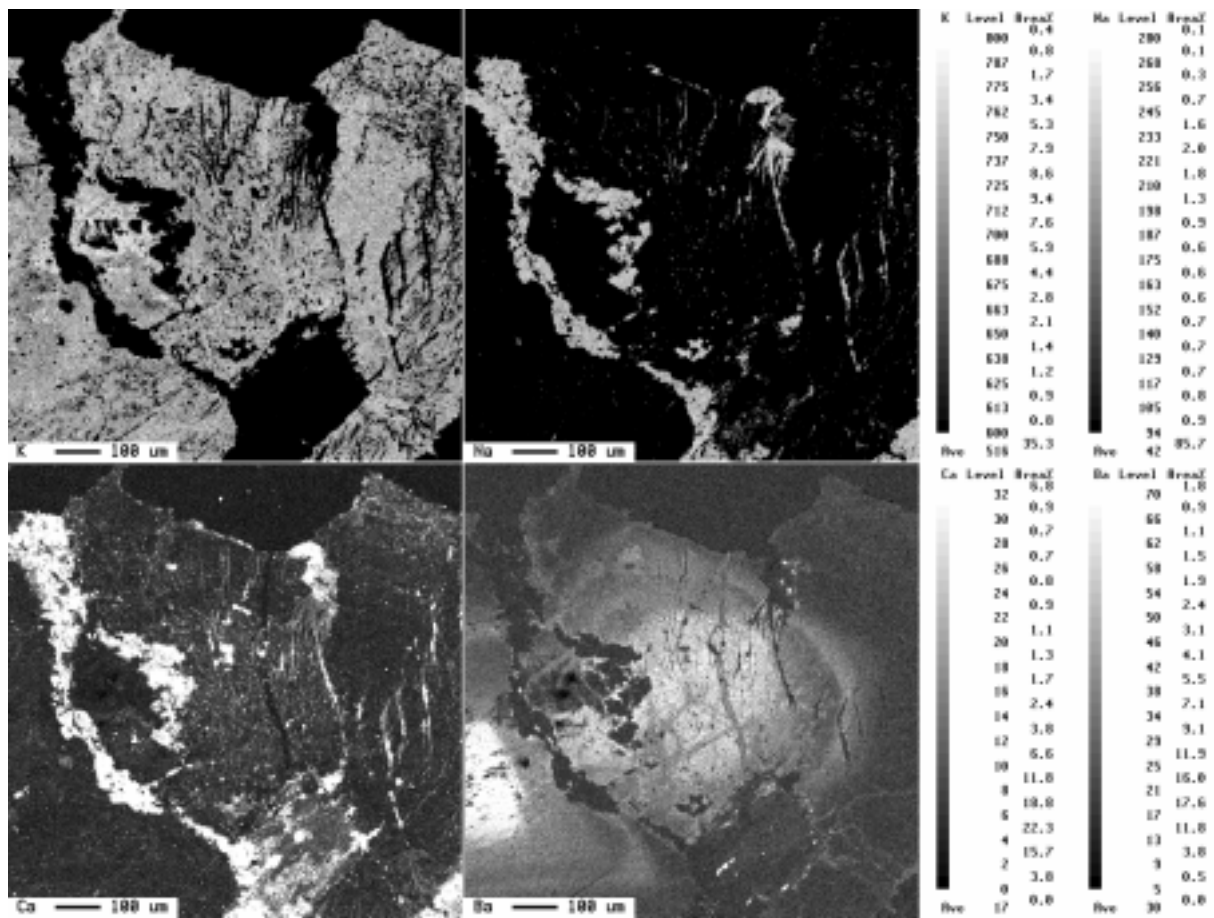


Fig. 3.9c. Element mapping (Na, K, Ca, Ba) of two neighbouring, albitised K-feldspar grains within GSB 10. Along microcracks Ba²⁺ and Ca²⁺ has been leached. See also corresponding BSE- and CL-pictures in Figs. 3.9a,b. For further discussion see chapter 3.6.

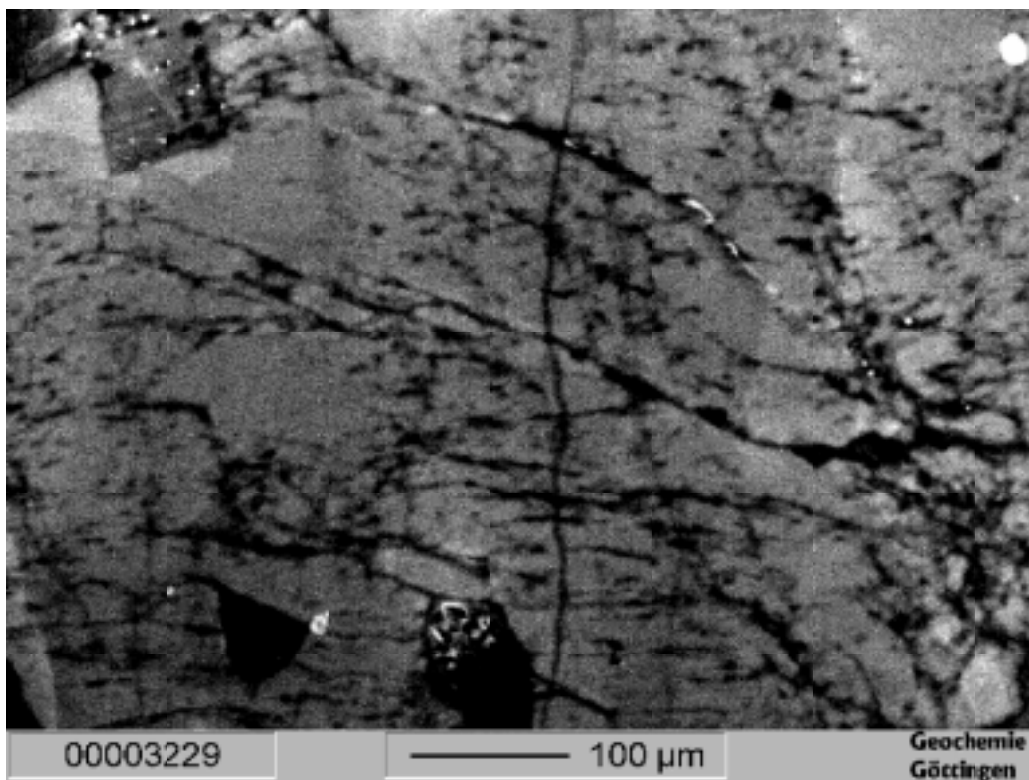
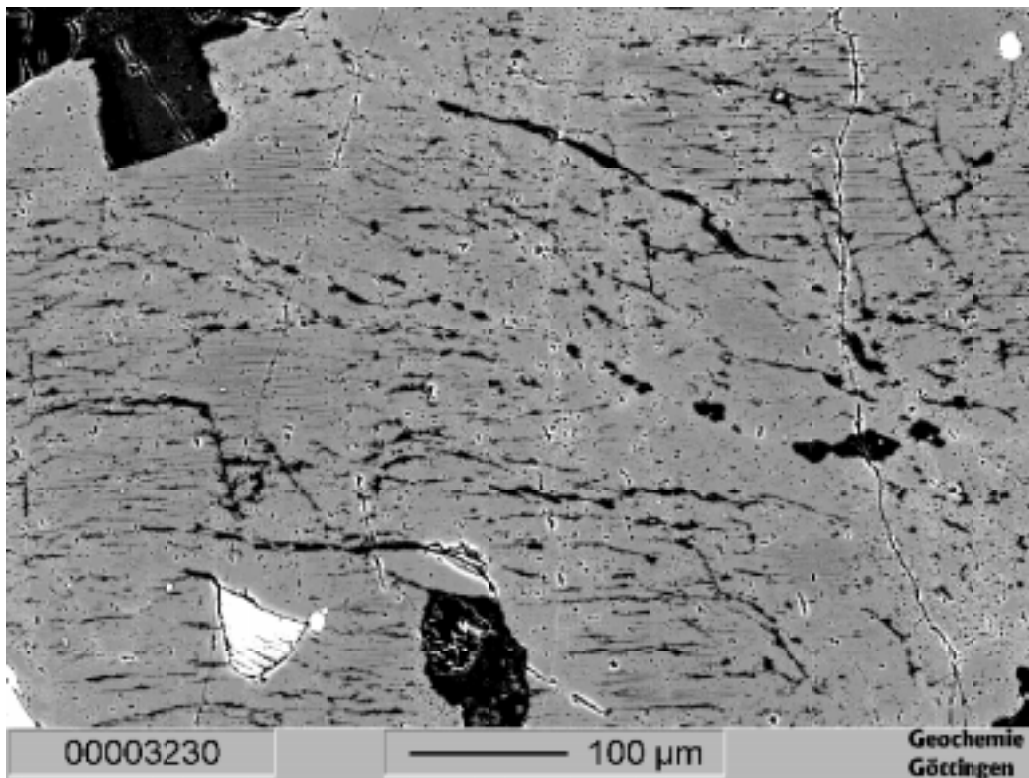


Fig. 3.10a,b. BSE (a)- and CL (b)-picture of a single K-feldspar-grain within GSB 6b. In contrast to K-feldspar within GSB 10, much less microcracks are observed, along which fluid-rock interaction took place. Most "channels" represent primary magmatic perthitic lamellae. See also discussion in chapter 3.6.

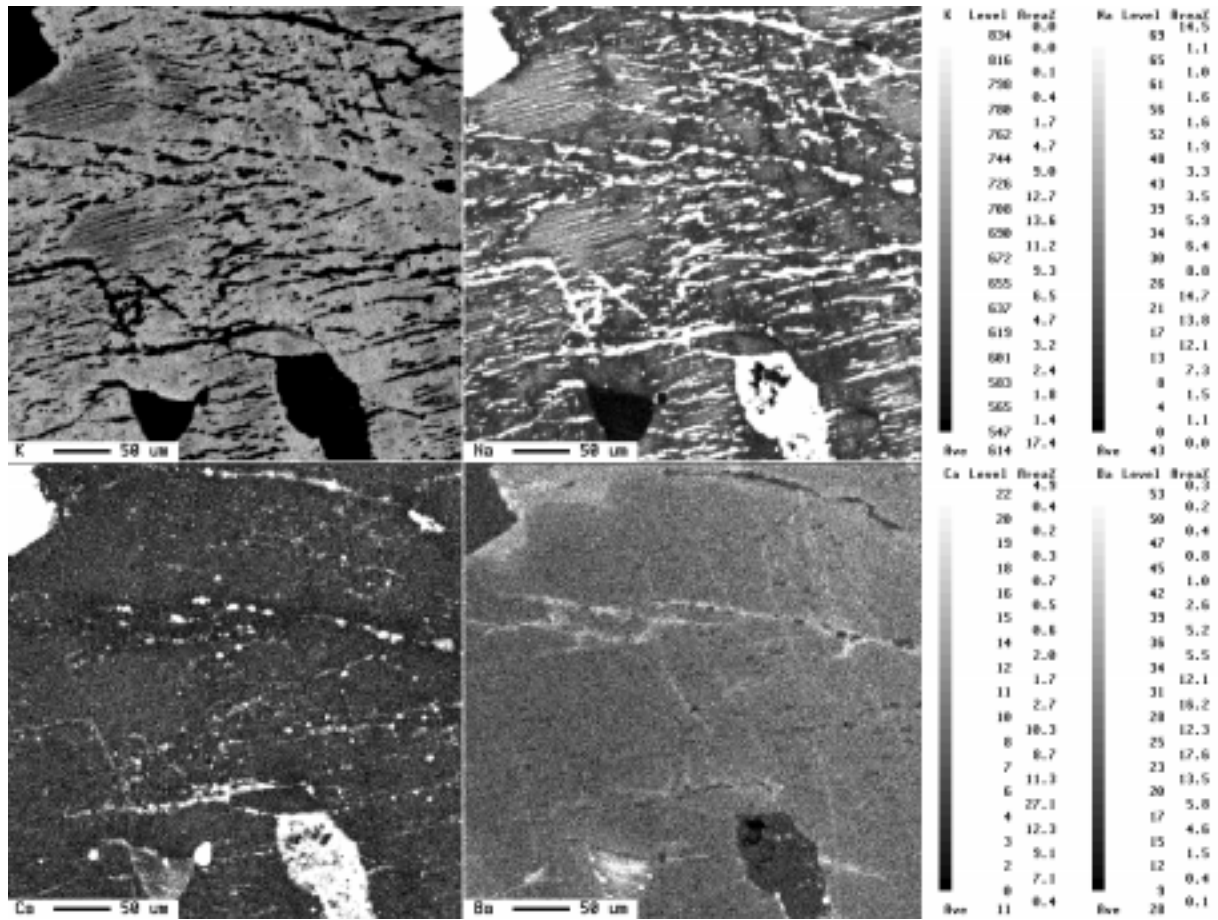


Fig. 3.10c. Element mapping (Na, K, Ca, Ba) of a single K-feldspar-grain within GSB 6b. As from Figs. 3.10a,b it can easily be seen that most "channels" represent primary magmatic perthitic lamellae. See also discussion in chapter 3.6.

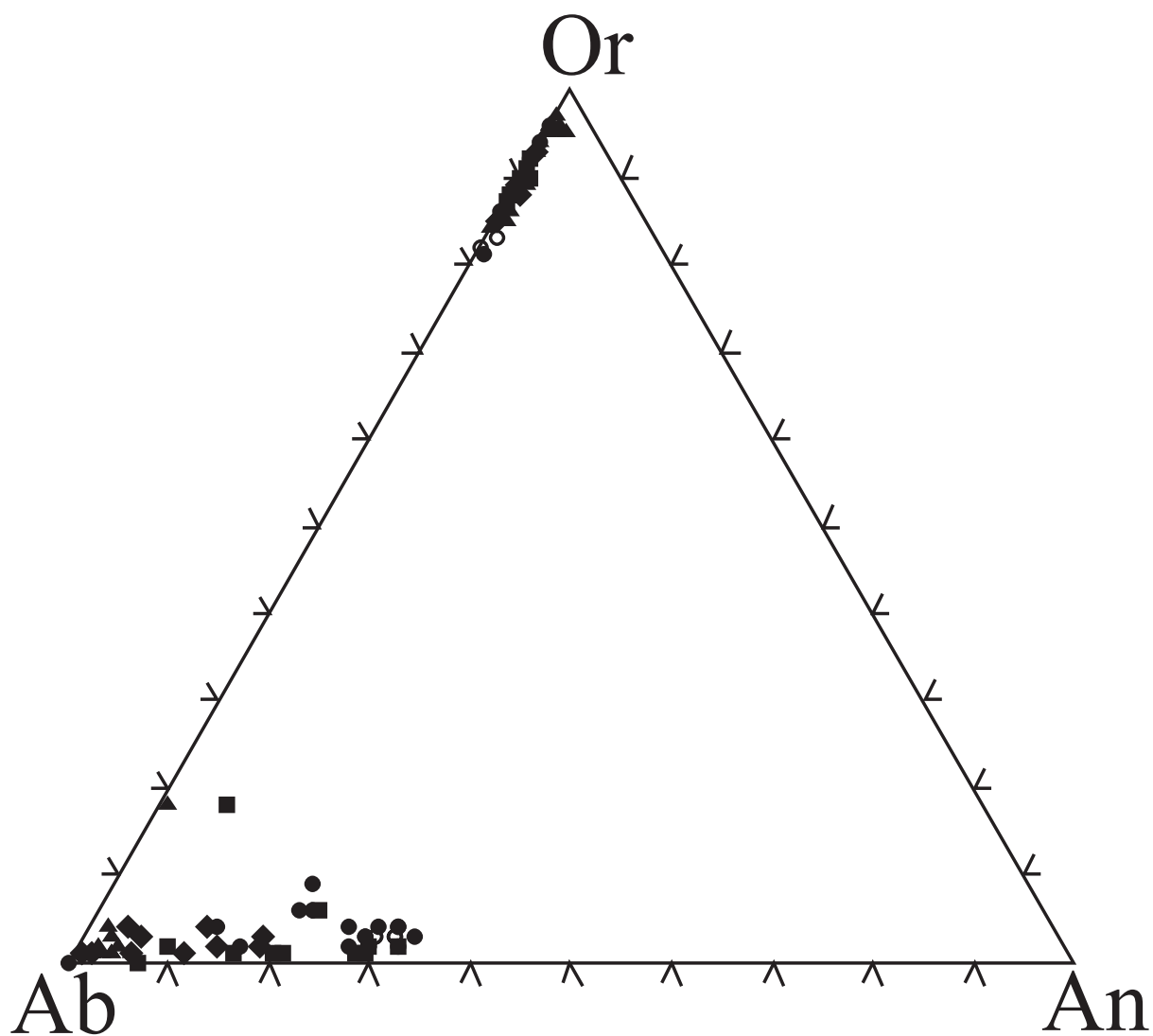


Fig. 3.11. Chemical composition of the feldspars of the St. Blasien pluton as discussed in chapter 3.6. Feldspars of different locations are marked as in Fig. 3.2.

To summarize, for the two end-members of fluid-rock interaction, GSB 6 and GSB 10, coexisting minerals partly exhibit strong disequilibrium fractionations. As a consequence, the hydrothermal interaction must have taken place under open system conditions (see chapter 3.5.1). Fluid flux and duration of interaction have been highest for GSB 10 such that large amounts of secondary minerals have been formed, which could have been analysed separately from coexisting primary minerals. These have locally equilibrated with the mother fluid -at least at a scale of less than 1 cm- at temperatures of about 300 °C. Disequilibrium is observed for systems, where it has not been possible to analyse primary and secondary minerals separated from each other.

3.6. Mechanisms and interfaces of hydrothermal interaction

A brief summary of general mechanisms and interfaces of oxygen isotope exchange between fluid and granite has already been given in chapter 3.4. For a discussion, which mechanisms and interfaces are relevant for the investigated St. Blasien granite, each mineral will be treated separately:

3.6.1. Biotite

An exchange of oxygen isotopes between biotite and chlorite exclusively occurs by chemical reaction. Figs. 3.4a,b clearly demonstrate that oxygen isotope composition within a single biotite grain correlates with the degree of chloritisation. The $\delta^{18}\text{O}$ -value of primary magmatic feldspar is given by the intersect of the qtz-fsp isotherm of 600 °C and the qtz-fsp exchange trajectory in Fig. 3.2a to be about 9.0 ‰. Assuming a fractionation of 2.1 ‰ between biotite and plagioclase (an_{30}) (Zheng, 1993a,b), primary biotite can be calculated to have a $\delta^{18}\text{O}$ of about 6.9 ‰. This is very close to $\delta^{18}\text{O}$ -values obtained for less chloritised parts of biotite (e.g. 6.2 ‰), suggesting that biotite, which is in direct contact to ^{18}O depleted chlorite, has still preserved its primary isotopic composition. Obviously, an exchange by dissolution-recrystallisation did not take place. Additionally, a significant diffusional anionic oxygen isotope exchange between biotite and chlorite (re-equilibration) and/or between biotite and fluid can be ruled out. According to Fortier & Giletti (1991) diffusional exchange between biotite and water still occurs at temperatures as low as 300 °C. However, the preservation of the primary magmatic character of biotite does not contradict their observations: Fortier & Giletti (1991) assumed water to be the oxygen bearing diffusive species. It can be seen by Figs. 3.4a,b that chloritisation of biotite not only took place along microcracks, but also along cleavages. It is therefore likely that the fluid -once it was infiltrated into the biotite from microcracks- also migrated along cleavages by a diffusional mechanism. But wherever the fluid has been in contact with biotite an

immediate formation of chlorite has been triggered. Hence, the existence of primary biotite in direct contact to ^{18}O -depleted chlorite only rules out a significant diffusion of anionic oxygen.

The degree of chlorite formation has been observed to increase from GSB 6 over GSB 14 to GSB 10 in such a way that biotite within GSB 10 has been completely converted to chlorite. Thus total water-rock ratios must have increased in the same sequence.

3.6.2. Plagioclase

The composition of the feldspars is shown in Fig. 3.11. This diagram was constructed from single spot analyses using the electron microprobe.

The anorthite content of plagioclase continuously decreases from GSB 6 (an_{0-40}) over GSB 14 (an_{0-20}) towards GSB 10 (an_{0-10}). In the same direction, water-rock ratios and the degree of chloritisation of biotite have been found to increase (see chapter 3.6.1). Within GSB 10, calcite precipitates occur over single plagioclase grains, especially along microcracks (Figs. 3.6, 3.7a). These also exhibit minor amounts of Fe-oxides. The fluid must therefore have been enriched in Na, CO_2 and SiO_2 , when it interacted with the St. Blasien granite. At high water-rock ratios plagioclase was completely albitised after



as it has already been observed for Na-metasomatism of basaltic (e.g. Moody et al., 1985; Rosenbauer et al., 1988), detrital (e.g. Boles, 1982) and synthetic plagioclase (e.g. Eskola et al., 1937; Orville, 1972).

For GSB 6 water-rock ratios have been the lowest. Here, the extent of albitisation of plagioclase is much lower than for GSB 10 (see also petrographic description in chapter 3.2). If at all, plagioclase is slightly albitised at the rim of single grains (Fig. 3.8). As for GSB 10, in single microcracks minor amounts of Fe-oxides are found.

3.6.3. K-feldspar

K-feldspar in GSB 10 is partly replaced by albite. Fig. 3.9a shows a BSE-picture of K-feldspar within GSB 10, while Figs. 3.9b and 3.9c exhibit corresponding pictures of the same area obtained by CL and element mapping. In Fig. 3.9c two Ba-rich zones can be recognised. Usually, cores of primary crystals of granitic K-feldspar show the highest Ba-contents (Mehnert & Büsch, 1981). Thus, these Ba-enriched zones are most likely the relics of cores of two feldspar grains originally neighbouring each other. Along the grain boundary between those two grains, K-feldspar is replaced by a thin band of secondary albite. Secondary albite is assumed to derive from Na-metasomatism of primary K-feldspar, as it has been described by Orville (1962).

Cole et al. (1992) also observed an albitisation of K-feldspar by alteration experiments on granites with Na-containing solutions. The luminescence of secondary albite is similar to that of K-feldspar (Fig. 3.9b), implying that the albite inherits its trace element composition by K-feldspar. Of course, the main element composition of secondary albite is different from K-feldspar, so that it can be differentiated between both phases by Na-, K- and Ca-mapping (Fig. 3.9c) as well as by the BSE-picture (Fig. 3.9a).

Albitisation of primary K-feldspar along grain boundaries occurred also for the feldspar grain shown in Fig. 3.7a. In contrast to albitisation of plagioclase, albitisation of K-feldspar generally occurred at a lower reaction rate. For GSB 10, plagioclase is completely replaced by albite, whereas K-feldspar is only partly converted.

However, the exchange between K-feldspar and fluid was not only restricted to chemical reaction, but also to dissolution-recrystallisation. From comparison of Figs. 3.9a and 3.9b it is evident that a multiple set of microcracks runs through primary K-feldspar, along which secondary K-feldspar has been formed. The same can be seen in Figs. 3.7a and 3.7b for another investigated K-feldspar within GSB 10. The luminescence of secondarily formed K-feldspar is different from primary one, since K-feldspar of secondary origin inherits its trace element composition mainly from the fluid. Obviously, Ca^{2+} and Ba^{2+} have been leached during dissolution-recrystallisation of K-feldspar (Fig. 3.9c). Subsolidus diffusion of Ca^{2+} and Ba^{2+} seems to be of minor importance since leaching is directly restricted to the "flow-channels" which are given by the microcracks.

Again, GSB 6 shows much less symptoms of water-rock interaction: BSE- (Fig. 3.10a) and CL-picture (Fig. 3.10b) as well as element mapping (Fig. 3.10c) of K-feldspar mostly exhibit primary perthitic lamellae. In contrast to GSB 10, less microcracks are observed along which secondary K-feldspar has been formed. Additionally, K-feldspar has not been found to be replaced by albite.

3.6.4. Quartz

Given that volume diffusion is the rate-limiting factor, diffusion in quartz has been shown to be too slow to account for an oxygen isotope exchange between fluid and quartz at temperatures as low as 300 °C (Eiler et al., 1992, 1993; Jenkin et al., 1994). Hence, in the low temperature region of hydrothermal alteration of granites, quartz is only able to exchange with the fluid by dissolution-recrystallisation. The CL-picture in Fig. 3.7b shows quartz neighbouring K-feldspar within GSB 10. As for K-feldspar, many microcracks run through the quartz grain. It is most likely that secondary quartz has been precipitated along these fractures, thus leading to the observed slight depletion in ^{18}O for quartz within GSB 10 (see Tab. 3.2). An isotopic exchange between quartz and fluid by dissolution-recrystallisation has also been found by Valley &

Graham (1996) and King et al. (1997) for quartz from Skye granites and quartz phenocrysts within the Kidd Creek mine, Ontario, respectively.

Summing up, an exchange of oxygen isotopes between fluid and granite occurs by chemical reaction and dissolution-recrystallisation. Diffusional exchange of anionic (O^{2-}) and cationic (Ca^{2+} , Ba^{2+}) species has not been observed. The fluid by which large parts of the St. Blasien pluton have been altered, must have had locally high Na/K-ratios enabling albitisation of plagioclase and chloritisation of biotite to be the fastest exchange mechanisms. For GSB 10, water-rock ratios have been the highest, such that both reactions went to completion and equilibrium between secondary minerals is observed. An interaction between fluid and rock is observed to take preferentially place along microcracks. For large water-rock ratios, interaction also occurs along grain boundaries. It is therefore assumed that microcracks do serve as precursor pathways for the fluid to get into contact with grain boundaries.

3.7. Fluid evolution and alteration history

The extent and evolution of hydrothermal activity in the Schwarzwald is still a matter of debate. According to Taylor et al. (1991) hydrothermal activity was restricted to a 10-15 km wide zone north and south from the Badenweiler-Lenzkirch tectonic line. In contrast, Simon (1990) and Simon & Hoefs (1998) found evidence that hydrothermal activity occurred over a much wider area of at least 6000 km² and affected oxygen isotope compositions of granites and gneisses both in the Middle and Southern Schwarzwald.

However, there is agreement about the original isotopic composition of the fluid. By D/H-investigations of biotite both Simon (1990) and Taylor et al. (1991) proposed an initial $\delta^{18}O$ -value of -10 ‰ to -12 ‰, and thus the fluid to be of meteoric origin. Rift-zone magmatism along the Badenweiler-Lenzkirch tectonic line and subsequent emplacement of the sheared syn-tectonic Rand Granite in the Lower Carboniferous (ca. 320-360 Ma) initiated a first large hydrothermal interaction, by which large parts of the Rand-Granite and surrounding gneisses became extremely depleted in whole-rock $\delta^{18}O$ (< 3‰; Taylor et al., 1991). In contrast, post-tectonic Hercynian granites (e.g. Bärhalde), which intruded ca. 290-315 Ma ago, partly exhibit negative oxygen isotope fractionations between quartz and feldspar (Simon, 1990). It is assumed that these later intruded granites have been altered by a fluid, which has been continuously enriched in ^{18}O during previous fluid-rock interactions, while D/H-ratios nearly stayed constant (Simon, 1987; Simon 1990).

In order to prove this hypothesis, averaged in situ data -as expressed in δ - δ -space in Figs. 3.2a,b,c- has been fitted to fluid-rock exchange curves. These curves have been calculated using the computer programm XCHANGE (Simon, 1990), which bases on the kinetic exchange theory

of Criss et al. (1987). All calculations have been carried out for a temperature of 300 °C, which has been obtained by chlorite-albite equilibrium fractionation of GSB 10 (see chapter 3.5.2). Corresponding mineral-mineral and mineral-fluid fractionations rely on theoretical calculations by Zheng (1993a,b). Modelled exchange curves are presented in Figs. 3.12a,b,c:

All data can be modelled with an initial isotopic composition of the fluid of -5‰ . For GSB 6a,b and 14, which have been taken within 1 km distance (Fig. 3.1), averaged in situ data of coexisting minerals can be best explained by water-rock ratios as low as 10 atom-% and a fluid flux u (expressed as ratio of u/k_{qtz} , where u is the fluid flux in s^{-1} and k_{qtz} is the exchange rate of quartz in s^{-1} ; Gregory & Criss, 1986 and Criss et al., 1987) of 1.0. Additionally, these locations exhibit a constant ratio of exchange rates $k_{\text{bio}}:k_{\text{fsp}}:k_{\text{qtz}}$ as 9:3:1. Obviously, rock- and fluid-specific parameters -such as the reactive surface area, permeability and chemical composition of the fluid- may have been constant within a range of about 1 km. However, one has to keep in mind that the kinetic exchange theory of Criss et al. (1987) relies on integrated fluid-rock parameters. Though average values seem to be constant, variations by time and space can not be excluded.

Variation of integrated fluid-rock parameters is at least observed on a scale of a few kilometers. Given that chlorite within GSB 10 is already in equilibrium with the fluid, while feldspar- because of lower exchange rates of K-feldspar- still has been on its way of attaining equilibrium, the corresponding bio-fsp exchange curve in Fig. 3.12c is expected to approach the isotherm of 300 °C parallel to the fsp-axis. Such a run requires water-rock ratios as large as 100 atom-% and a high fluid flux of 10.0, which is in agreement with observations made by electron microprobe investigations within chapter 3.6. GSB 10 exhibits much more microcracks than GSB 6, which in turn leads to a higher permeability. Simultaneously, an increase of the reactivity of feldspar and biotite relative to quartz ($k_{\text{bio}}:k_{\text{fsp}}:k_{\text{qtz}} = 15:5:1$) indicates a change in the chemical composition of the fluid, most presumably in the Na/K-ratio:

The rate of chloritisation of biotite and albitisation of feldspar directly depends on the Na-content of the fluid. The higher the Na-content the faster chloritisation and albitisation occurs (Cole et al., 1992). For a fluid, which initially has been homogeneous in its isotopic and chemical composition, local variations in the Na/K-ratio may arise from different water-rock ratios and fluid fluxes, as can be shown by using oxygen isotopes as a tracer (Figs. 3.13a,b). Because of low water-rock ratio and low fluid flux, the isotopic composition of the fluid interacting with GSB 6 shifted to a final $\delta^{18}\text{O}$ -value of 1‰ (Fig. 3.13a). The change in oxygen isotope composition of the interacting fluid along with the observed chloritisation of biotite and weak albitisation of plagioclase indicates that the Na/K-ratio of the fluid must have changed, too. Generally, chloritisation of biotite goes along with a leaching of K (e.g. Ferry, 1979) as well as albitisation of feldspar does. Thus, for GSB 6, the Na/K-ratio of the fluid must have decreased with increasing time of interaction. For GSB 10, because of high water-rock ratio and high fluid

flux, the oxygen isotope composition of the fluid stayed nearly constant throughout the hydrothermal event (Fig. 3.13b), suggesting that the Na/K-ratio stayed nearly constant, too. Given that the Na/K-ratio initially has been high, it is straightforward that chloritisation and albitisation occurred faster for GSB 10 than for GSB 6.

For the different locations, various values for $t \cdot k_{\text{qtz}}$ are obtained, but are nearly constant for coexisting feldspar and biotite for a single location (Figs. 3.13a,b). For quartz, slightly higher $t \cdot k_{\text{qtz}}$ intercepts are obtained. These are most probably due to small amounts of feldspar which have been vaporised together with quartz during in situ analysis (see chapter 3.8). Gregory et al. (1989) have proposed values in the range of 10^{-13} to 10^{-15} s^{-1} for exchange rates k of quartz. Since upper limits on hydrothermal activity are not likely to exceed 1 Ma (Norton & Taylor, 1979), k_{qtz} for GSB 14 (which has an intercept of $t \cdot k_{\text{qtz}} \approx 0.4$, Fig. 3.13a) must have been greater than $1.3 \cdot 10^{-14} \text{ s}^{-1}$. As exchange rates depend on reactive surface areas and GSB 10 exhibits more microcracks than GSB 6, k_{qtz} for GSB 10 (with an intercept of $t \cdot k_{\text{qtz}} \approx 0.6$, Fig. 3.13b) should have been even greater than for GSB 6. Assuming values of $k_{\text{qtz}} = 4.0 \cdot 10^{-14} \text{ s}^{-1}$ for GSB 10 and $2.0 \cdot 10^{-14} \text{ s}^{-1}$ for GSB 6a,b and 14, time-spans of water-rock interaction are estimated to be 0.16 Ma for GSB 6a,b, 0.63 Ma for GSB 14 and 0.48 Ma for GSB 10. For GSB 6 and 14, these calculations demonstrate that time-spans of fluid-rock interaction vary on a smaller scale than integrated fluid-rock parameters do. This feature arises from a channelised fluid flow (see chapter 3.6).

Due to an interaction with large amounts of water, whole rock $\delta^{18}\text{O}$ of GSB 10 is less than 3 ‰ (Tab. 3.2). Similar ^{18}O -depletions as for GSB 10 have been found by Taylor et al. (1991) for large parts of the highly deformed syn-tectonic Rand-Granite and also by Simon & Hoefs (1998) for the Triberg-Granite from the Middle Schwarzwald, which exhibits the same age than the late-tectonic granites in the southeastern Schwarzwald (Leutwein & Sonet, 1974). It is therefore assumed that initially huge amounts of meteoric water have not only been restricted to the B-L-zone, but have been infiltrated nearly all over the South- and Middle Schwarzwald. For a single location, the degree of fluid-rock interaction has been most likely determined by the amount of preexisting cracks and microcracks.

The above calculations indicate that the meteoric fluid became continuously enriched in ^{18}O during water-rock interaction. A shift from -10 ‰ to -5 ‰ is observed for the time-span inbetween rainfall and interaction with the late-tectonic St. Blasien pluton and is attributable to preceding interactions of the meteoric water with basement rocks as well as syn-tectonic granites and gneisses along the Badenweiler-Lenzkirch tectonic line. For hydrothermal interaction of the later intruded St. Blasien pluton, water-rock ratios are observed to decrease from GSB 10 to GSB 6 and 14. In the same direction, the interacting fluid becomes enriched to final $\delta^{18}\text{O}$ -values of about 1 ‰.

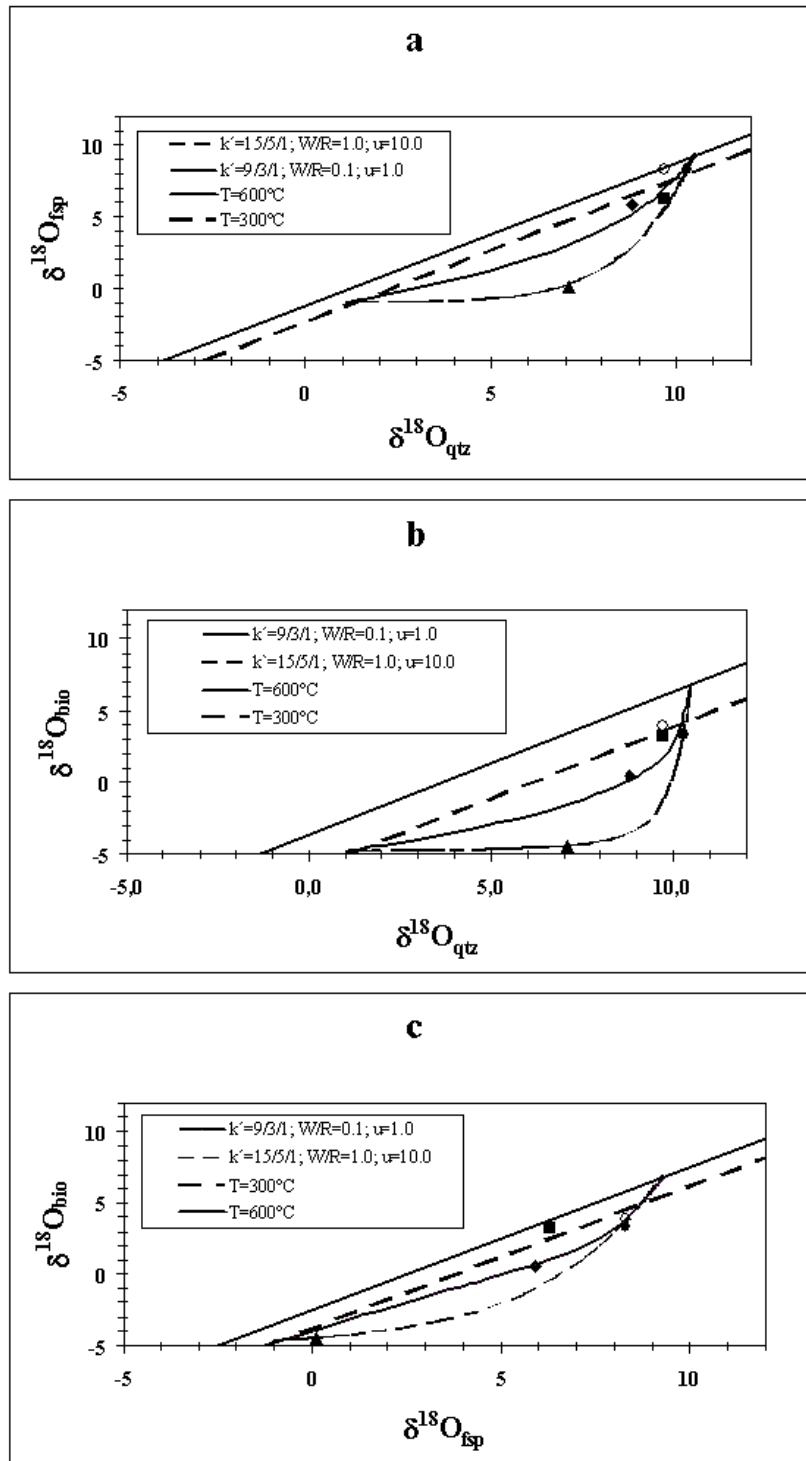


Fig. 3.12. Oxygen isotope exchange curvatures between fluid and granite performed in δ - δ -space of coexisting minerals. Calculations base on the kinetic exchange theory of Criss et al. (1987). For modelling fluid-granite interactions, mineral-mineral and mineral-water fractionations after Zheng (1993a,b) have been used. Initial $\delta^{18}\text{O}$ -compositions at $T = 600^\circ\text{C}$ have been chosen as follows: 10.5‰ (qtz), 9.3‰ (fsp), 6.8‰ (bio) with $x_{\text{bio}} = 0.1$, $x_{\text{fsp}} = 0.6$ and $x_{\text{qtz}} = 0.3$. Mineral-water fractionations at $T = 300^\circ\text{C}$: $\alpha_{\text{qtz-water}} = 1.0064$, $\alpha_{\text{fsp-water}} = 1.0040$, $\alpha_{\text{chl-water}} = 1.0002$. $\alpha_{\text{chl-water}}$ has been used instead of $\alpha_{\text{bio-water}}$, since biotite-fluid interaction goes along with chlorite formation. For feldspar, fractionations are referred to albite. k' represents the ratio of proposed exchange rates $k_{\text{bio}}/k_{\text{fsp}}/k_{\text{qtz}}$. Diagram sequence: (a) qtz-fsp, (b) qtz-bio, (c) fsp-bio. For each location averaged in situ data is plotted as in Fig. 3.2. See also discussion in section 3.7.

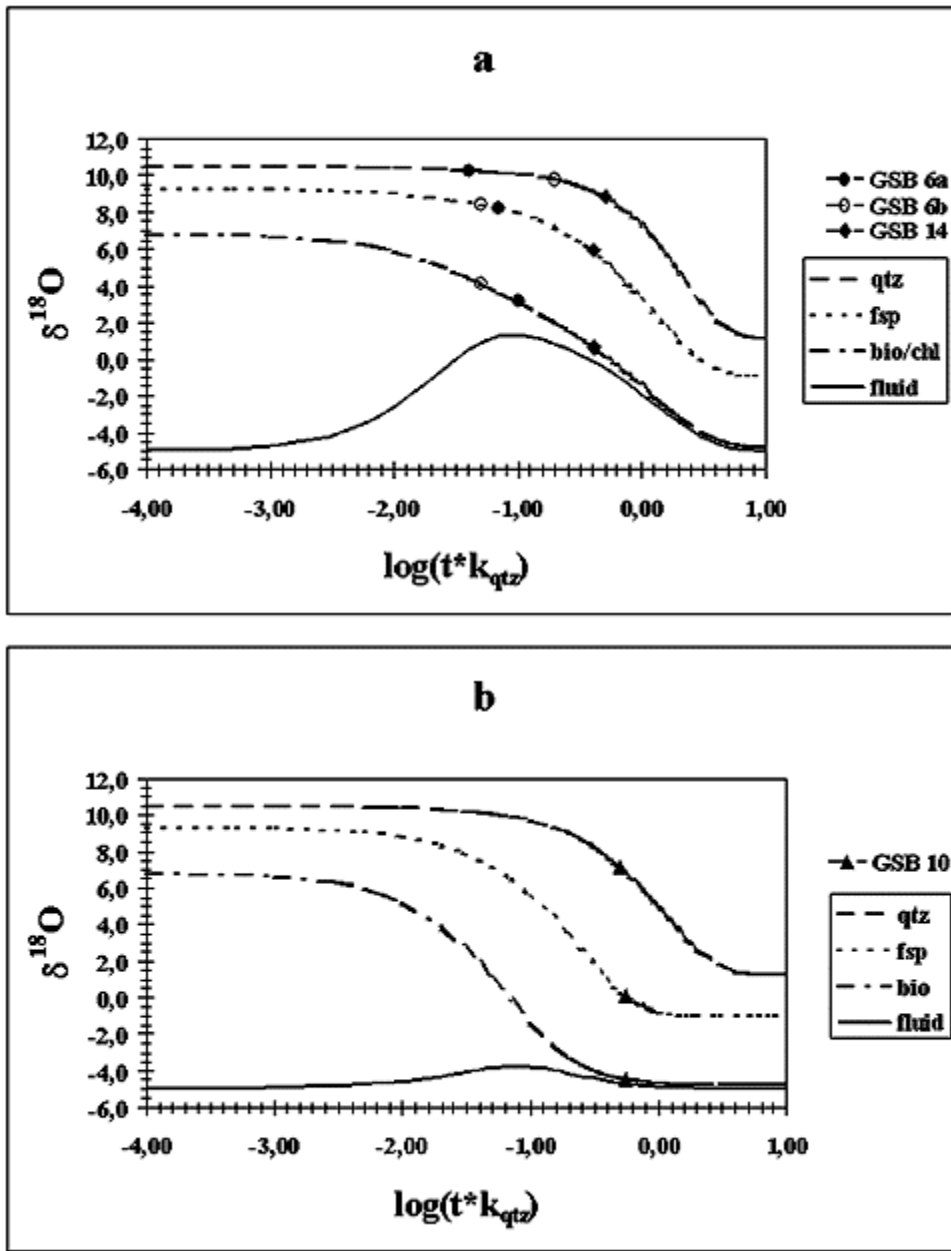


Fig. 3.13. Isotopic variation of granitic minerals and interacting fluid by time. (a): $W/R = 1.0$, $u/k_{\text{qtz}} = 10.0$; (b): $W/R = 0.1$, $u/k_{\text{qtz}} = 1.0$. All other parameters like Fig 3.12. See discussion in chapter 3.7.

For the St. Blasien-Granite, oxygen isotope composition of GSB 7 can not be simply modelled. Its alteration history is different from those of GSB 6, 10 and 14, because biotite of GSB 7 has been enriched in ^{18}O relative to feldspar (see Figs. 3.2c and 3.12c). GSB 12 exhibits a similar enrichment in ^{18}O as GSB 7 (Simon, 1990). Both locations are within 1 km distance of the Bärhalde pluton. It is therefore suggested that the oxygen isotope compositions of GSB 7 and GSB 12 have additionally been affected by a hydrothermal interaction accompanied with the subsequent emplacement of the Bärhalde pluton. Granites from locations nearby later intruded plutons may have interacted with both fluids depleted in ^{18}O and subsequently -to a much lesser extent- with fluids enriched in ^{18}O , as proposed by Simon (1990) for parts of the Bärhalde pluton. The alteration history of GSB 7 might be even more complex, because of its additional proximity to the Schluchsee pluton.

To sum up, kinetic exchange calculations for granites from St. Blasien support the model by Simon (1990), after which oxygen isotope signatures of subsequently intruded granites in the Southeastern Schwarzwald are due to interactions with a fluid of meteoric origin, that became continuously enriched in ^{18}O . Water-rock ratios and fluid fluxes depend on the amount of preexisting fluid-pathways. With decreasing total water-rock ratios, the chemical and isotopic composition of the fluid is changing, which results in different alteration kinetics for GSB 10 and GSB 6. Time-spans of water-rock interaction have been found to vary at least on a scale of less than 1 km, which is in agreement with a channelised fluid flow.

3.8. Comparison of conventional and in situ data

Conventional oxygen isotope analysis on mineral separates for GSB 6, 7, 10 and 14 has been carried out by Simon (1990). For a comparison with in situ data, conventional data is plotted in δ - δ -space in Figs. 3.3a,b,c and is also listed in Tab. 3.2.

Both data sets exhibit similar trends: Steep positive qtz-fsp (Fig. 3.3a) and qtz-bio/chl-exchange trajectories (Fig. 3.3b) indicate that equilibrium has not been attained (Simon, 1990). Additionally, it is obvious that fluid and granite interacted under open system conditions. However, there are still some systematic differences in both data sets:

First, quartz analysed in situ gives systematically lower $\delta^{18}\text{O}$ -values than quartz conventionally determined: Exchange trajectories in Figs. 3.3a and b intersect primary magmatic qtz-fsp-isotherm and qtz-bio/chl-isotherm between 12-13 ‰. In contrast, for in situ data intersections are obtained which imply a primary magmatic composition of quartz of 10-11 ‰ (Figs. 3.2a,b). This lowering of in situ quartz data compared to conventional data may be explained by a mixing of different minerals during in situ ablation of quartz: Generally, quartz sampling by UV-laser light occurred on a mm-scale (see chapter 3.3). It can therefore not be

excluded, that small amounts of feldspar or biotite/chlorite have been vaporised together with quartz.

Secondly, by a comparison of calculated whole rock- and conventionally determined whole rock data (Tab. 3.2) it appears that results from in situ analysis contradicts those from conventional analysis: For all samples, calculated in situ whole rock data is lower than conventionally determined whole rock $\delta^{18}\text{O}$. For in situ analysis, thick sections have been cut from hand samples which had been taken in the field. Thick sections are cm-extracts of whole rocks, in which the original mineral assemblage is well preserved. Thus, oxygen isotope data obtained by a single thick section analysis represents the original isotopic composition of minerals on a cm-scale. The difference between conventionally determined and calculated in situ whole rock $\delta^{18}\text{O}$ is most probably due the channelised fluid flow (see chapter 3.7). If one assumes that the conventionally determined whole rock data is representative for the average oxygen isotope composition of a single location, for in situ analysis more altered sections have been chosen by accident.

Conversely, calculated whole rock data derived from conventional analysis of mineral separates is higher than conventionally determined whole rock data. Consequently, for conventional analysis of mineral separates less altered material has been selected. However, this does not seem to be just a coincidence: In contrast to thick section analysis, the original mineral assemblage is destroyed prior to conventional analysis. A preferential selection of less altered material by hand-picking after sample crushing leads to $\delta^{18}\text{O}_{\text{fsp,bio/chl}}$ - values which are not representative for the original assemblage.

Selective sampling of mineral separates might explain why $\delta^{18}\text{O}_{\text{fsp,bio/chl}}$ of GSB 10 lies above the primary magmatic fractionation line of 600 °C (Fig. 3.3c). In fact, of all reasons that could account for this "unusual" $\delta^{18}\text{O}$ -value, this is the most convincing:

(1) An additional interaction of GSB 10 with a fluid enriched in ^{18}O may be ruled out, since such interactions are likely to be restricted to a zone within 1 km distance from the Bärhalde pluton (see chapter 3.7).

(2) Points above the primary magmatic fractionation line can also be attained, if $k_{\text{fsp}} > k_{\text{bio}}$. Ferry (1985) reported for granites from the Isle of Skye, Scotland, that feldspar was more susceptible towards mineralogical alteration than biotite in a temperature range of 350 - 450 °C. However, the variation of conventionally determined $\delta^{18}\text{O}_{\text{fsp,bio/chl}}$ over all locations would require a large change in the exchange kinetics of biotite and feldspar. This is in contrast to findings derived from in situ analysis: $\delta^{18}\text{O}_{\text{fsp,bio/chl}}$ of GSB 6, 10 and 14 are best explained by $k_{\text{fsp}} < k_{\text{bio}}$ and a narrow range of variation (see chapter 3.7). The higher susceptibility of biotite towards alteration is in agreement with observations by Cole et al. (1992), who carried out hydrothermal experiments on granites between 170 and 300 °C with NaCl containing solutions.

To conclude, oxygen isotope data derived from conventional- and in situ-analysis show a similar trend of fluid-rock interaction for quartz-feldspar and quartz-biotite-systems. However, large differences have been obtained for biotite-feldspar fractionations, which are most presumably due to a selective sampling of mineral separates prior to conventional analysis.

B. Conclusions

In order to investigate the process of hydrothermal alteration of granites a UV-laser based oxygen isotope microprobe was set up. Spatial resolution is about 250 μm , but can easily be improved. Throughout the analytical procedure only a small proportion of silicate extracted oxygen is finally purged into the ion source, which results in analysis durations of less than 15 minutes. The mass spectrometer used is a DeltaPlus (Finnigan, Inc.) with continuous flow inlet and detector system for masses 32, 33 and 34. For a reproducible quantification of oxygen isotopes in a continuous flow mode, a differential pumping system is necessary. Linearity is fulfilled when analyte oxygen is cryofocused prior to analysis. As long as more than 300 nmol of oxygen is extracted from the silicate, the GC-technique is not necessarily needed to obtain accuracy and precision better than 0.2%.

UV-laser induced fluorination of silicates results in a fractionation-free extraction of oxygen, even if oxygen yields are not quantitative. Hence, the use of UV-lasers allows real in situ oxygen isotope analyses of silicates. UV-lasers with a single photon energy ≥ 5 eV even enable in situ analysis of highly transparent minerals like quartz. The higher the single photon energy of the laser, the higher the oxygen yields at constant energy density. Additionally, for a constant single photon energy, oxygen yields increase with increasing energy density of the focused beam. From all easy handable UV-lasers the ArF-laser is most suitable to carry out in situ oxygen isotope analysis of quartz.

Quartz analysis of thick sections should be preferred over single grain analysis, since the latter gives rise to slight fractionations. However, during in situ analysis of granitic thick sections the high reactivity of fluorine easily produces oxygen blanks. In order to correct for oxygen blanks, it is not sufficient to measure only one standard along with the samples. For reasons of accuracy, oxygen blanks must be corrected both for their quantity and $\delta^{18}\text{O}$. Therefore two standards of distinct isotopic composition have to be measured along with the sample.

The newly developed technique was applied to in-situ oxygen isotope analysis of thick sections of a hydrothermally altered granitic pluton from St. Blasien, southeastern Schwarzwald, Germany. All thick sections investigated for oxygen isotopes were additionally analysed by electron microprobe. The combination of both methods was used to investigate the kinetics of oxygen isotope exchange between granite and fluid.

Large parts of the St. Blasien pluton were altered by a fluid with an initial $\delta^{18}\text{O}$ -value of about -5%. The fluid presumably infiltrated the rock along cracks and microcracks, where an exchange of oxygen isotopes preferentially took place. For high water-rock ratios an exchange along grain boundaries was also observed. Chemical reaction and dissolution-recrystallisation were found to be the primary exchange mechanisms. Due to low temperatures, subsolidus

diffusion of anionic and cationic species like O^{2-} , Ca^{2+} and Ba^{2+} was too slow to show any significant influence. Primary magmatic biotite is in direct contact with secondary, ^{18}O -depleted chlorite and element mappings of K-feldspar demonstrate that Ca^{2+} and Ba^{2+} are only leached along fluid-pathways.

The fluid initially had high Na/K-ratios, such that chloritisation of biotite and albitisation of plagioclase occurred most rapidly. The amount of microcracks drives kinetic parameters like water-rock ratio and fluid flux. At least on a cm-scale, fluid-rock ratio and fluid flux were high and both chloritisation of biotite and albitisation of plagioclase went to completion. Fractionation between secondarily formed chlorite and albite yields an equilibrium temperature of 300 °C. At other locations water-rock ratios and fluid flux were low, such that the chemical composition of the fluid was shifted to lower Na/K-values during water-rock interaction and absolute values of the rates of chloritisation and albitisation decreased.

Since oxygen diffusion can be disregarded, an interaction between meteoric fluid and mineral was restricted to those parts of a mineral that were in direct contact with the fluid. On a molecular dimension and temperatures of 300 °C, each secondarily formed phase is assumed to be in local equilibrium with the interacting fluid. The amount of secondarily formed phases, which are for a given temperature in equilibrium with the fluid, depends on reaction rates, water-rock ratios and time-spans of interaction at the corresponding temperature. Because of a channelised fluid flow, mineral phases with primary magmatic character exist in direct contact with those which locally reached equilibrium with the fluid. Disequilibrium obtained by bulk analysis may arise from an insufficient spatial resolution of the applied analytical technique, such that primary and fluid equilibrated secondary minerals are analysed together. This is confirmed by in-situ analysis on a 250 μm scale. Wherever water-rock ratios were low, amounts of secondarily formed mineral phases were too small to be analysed separately from primary phases and disequilibrium fractionations between coexisting mineral pairs were obtained. In contrast, at locations where water-rock ratios were high, large amounts of secondary phases were formed. These could be analysed separately from primary phases exhibiting equilibrium fractionation ($T = 300^{\circ}C$) on a cm-scale. In order to evaluate whether equilibrium was attained within a fluid-rock system or not, it is therefore imperative to define the size and the components of the investigated system.

Calculations using the kinetic exchange theory of Criss et al. (1987) confirm the model by Simon (1990), which suggests that large parts of granites in the southeastern Schwarzwald were hydrothermally altered by a fluid of meteoric origin, which locally became significantly enriched in ^{18}O during fluid-rock interaction. During hydrothermal alteration of the St. Blasien-Granite water-rock ratios varied at least on a km-scale, so that the final fluid locally became enriched in ^{18}O about 6%. Hydrothermal activity with ^{18}O -enriched fluids was revived by the intrusion of

late-stage Bärhalde- and Schluchsee-Granite and additionally affected oxygen isotope composition of surrounding parts of the St. Blasien-granite.

References

- Akagi T., Franchi I. A., and Pillinger C. T. (1995) Isotope analysis of oxygen in minerals using Nd:YAG laser-fluorination: the use of stainless-steel wool trap as a fluorine remover. *Geochem. J.* **29**, 115-122.
- Arita, Z. and Wada, H. (1990) Stable isotope evidence for migration of metamorphic fluids along grain boundaries of marbles. *Geochem. J.* **24**, 173-186.
- Asprey, L.B. (1976) The preparation of very pure fluorine gas. *J. Fluor. Chem.* **7**, 359-361.
- Behr, H.J. and Gerler, J. (1987) Inclusions of sedimentary brines in post-Variscan mineralizations in the Federal Republic of Germany - a study by neutron activation analysis. *Chem. Geol.* **61**, 65-77.
- Boles, J.R. (1982) Active albitization of plagioclase, Gulf Coast Tertiary. *Am. Jour. Sci.* **282**, 165-180.
- Borthwick J. and Harmon R. S. (1982) A note regarding ClF_3 as an alternative to BrF_5 for oxygen isotope analysis. *Geochim. Cosmochim. Acta* **46**, 1665-1668.
- Bottinga, Y. and Javoy, M. (1973) Comments on oxygen isotope geothermometry. *Earth Planet. Sci. Lett.* **20**, 250-265.
- Bridger, N.I., Craig, R.D., and Sercombe, J.S.F. (1974) New mass spectrometer for isotopic analysis of small gas samples. *Adv. Mass Spectrom.* **6**, 365-375.
- Chamberlain, C.P. and Conrad, M.E. (1991) Oxygen isotope zoning in garnet. *Science* **254**, 403-406.
- Chamberlain, C.P. and Conrad, M.E. (1993) Oxygen isotope zoning in garnet: A record of volatile transport. *Geochim. Cosmochim. Acta* **57**, 2613-2629.
- Clayton, R.N. and Mayeda, T.K. (1963) The use of bromine pentafluoride in the extraction of oxygen from oxides and silicates for isotopic analysis. *Geochim. Cosmochim. Acta* **27**, 43-52.
- Clayton, R.N. and Mayeda, T.K. (1983) Oxygen isotopes in eucrites, shergottites nakhlites and chassignites. *Earth Planet. Sci. Lett.* **62**, 1-6.
- Clayton, R.N. and Kieffer, S.W. (1991) Oxygen isotopic thermometer calibrations. In: Taylor, H.P., Jr, O'Neil, J.R., and Kaplan, I.R. (eds) Stable isotope geochemistry: A tribute to Samuel Epstein. Geochemical Society, Special Publication No. 3, 3-10.

- Cole, D.R., Ohmoto, H., and Lasaga, A.C. (1983) Isotopic exchange in mineral-fluid systems. I. Theoretical evaluation of oxygen isotopic exchange accompanying surface reactions and diffusion. *Geochim. Cosmochim. Acta* **47**, 1681-1693.
- Cole, D.R. and Ohmoto, H. (1986) Kinetics of isotopic exchange at elevated temperatures and pressures. In: Valley, J.W., Taylor, H.P., Jr., and O'Neil, J.R. (eds) Stable isotopes in high temperature geological processes. *Mineral. Soc. Am. Rev. Mineral.* **16**, 41-90.
- Cole, D.R., Ohmoto, H., and Jacobs, G.K. (1992) Isotopic exchange in mineral-fluid systems: III. Rates and mechanisms of oxygen isotope exchange in the system granite-H₂O ± NaCl ± KCl at hydrothermal conditions. *Geochim. Cosmochim. Acta* **56**, 445-466.
- Cole, D.R. and Ripley, E.M. (1999) Oxygen isotope fractionation between chlorite and water from 170 to 350°C: A preliminary assessment based on partial exchange and fluid/rock experiments. *Geochim. Cosmochim. Acta* **63**, 449-457.
- Conrad, M.E. and Chamberlain, C.P. (1992) Laser-based, in situ measurements of fine-scale variations in the $\delta^{18}\text{O}$ values of hydrothermal quartz. *Geology*, **20**, 812-816.
- Criss, R.E., Gregory, R.T., and Taylor, H.P., Jr. (1987) Kinetic theory of oxygen isotopic exchange between minerals and water. *Geochim. Cosmochim. Acta* **51**, 1099-1108.
- Devine, R.A.B. (1989) Defect creation and two-photon absorption in amorphous SiO₂. *Phys. Rev. Lett.* **62**, 340.
- Echtler, H.P. and Chauvet, A. (1991-1992) Carboniferous convergence and subsequent crustal extension in the southern Schwarzwald (SW Germany). *Geodin. Acta* **5**, 37-49.
- Eiler, J.M., Baumgartner, L.P., and Valley, J.W. (1992) Interdiffusion of stable isotopes: A fast grain boundary model. *Contrib. Mineral. Petrol.* **112**, 543-557.
- Eiler, J.M., Valley, J.W., and Baumgartner, L.P. (1993) A new look at stable isotope thermometry. *Geochim. Cosmochim. Acta* **57**, 2571-2583.
- Eiler, J.M., Valley, J.W., Graham, C.M., and Baumgartner, L.P. (1995) Ion microprobe evidence for the mechanisms of stable isotope retrogression in high-grade metamorphic rocks. *Contr. Mineral. Petrol.* **118**, 365-378.
- Eiler J. M., Farley K. A., Valley J. W., Hofmann A. W., and Stolper E. M. (1996) Oxygen isotope constraints on the sources of Hawaiian volcanism. *Earth Planet. Sci. Lett.* **144**, 453-468.
- Eiler, J.M., Farley, K.A., Valley, J.W., Hauri, E., Craig, H., Hart, S.R., and Stolper, E.M. (1997) Oxygen isotope variations in ocean island basalt phenocrysts. *Geochim. Cosmochim. Acta* **61**, 2281-2293.

- Elsenhaimer, D. and Valley, J.W. (1992) In situ oxygen analysis of feldspar and quartz by Nd:YAG laser microprobe. *Chem. Geol.* **101**, 21-42.
- Elsenhaimer, D. and Valley, J.W. (1993) Submillimeter scale zonation of $\delta^{18}\text{O}$ in quartz and feldspar, Isle of Skye, Scotland. *Geochim. Cosmochim. Acta* **57**, 3669-3676.
- Emmerrmann, R. (1977) A petrogenetic model for the origin and evolution of the Hercynian granite series of the Schwarzwald. *N. Jb. Miner. Abh.* **128**, 219-253.
- Eskola, P., Vuoristo, U., and Rankama, K. (1937) An experimental illustration of the spilite reaction. *Comm. geol. Finlande Bull.* **119**, 61-68.
- Farquhar, J. and Rumble, D. (1998) Comparison of oxygen isotope data obtained by laser fluorination of olivine with KrF excimer laser and CO_2 laser. *Geochim. Cosmochim. Acta* **62**, 3141-3149.
- Fein, J.B., Graham, C.M., Holness, M.B., Fallick, A.E., and Skelton, A.D.L. (1994) Controls on the mechanisms of fluid infiltration and front advection during regional metamorphism: a stable isotope and textural study of retrograde Dalradian rocks of the SW Scottish Highlands. *J. metamorphic Geol.* **12**, 249-260.
- Ferry, J.M. (1979) Reaction mechanisms, physical conditions, and mass transfer during hydrothermal alteration of mica and feldspar in granitic rocks from South-Central Maine, USA. *Contrib. Mineral. Petrol.* **68**, 125-139.
- Ferry, J.M. (1985) Hydrothermal alteration of Tertiary igneous rocks from the Isle of Skye, northwest Scotland. II. Granites. *Contrib. Mineral. Petrol.* **91**, 283-304.
- Fiebig, J., Wiechert, U., Rumble, D., and Hoefs, J. (1999) High-precision in-situ oxygen isotope analysis of quartz using an ArF laser. *Geochim. Cosmochim. Acta* **63**, 687-702.
- Fortier, S.M. and Giletti, B.J. (1991) Volume self-diffusion of oxygen in biotite, muscovite, and phlogopite micas. *Geochim. Cosmochim. Acta* **55**, 1319-1330.
- Fouillac, A.M. and Girard, J.P. (1996) Laser oxygen analysis of silicate/oxide grain separates: evidence for a grain size effect? *Chem. Geol.* **130**, 31-54.
- Giletti, B.J. (1985) The nature of oxygen transport within minerals in the presence of hydrothermal water and the role of diffusion. *Chem. Geol.* **53**, 197-206.
- Giletti, B.J. (1986) Diffusion effect on oxygen isotope temperatures of slowly cooled igneous and metamorphic rocks. *Earth Planet. Sci. Lett.* **77**, 218-228.
- Gilliam, C.E. and Valley, J.W. (1997) Low $\delta^{18}\text{O}$ magma, Isle of Skye, Scotland: Evidence from zircons. *Geochim. Cosmochim. Acta* **61**, 4975-4981.

- Gregory, R.T. and Criss, R.E. (1986) Isotopic exchange in open and closed systems. In: Valley, J.W., Taylor, H.P., Jr., and O'Neil, J.R. (eds) Stable isotopes in high temperature geological processes. *Mineral. Soc. Am. Rev. Mineral.* **16**, 91-127.
- Gregory, R.T., Criss, R.E., and Taylor, H.P., Jr. (1989) Oxygen isotopic exchange kinetics of mineral pairs in closed and open systems: application to problems of hydrothermal alteration of igneous rocks and precambrian iron formations. *Chem. Geol.* **75**, 1-42.
- Haglund, R.F.J. and Itoh, N. (1994) Electronic processes in laser ablation of semiconductors and insulators. In *Laser Ablation*, Vol. **28**, (ed. J.C.Miller), *Springer Series in Material Sciences*, pp 11-52. Springer.
- Hayes, J.M., Freeman, K.H., Popp, B.N., and Hoham, C.H. (1990) Compound-specific isotopic analyses; a novel tool for reconstruction of ancient biogeochemical processes. *Org. Geochem.* **16**, 1115-1128.
- Hoefs, J. and Emmermann, R. (1983) The oxygen isotope composition of Herynian granites and pre-Hercynian gneisses from the Schwarzwald, SW-Germany. *Contrib. Mineral. Petrol.* **83**, 320-329.
- Hoefs, J. (1997) Stable isotope geochemistry. 4th completely revised, updated and enlarged edition, Springer, 201 pp.
- Holness, M.B. and Graham, C.M. (1995) P-T-X-effect on equilibrium carbonate-H₂O-CO₂-NaCl dihedral angles: constraints on carbonate permeability and the role of deformation during fluid infiltration. *Contrib. Mineral. Petrol.* **119**, 301-313.
- Horita, J. and Wesolowski, D.J. (1994) Liquid-vapor fractionation of oxygen and hydrogen isotopes of water from the freezing to the critical temperature. *Geochim. Cosmochim. Acta* **58**, 3425-3437.
- Ihleman, J., Wolff, B., and Simon, P. (1992) Nanosecond and femtosecond excimer laser ablation of fused silica. *Appl. Phys.* **A54**, 363-368.
- Jenkin, G.R.T., Farrow, C.M., Fallick, A.E., and Higgins, D. (1994) Oxygen isotope exchange and closure temperatures in cooling rocks. *J. metamorphic Geol.* **12**, 221-235.
- King, E.M., Barrie, C.T., and Valley, J.W. (1997) Hydrothermal alteration of oxygen isotope ratios in quartz phenocrysts, Kidd Creek mine, Ontario: Magmatic values are preserved in zircon. *Geology* **25**, 1079-1082.
- Kirschner, D.L., Sharp, Z.D., and Teyssier, C. (1993) Vein growth mechanisms and fluid sources revealed by oxygen isotope laser microprobe. *Geology* **21**, 85-88
- Kirschner, D.L. and Sharp, Z.D. (1997) Oxygen isotope analysis of fine-grained minerals and rocks using the laser-extraction technique. *Chem. Geol.* **137**, 109-115.

- Krantz, R.L. (1983) Micro-cracks in rocks: a review. *Tectonophysics* **100**, 449-480.
- Lasaga, A.C. (1981a) Rate laws of chemical reactions. In: Lasaga, A.C. and Kirkpatrick, R.J. (eds) Kinetics of geological processes. *Rev. Mineral.* **8**, 1-68.
- Lasaga, A.C. (1981b) The atomistic basis of kinetics: Defects in minerals. In: Lasaga, A.C. and Kirkpatrick, R.J. (eds) Kinetics of geological processes. *Rev. Mineral.* **8**, 261-320.
- Leutwein, F. and Sonet, J. (1974) Geochronological studies in the Southern Black Forest. *N. Jb. Miner. Abh.* **121**, 252-271.
- Magaritz, M. and Taylor, H.P., Jr. (1981) Low ^{18}O migmatites and schists from the tectonic contact zone between Hercynian (= Variscan) granites and the older gneissic core complex of the Black Forest (Schwarzwald), West Germany. *Geol. Soc. Amer. Abstr. Prog.* **13**, 501.
- Magaritz, M. and Taylor, H.P., Jr. (1986) Oxygen 18/oxygen 16 and D/H studies of plutonic granitic and metamorphic rocks across the Cordilleran Batholiths of Southern British Columbia. *J. Geophys. Res.* **91**, 2193-2217.
- Mattey, D. and Macpherson, C. (1993) High-precision oxygen isotope microanalysis of ferromagnesian minerals by laser-fluorination. *Chem. Geol.* **105**, 305-318.
- Mattey D., Lowry D., and Macpherson C. (1994) Oxygen isotope composition of mantle peridotite. *Earth Planet. Sci. Lett.* **128**, 231-241.
- Matthews, A. Goldsmith, J.R., and Clayton, R.N. (1983) On the mechanisms and kinetics of oxygen isotope exchange in quartz and feldspars at elevated temperatures and pressures. *Geol. Soc. Am. Bull.* **94**, 396-412.
- Matthews, D.E. and Hayes, J.M. (1978) Isotope-ratio-monitoring gas chromatography mass spectrometry. *Anal. Chem.* **50**, 1465-1473.
- Mehnert, K.R. and Büsch, W. (1981) The Ba content of K-feldspar megacrysts in granites: a criterion for their formation. *N. Jb. Miner. Abh.* **140**, 221-252.
- Merrit, D.A. and Hayes, J.M. (1994) Factors controlling precision and accuracy in Isotope-Ratio-Monitoring Mass Spectrometry. *Anal. Chem.* **66**, 2336-2347.
- Metz, R. and Rein, G. (1958) Erläuterungen zur geologisch-petrographischen Übersichtskarte des Südschwarzwaldes 1:50.000. Moritz-Schauenburg Verlag, Lahr.
- Metz, R. (1964) Der Granit von St. Blasien im Südschwarzwald und seine Randzonen. *Jber. Mitt. oberrh. geol. Ver.* **46**, 69-96.
- Moody, J.B., Jenkins, J.E., and Meyer, D. (1985) An experimental investigation of the albitization of plagioclase. *Can. Mineral.* **23**, 583-596.

- Müller-Sohnius, D., Propach, G., and Köhler, H. (1976) Gleichzeitige Intrusion von Bärhalde- und Schluchseegranit. *N. Jb. Miner. Abh.* **127**, 174-186.
- Newman, A. (1996) The precise world of isotope ratio mass spectrometry. *Anal. Chem.* **A**, 373-377.
- Norton, D.L. and Taylor, H.P. (1979) Quantitative simulation of the hydrothermal systems of crystallizing magmas on the basis of transport theory and oxygen isotope data: an analysis of the Skaergaard Intrusion. *J. Petrol.* **20**, 421-486.
- Onasch, C.M. and Vennemann, T.W. (1995) Disequilibrium partitioning of oxygen isotopes associated with sector zoning in quartz. *Geology* **23**, 1103-1106.
- Orville, P.M. (1962) Alkali metasomatism and feldspars. *Norsk Geol. Tidsskr.* **42**, 283-316.
- Orville, P.M. (1972) Plagioclase cation exchange equilibria with aqueous chloride solution: Results at 700°C and 2000 bars in the presence of quartz. *Am. Jour. Sci.* **272**, 234-272.
- Pompe, W., Völlmar, S., Schöneich, B., and Panzner, M. (1992) Laser sputtering of insulators. *Nucl. Instr. and Meth.* **B65**, 200-205.
- Rosenbauer, R.J., Bischoff, J.L., and Zierenberg, R.A. (1988) The laboratory albitization of Mid-Ocean Ridge Basalt. *J. Geol.* **96**, 237-244.
- Rothschild, M., Ehrlich, D.J., and Shaver, D.C. (1989) Effects of excimer laser irradiation on the transmission, index of refraction and density of ultraviolet grade fused silica. *Appl. Phys. Lett.* **55**, 1276-1278.
- Rumble, D., Ferry, J.M., and Hoering, T.C. (1986) Oxygen isotope geochemistry of hydrothermally-altered synmetamorphic granitic rocks from South-Central Maine, USA. *Contrib. Mineral. Petrol.* **93**, 420-428.
- Rumble, D.R., Farquhar, J., Young, E.D., and Christensen, C.P. (1997) In situ oxygen isotope analysis with an excimer laser using F₂ and BrF₅ reagents and O₂ gas as analyte. *Geochim. Cosmochim. Acta* **61**, 4229-4234.
- Santrock, J., Studley, S.A., and Hayes, J.M. (1985) Isotopic analyses based on the mass spectrum of carbon dioxide. *Anal. Chem.* **57**, 1444-1448.
- Sharp, Z.D. (1990) A laser-based microanalytical method for the in-situ determination of oxygen isotope ratios of silicates and oxides. *Geochim. Cosmochim. Acta* **54**, 1353-1357.
- Sharp, Z.D. (1992) In situ laser microprobe techniques for stable isotope analysis. *Chem. Geol. (Isot. Geosci. Sect.)* **101**, 3-19.
- Sheppard, S.M.F., Nielsen, R.L., and Taylor, H.P. (1969) Oxygen and hydrogen isotope ratios of clay minerals from Porphyry Copper Deposits. *Econ. Geol.* **64**, 755-777.

- Simon, K. and Hoefs, J. (1987) Effects of meteoric water interaction on Hercynian granites from the Südschwarzwald, Southwest Germany. *Chem. Geol.* **61**, 253-261.
- Simon, K. (1988) Wasser/Gestein Wechselwirkungen in der Granitserie des südöstlichen Schwarzwaldes. Dissertation, Georg-August University, Göttingen, Germany.
- Simon, K. (1990) Hydrothermal alteration of Variscan granites, southern Schwarzwald, Federal Republic of Germany. *Contrib. Mineral. Petrol.* **105**, 177-196.
- Simon, K. and Hoefs, J. (1998) Large fossil hydrothermal systems in Variscan granites and pre-Variscan gneisses of the Schwarzwald. *Mineral. Mag.* **62A**, 1405-1406.
- Spicuzza, M.J., Valley, J.W., Kohn, M.J., Girard, J.P., and Fouillac, A.M. (1998) The rapid heating, defocused beam technique: a CO₂-laser based method for highly precise and accurate determination of $\delta^{18}\text{O}$ values of quartz. *Chem. Geol.* **144**, 195-203.
- Taylor, H.P. (1974) The application of oxygen and hydrogen isotope studies to problems of hydrothermal alteration and ore deposition. *Econ. Geol.* **69**, 843-883.
- Taylor, H.P., Jr. (1977) Water/rock interactions and the origin of H₂O in granitic batholiths. *J. Geol. Soc. Lond.* **133**, 509-558.
- Taylor, H.P., Jr. (1978) Oxygen and hydrogen isotope studies of plutonic granitic rocks. *Earth Planet. Sci. Lett.* **38**, 177-210.
- Taylor, H.P., Jr., Magaritz, M., and Wickham, S.M. (1991) Application of stable isotopes in identifying a major Hercynian synplutonic rift zone and its associated meteoric-hydrothermal activity, southern Schwarzwald, Germany. In: Taylor, H.P., Jr, O'Neil, J.R., and Kaplan, I.R. (eds) Stable isotope geochemistry: A tribute to Samuel Epstein. Geochemical Society, Special Publication No. 3, 355-371.
- Techmer, A. (1992) Die Nordschwarzwälder und Odenwälder Granite: Kennzeichen von hydrothermalen Alterationsreaktionen. Dissertation, Georg-August Universität, Göttingen, Germany.
- Tsai, T.E., Griscom, D.L., and Friebele, E.J. (1988) Mechanism of intrinsic Si E'-center photogeneration in high-purity silica. *Phys. Rev. Lett.* **61**, 444-446.
- Urey, H.C. (1947) The thermodynamic properties of isotopic substances. *J. Chem. Soc.* **1947** 562-581.
- Valley J. W., Chiarenzelli J. R., and McLelland J. M. (1994) Oxygen isotope geochemistry of zircon. *Earth Planet. Sci. Lett.* **126** (4), 187-206.
- Valley J.W., Kitchen N., Kohn M. J., Niendorf C. R., and Spicuzza M. (1995) UWG-2, a garnet standard for oxygen isotope ratios: Strategies for high precision and accuracy with laser heating. *Geochim. Cosmochim. Acta* **59** (24), 5223-5231.

- Valley, J.M. and Graham, C.M. (1996) Ion microprobe analysis of oxygen isotope ratios in quartz from Skye granite: healed micro-cracks, fluid flow, and hydrothermal exchange. *Contrib. Min. Petrol.* **124**, 225-234.
- Wendt, I., Lenz, H., and Hohndorf, A. (1974) Das Alter des Bärhalde-Granites (Schwarzwald) und der Uranlagerstätte Menzenschwand. *Geol. Jahrb.* **E2**, 131-143.
- Wiechert, U. and Hoefs, J. (1995) An excimer laser-based micro analytical preparation technique for in-situ oxygen isotope analysis of silicate and oxide minerals. *Geochim. Cosmochim. Acta* **59**, 4093-4101.
- Wiechert U., Ionov D. A., and Wedepohl K. H. (1997a) Spinel peridotite xenoliths from the Atsagin-Dush volcano, Dariganga Plateau, Mongolia: A story of partial melting and cryptic metasomatism in the mantle. *Contrib Mineral Petrol* **126**, 345-364.
- Wiechert U., Hoernle K., and Graham D. (1997b) Oxygen isotope evidence for high temperature altered oceanic crust in the Canary Plume. *Trans. AGU* **87**, 825-826.
- Wood, B.J. and Walther, J.V. (1983) Rates of hydrothermal reactions. *Science* **222**, 413-415.
- Worden, R.H., Walker, F.D.L., Parsons, I., and Brown, W.L. (1990) Development of microporosity, diffusion channels and deuteric coarsening in perthitic alkali feldspars. *Contrib. Mineral. Petrol.* **104**, 507-515.
- Young, E.D. and Rumble, D. (1993) The origin of correlated variations in in-situ $^{18}\text{O}/^{16}\text{O}$ and elemental concentrations in metamorphic garnet from southeastern Vermont, USA. *Geochim. Cosmochim. Acta* **57**, 2585-2597.
- Young, E.D., Fogel, M.L., Rumble, D., and Hoering, T.C. (1998a) Isotope-ratio-monitoring of O_2 for microanalysis of $^{18}\text{O}/^{16}\text{O}$ and $^{17}\text{O}/^{16}\text{O}$ in geological materials. *Geochim. Cosmochim. Acta* **62**, 3087-3094.
- Young, E.D., Coutts, D.W., and Kapitan, D. (1998b) UV laser ablation and irm-GCMS microanalysis of $^{18}\text{O}/^{16}\text{O}$ and $^{17}\text{O}/^{16}\text{O}$ with application to a calcium-aluminium-rich inclusion from the Allende meteorite. *Geochim. Cosmochim. Acta* **62**, 3161-3168.
- Yui T. F., Rumble III D., and Lo C. H. (1995) Unusually low $\delta^{18}\text{O}$ ultra-high-pressure metamorphic rocks from the Sulu Terrain, eastern China. *Geochim. Cosmochim. Acta* **59**, 2859-2864.
- Zheng, Y.F. (1993a) Calculation of oxygen isotope fractionation in hydroxyl-bearing silicates. *Earth Planet. Sci. Lett.* **120**, 247-263.
- Zheng, Y.F. (1993b) Calculation of oxygen isotope fractionation in anhydrous silicate minerals. *Geochim. Cosmochim. Acta* **57**, 1079-1091.

Curriculum vitae

Date & place of birth: 5 November 1968, Bremen, Germany

Education: 1975-1979; Grundschule, Schwanewede
1979-1981; Orientierungsstufe, KGS Schwanewede
1981-1988; Gymnasiale Oberstufe, KGS Schwanewede

1988-1990; Civil Service

1990-1996; University Göttingen

Diploma in Chemistry

Advisor: H-Gg. Wagner

Co-advisor: J. Hoefs

Thesis: Matrix-interferences during quantitative determinations of trace elements by Graphite Furnace-Atomic Absorption Spectrometry (GF-AAS) [in German]

1997-1999; *Ph.D.* studies in Earth Sciences, Geochemistry

Institute of Geochemistry, University of Göttingen

Advisor: J. Hoefs

Co-advisor: G. Wörner

Thesis: Oxygen isotope microanalysis of silicates with application to fluid-rock interfaces